UTS UNIVERSITY OF TECHNOLOGY SYDNEY

Factors Affecting the Stability of Gold Nanoparticles

by Paige Summers

Thesis submitted in fulfilment of the requirements for the degree of:

Doctor of Philosophy

under the supervision of:
Andrew McDonagh
Michael Cortie

University of Technology
Sydney Faculty of Science
School of Mathematical and Physical Sciences

March 2025

Certificate of Original Authorship

I, *Paige Summers,* declare that this thesis is submitted in fulfilment of the requirements for the award of *Doctor of Philosophy*, in the *Faculty of Science* at the University of Technology Sydney.

This thesis is wholly my own work unless otherwise referenced or acknowledged. In addition, I certify that all information sources and literature used are indicated in the thesis.

This document has not been submitted for qualifications at any other academic institution.

This research was supported by the Australian Government Research Training Program (RTP) Scholarship doi.org/10.82133/C42F-K220.

Signature: Production Note:
Signature removed prior to publication.

Date: 27.03.2025

For my mother

Table of Contents

Certificate of Original Authorship ..... **i**
Publications Arising from This Work ..... **iv**
List of Figures ..... **v**
List of Tables ..... **viii**
List of Abbreviations ..... **ix**
Abstract ..... **x**
Chapter 1 ..... **1**
1.1 Introduction and Overview of the Thesis 2
1.2 Gold Nanoparticles Stabilised with Thiol and Alkyne Compounds 3
1.2.1 Thiyl-stabilised Gold Nanoparticles 3
1.2.2 Alkynide-stabilised Gold Nanoparticles 4
1.3 Sintering of Ligand-stabilised Gold Nanoparticles 5
1.3.1 Analysis of AuNPs Before, During and After the Sintering Event 6
1.3.2 Factors Affecting the Temperature of the Sintering Event 6
1.4 Project Aim and Objectives 8
Chapter 2 ..... **13**
2.1 Preamble 14
2.2 Certificate of Authorship 15
2.3 Authorship Contributions 15
2.4 The Fate of Organic Species Upon Sintering of Thiol-Stabilised Gold Nanoparticles Under Different Atmospheric Conditions 16
2.5 Supplementary Information 28
Chapter 3 ..... **35**
3.1 Preamble 36
3.2 Certificate of Authorship 37
3.3 Authorship Contributions 37
3.4 Nano to Macro Transition of Gold Nanoparticles Prior to Sintering 38
3.5 Supplementary Information 48
Chapter 4 ..... **54**
4.1 Preamble 55
4.2 Certificate of Authorship 56
4.3 Authorship Contributions 56
4.4 Electrically Conductive Gold Films Formed By Sintering of Gold Nanoparticles At Room Temperature Initiated By Ozone 57
4.5 Supplementary Information 64
Chapter 5 ..... **69**
5.1 Preamble 70
5.2 Certificate of Authorship 71
5.3 Authorship Contributions 71
5.4 Alkynide-Stabilised Gold Nanoparticles: A Synthetic Investigation 72
5.5 Supplementary Information 85
Chapter 6 ..... **91**
6.1 Conclusions 92
6.2 Future Directions 93

Publications Arising from This Work

Summers, P.K., Angeloski, A., Wuhrer, R., Cortie, M., & McDonagh, A.M. The fate of organic species upon sintering of thiol-stabilised gold nanoparticles under different atmospheric conditions *Phys. Chem. Chem. Phys.*, 2023, 25, 7170-7175 https://doi.org/10.1039/D2CP05822G

Summers, P.K., Wuhrer, R. & McDonagh, A.M. Electrically conductive gold films formed by sintering of gold nanoparticles at room temperature initiated by ozone. *J Nanopart Res*., 2024, 26, 97. https://doi.org/10.1007/s11051-024-06012-4

Summers, P.K., & McDonagh, A.M. Alkynide-stabilised Gold Nanoparticles: A Synthetic Investigation. *Nano Futures*., 2025, 9, 021001. https://doi.org/10.1088/2399-1984/addb18

Summers, P.K., Angeloski, A., Cortie, M., Wuhrer, R., & McDonagh, A.M. Nano to Macro Transition of Gold Nanoparticles Prior to Sintering. *J Mat Sci: Mater Electron*., 2025, 35, 1797. https://doi.org/10.1007/s10854-025-15854-0

List of Figures

Figure 1.1 Au(0)-thiyl model in equilibrium with the activated self-assembled monolayer (SAM) and thiolates. Reproduced from 31 4

Figure 1.2 Reaction scheme and chemical structure of alkynylated molecules used for surface functionalisation of poly(ethylene glycol) capped-gold nanoparticles. Reproduced from 40 5

Figure 1.3 a) Potential energy (U) curve depicting the energy barrier (ΔGact) for ligand-stabilised AuNPs separated by a distance, r, b) Schematic diagram of the sintering of two AuNPs, showing the required partial disruption of the stabilising ligands. Reproduced from 44 5

Figure 2.1 Schematic depicting the removal thiyl bound ligands in various atmosphere leaving the vicinity of the AuNPs as a disulfide species. 14

Figure 2.2 Schematic depicting the removal of short (a) and long (b) chain thiyl ligands from the surface of gold nanoparticles under ambient pressures. Initially, an equilibrium exists between bound thiyl and disulfide. (a) Short chain butanethiyl produces volatile dibutyl disulfide that leave the vicinity of the particle surface at moderate temperatures. (b) Long chained hexadecanethiyl ligands produce dihexadecyl disulfide with relatively low volatility that leave the surface at significantly higher temperatures. 18

Figure 2.3 Resistance data of (a) BT@AuNPs and (c) HDT@AuNP, and the corresponding derivatives of the resistance vs temperature curves (b) BT@AuNPs d/dT $\log_{10}$(R), s, (d) HDT@AuNPs d/dT $\log_{10}$(R). 21

Figure 2.4 ^{1}H NMR spectra of sintering residue of (a) BT@AuNP in hydrogen and nitrogen and (b) HDT@AuNP in hydrogen and nitrogen (* denotes H_2O at 1.58 ppm). 23

Figure 2.5 Thermogravimetric analysis data of (a) BT@AuNPs, (b) BT@AuNPs d/dT $\log_{10}$(R), (c) dibutyl disulfide, (d) dibutyl disulfide d/dT $\log_{10}$(R). 24

Figure 2.6 Thermogravimetric analysis data of (a) HDT@AuNPs, (b) HDT@AuNPs d/dT $\log_{10}$(R), (c) dihexadecyl disulfide, (d) dihexadecyl disulfide d/dT $\log_{10}$(R). 25

Figure 2.7 TEM images of (1) BT@AuNP and (2) HDT@AuNP. 28

Figure 2.8 ^{1}H NMR spectra of (a)/(c) BT@AuNP and (b)/(d) HDT@AuNP in $CDCl_3$. * indicates water (1.58 ppm). 29

Figure 2.9 SEM images of (a) BT@AuNPs and (c) HDT@AuNPs deposited using chloroform before heating and (b/d) after heating 10°C min^{-1} in air to 350°C.....30
Figure 2.10 TGA-MS data for BT@AuNPs (a) mass loss and (b) counts under a helium atmosphere. 30
Figure 2.11 ^{1}H NMR spectra of 1-butanethiol spiked with dibutyl disulfide. 31
Figure 2.12 Heat flow peaks (exothermic) under open and closed environments for HDT@AuNP(a/b) and BT@AuNP(c/d) respectively. 31
Figure 3.1 SEM images (obtained at 21°C) of BT@AuNPs after exposure to the following temperatures for 2 hours: (a) and (b), room temperature; (c) and (d), 100°C; (e) and (f), 150°C.....41
Figure 3.2 SEM images (obtained at 21°C) of HDT@AuNPs after exposure to the following temperatures for 2 hours: (a) and (b), room temperature; (c) and (d), 100°C; (e) and (f), 150°C;(g) and (h), 200°C. 42
Figure 3.3 Graph showing the resistances of HDT@AuNP films (a) and BT@AuNP films (b) from room temperature to 100°C. 44
Figure 3.4 Heat map of SAXS data for BT@AuNPs heated to 165°C at 3°C min^{-1}. 46
Figure 3.5 Heat map of SAXS data for HDT@AuNPs heated to 250°C at 3°C min^{-1}. .47
Figure 3.6 TEM images of HDT@AuNPs (left) and BT@AuNPs (right).....48
Figure 3.7 UV-vis of (a) BT@AuNPs and (b) HDT@AuNPs. 49
Figure 3.8 Resistance of BT@AuNPs held at 24 for 10 hours. 49
Figure 3.9 Graph showing the resistances of (a) HDT@AuNP films and (b) BT@AuNP films heated at temperatures shown on (c).....50
Figure 4.1 Resistance data obtained from films of BT@AuNPs during heating. Conditions: (a) ozone-rich environment, (c) air. (b) and (d) are the corresponding derivatives of the resistance vs temperature curves. 60
Figure 4.2 BT@AuNP ink film (left) before and (right) after exposure to a stream of ozone for 3 hours.....60
Figure 4.3 Resistance data of BT@AuNPs at (a) room temperature in air and (b) an ozone rich environment over 15h. 61
Figure 4.4 Schematic depicting the removal of butanethiyl ligands from the surface of gold nanoparticles in an ozone rich environment. 62

Figure 4.5 SEM images of gold films obtained by (left) heating BT@AuNPs in to 250°C at 10°C min^{-1}, and (right) exposing BT@AuNPs to an ozone-rich atmosphere for 6 h at room temperature. 63
Figure 4.6 TEM image of drop cast BT@AuNPs. 64
Figure 4.7 SEM image of drop cast BT@AuNPs (on silicon wafer). 64
Figure 4.8 ^{1}H NMR spectra of the DMSO-soluble residue from ozone-induced sintered BT@AuNPs. Top: full range spectrum, Bottom: Signals in the range 0 – 3 ppm (* denotes residual DMSO at δ 2.49). 65
Figure 4.9 ^{1}H NMR spectra of the residue from ozone-induced sintered BT@AuNPs as well as spectra for 1-butanesulfonic acid, 1-sodium 1-butanesulfonate, dibutyl disulfide and 1-butanethiol (* denotes residual DMSO at δ 2.49). 65
Figure 4.10 Mass spectrum of residue from ozone-induced sintered BT@AuNPs (Relative Mass Difference: -3.35 ppm) 66
Figure 5.1 Schematic showing new insights of (a) current synthetic technique of stabilising alkynides on AuNPs and (b) the synthetic technique developed in Chapter 5. 70
Figure 5.2 UV-visible spectra of (a) AuNPs synthesised using Method A, (b) AuNPs synthesised using Method B, (c) AuNPs synthesised using Method C (washed with water only), (d) AuNPs synthesised using Method E. 75
Figure 5.3 TEM of (a) Dec-1-ynide/TOAB-stabilised AuNPs (Method A); (b) Dec-1-ynide/TOAB-stabilised AuNPs (Method B); (c) TOAB-stabilised AuNPs (Method C). 76
Figure 5.4 UV-visible spectrum of (a) gold(I)dec-1-ynide; (b) dec-1-ynide@AuNPs (Method D). 77
Figure 5.5 (a) SEM and (b) TEM of Dec-1-ynide-stabilised AuNPs via Method D. 78
Figure 5.6 ^{1}H NMR spectra of (a) gold(I)dec-1-yn-1-ide; (b) dec-1-ynide@AuNPS (Method D); (c) 1-decyne. 79
Figure 5.7 TGA for (a) gold(I)dec-1-ynide; (b) dec-1-ynide@AuNPs (Method D). 80
Figure 5.8 TEM of (a) Method A; (b) Method B; (c) Method C and SEM of (d) Method D. 85
Figure 5.9 TEM Histogram of (a) Method A; (b) Method B; (c) Method C; (d) Method D. 86
Figure 5.10 ^{1}H NMR spectra of AuNPs synthesised by Method A, C and E, and tetraoctylammonium bromide (* denotes residual solvent). 86

List of Tables

Table 2.1 Summary of T_{SE} (°C) of BT@AuNP and HDT@AuNP determined using electrical resistance measurements in different atmospheres the T_{SE}. 26

Table 2.2.HDT@AuNPs Kruskal-Wallis test comparing gases argon, hydrogen and air (gases) and gases with high vacuum (atmospheres) T_{SE}. 31

Table 2.3 BT@AuNPs Kruskal-Wallis test comparing gases argon, hydrogen and air (gases), and between gases with high vacuum (atmospheres) T_{SE}. 31

Table 4.1 Summary of AuNP properties 81

List of Abbreviations

NMR	nuclear magnetic resonance
AuNC	gold nanocluster
AuNP	gold nanoparticle
BT@AuNP	1-butanethiol-stabilised AuNP
$CDCl_3$	deuterated chloroform
DMSO-d_6	deuterated dimethyl sulfoxide
DSC	differential scanning calorimetry
FEGSEM	field emission gun scanning electron microscope
HDT@AuNP	1-hexadecanethiol-stabilised AuNP
HRMS	high resolution mass spectrometry
NP	nanoparticle
PEG	phenylacetylene-polyethylene glycol
PVP	polyvinylpyrrolidone
SAM	self-assembled monolayer
SAXS	small-angle X-ray scattering
SEM	scanning electron microscope
TEM	transmission electron microscope
TGA	thermogravimetric analysis
TGA-MS	thermogravimetric analysis- mass spectrometry
TOAB	tetraocytlammonium bromide
T_{SE}	temperature of the sintering event
UV-vis	ultraviolet-visible

Abstract

Gold nanoparticles are utilised in a multitude of scientific disciplines. Their surfaces can be modified such that properties can be manipulated and so gold nanoparticles are employed across various applications. The stability of gold nanoparticles is of particular interest, as this affects their sintering behaviour and their utility in applications such as printed electronics, catalysis and sensing. Research investigating the stability of gold nanoparticles has focused primarily on modifying the heating rate, nanoparticle size, surface properties, and surrounding atmosphere to facilitate or hinder the sintering event. This thesis presents an investigation into the stability of gold nanoparticles with a focus on the physical and chemical changes that occur before, during and after the sintering event. Butanethiol and hexadecanethiol were selected as stabilising ligands with significantly different chain lengths to examine their influence on the stability of gold nanoparticles (in the size range of 2-4 nm). The physical and chemical properties were analysed using electrical resistance, scanning electron microscopy, differential scanning calorimetry, thermogravimetry analysis, nuclear magnetic resonance spectroscopy and small angle X-ray scattering before, during and after the sintering event. A comprehensive study of the stability of gold nanoparticles exposed to a variety of atmospheres including a strong oxidising atmosphere, with results having potential applications into the production of gold thin films at low temperatures. Important insights were also gained on the synthesis of new alkynide-stabilised gold nanoparticles (size range of 2-4 nm). A method was developed to produce monodisperse alkynide-stabilised gold nanoparticles.

Chapter 1
Introduction

This thesis is a compilation of published or submitted manuscripts. Thus, specific introductions are incorporated into the various chapters. This chapter provides a brief and general introduction to the field of study and themes of the current research work. Preambles to each of the chapters are included to indicate how each piece of work relates to the overall theme of the thesis.

1.1 Introduction and Overview of the Thesis

A nanoparticle (NP) is generally defined as a particle of any shape with a size ranging between 1 and 100 nm.[1] NPs are widely employed in multiple disciplines of science. Gold nanoparticles (AuNPs) have been of intense interest due to their controllable syntheses,[2] ease of surface functionalisation,[3-6] and excellent biocompatibility.[7] Ligand stabilised NPs present numerous applications and technological possibilities, ranging from energy (fuel cell catalysts,[8] steam methane reforming[9]) to environment (pollution,[10] wastewater treatment[11]), biology and medicine (drug delivery,[12] antibacterial agents,[13] food additives[14]). Ligand stabilised AuNPs have been examined in detail in the fields of nanotechnology and material science owing to their unique properties for thin film fabrication,[15, 16] printable inks[17] and electronic circuits.[18]

A distinctive optical feature of AuNPs is surface plasmon resonance, which leads to absorbance bands with maxima at approximately 520 nm. As nanoparticle core sizes decreases below ~3 nm, the intensity of the surface plasmon band diminishes sharply due to the onset of quantum size effects, accompanied by a slight blue shift and broadening of the plasmon band.[19-21] For ultrasmall, monodisperse AuNPs with core diameters between 1.1 and 1.9 nm, step-like spectral features emerge, reflecting electronic transitions to discrete, unoccupied energy levels of the conduction band.[22-24]

Despite the considerable advancements over the years, a detailed understanding of the mechanisms and factors affecting the processes by which AuNPs form gold films are still being explored.[25, 26] Many AuNP printing techniques (e.g. stencil, microcontact and nanoimprinting) rely on post-treatments such as heat treatment and washing with solvent to remove ligand residues following the formation of gold inks.[15, 27-29] Understanding factors that influence the AuNPs before, during and after gold film formation is important in improving the functionality of printed electronics.

The work presented here is an investigation of the stability of ligand stabilised AuNPs, focusing on the physical and chemical process before, during and after the formation of gold films.

The thesis is arranged as follows:

- Chapter 1 provides an overview of the literature relating to the analysis of the stability of ligand stabilised AuNPs and factors that effect it, along with a detailed description of the project aims.
- Chapter 2 provides an in-depth analysis of the effect of ligands during and after the sintering event.
- Chapter 3 presents an investigation of thiol-stabilised AuNPs while being heated prior to the sintering event.
- Chapter 4 describes a new chemical that allows thiol-stabilised AuNPs to be sintered at room temperature.
- Chapter 5 presents an in-depth investigation on the synthesis of alkynide-stabilised AuNPs.
- Chapter 6 presents the conclusions made from this work and suggests future work that can be done as a result.

1.2 Gold Nanoparticles Stabilised with Thiol and Alkyne Compounds

Surface modification of AuNPs is crucial in determining the AuNPs properties. Ligands are molecular entities or atoms that are coordinated to metal centres. Ligands can stabilise AuNPs via electrostatic and/or steric interactions.[30] Thus, modifications to the stabilising ligands will influence the particles' physical and chemical properties. This thesis focuses on stabilising AuNPs with thiol compounds and explores new methods to utilise alkyne functional groups.

1.2.1 Thiyl-stabilised Gold Nanoparticles

Thiol compounds are widely used to functionalise AuNPs surfaces and are a scaffold for a variety of applications, such as molecular electronics, catalysis, biosensing, and vaccine development. The nature of the bond at gold-sulfur interface may be described as a Au(0)-thiyl radical interation.[31] That is, the sulfhydryl group of the ligand is deprotonated, and a thiyl radical (RS·) is formed, as shown in Figure 1.1. The Au(0)-·SR bond formation involves interatomic chemical and physical (van der Waals) interactions

that leads to an equilibrium, Figure 1.1. The Au–S bond has been calculated to be stronger than that of the surface Au–Au bonds.

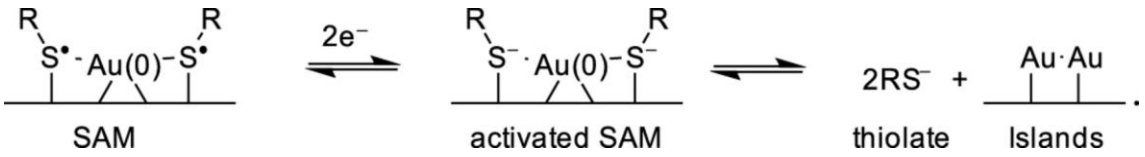

Figure 1.1 Au(0)-thiyl model in equilibrium with the activated self-assembled monolayer (SAM) and thiolates. Reproduced from ref 31.

The Brust–Schiffrin synthesis, a facile and versatile route, remains the most cited biphasic method used to prepare stable, monodispersed thiol-stabilised AuNPs.[32] The synthesis involves the reduction of Au(III) to Au(0) with the formation of Au(0)-·SR surface species (where R is most often organic aliphatic or aromatic groups).[33]

1.2.2 Alkynide-stabilised Gold Nanoparticles

Alkyne compounds have emerged as promising alternative stabilising ligands due to their stability when attached to gold.[34] Alkynes are relatively straightforward to prepare, and mild reaction conditions are sufficient for surface attachment to gold.[35] Binding to gold occurs through the deprotonation of the terminal alkyne, with the alkynide group shown to be in an upright linear configuration relative to gold surface.[36] The alkynide group has been reported to have strong σ-donating and π-back-bonding ability.[36] Self-assembled monolayers (SAMs) formed from alkynes on gold demonstrated their potential as biosensors with excellent performance, hydrolytic and thermal stability, and being less affected by biological thiol compounds compared to Au–S and Au–Se analogs.[34, 37]

Stability studies of terminal alkynes on gold utilise SAMs on Au(111), with the binding strengths greater than those of thiols, phosphines, aryl radicals and alkylamines.[38] Displacement experiments showed that a 1-ethynyl-4-fluorobenzene monolayer on Au exhibited a higher resistance to displacement compared to the monolayer formed from the thiol analog due to the enhanced stability of the Au–C bond.[39]

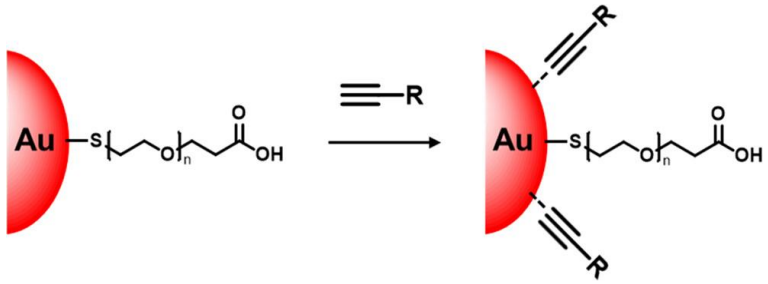

Figure 1.2 Reaction scheme and chemical structure of alkynylated molecules used for surface functionalisation of poly(ethylene glycol) capped-gold nanoparticles. Reproduced from ref 40.

Studies of alkynide-stabilised AuNPs are sparse, with reports focusing on their potential as chemicals sensors[40] and imaging,[41, 42] with most alkynide-stabilised AuNPs including an additional stabilising ligand (an example is shown in Figure 1.2).

1.3 Sintering of Ligand-stabilised Gold Nanoparticles

Sintering is the temperature-induced coalescence and densification of solid particles below the melting point of the core component.[43] Sintering of AuNPs can form electrically conductive films for use in thin-film transistors, field effect transistors, contacts, and conducting wires. AuNPs sinter when a sufficient amount of energy is applied and overcomes the activation energy barrier (ΔG_{act}) associated with the stabilising ligands (Figure 1.3a).[44] Sintering for most ligand-stabilised AuNPs occurs through particle migration and coalescence[7] where NPs move into close proximity whereupon the particle boundaries disappear and the overall surface area is reduced (Figure 1.3b).[8] Importantly, for AuNPs the temperature of the sintering event (T_{SE}) can be many hundreds of degrees below that of the melting point of gold (1064°C).

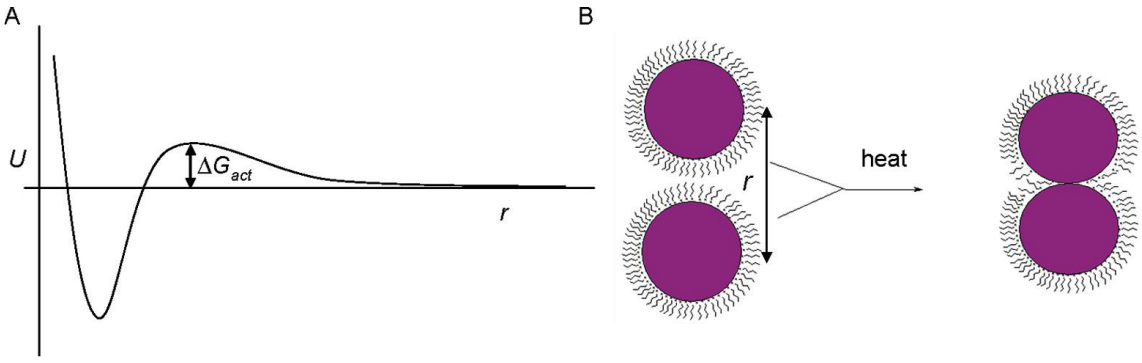

Figure 1.3 a) Potential energy (U) curve depicting the energy barrier (ΔGact) for ligand-stabilised AuNPs separated by a distance, r, b) Schematic diagram of the sintering of two AuNPs, showing the required partial disruption of the stabilising ligands. Reproduced from ref 44.

A number of factors influencing the T_{SE} have been investigated, permitting AuNPs to be employed in a diverse range of applications such as sensors, radio frequency

identification tags, and bioimaging. However, a detailed understanding of the AuNPs thermal stability surrounding the sintering event is essential for further development of these nanomaterials for applications.

1.3.1 Analysis of AuNPs Before, During and After the Sintering Event

During the heating of AuNPs to facilitate sintering, the associated surface area reduction is exothermic and results from a lowering of the surface energy.[45] The heat release increases the particle temperature rapidly and speeds up the coalescence.[46] These phenomena can be readily measured using differential scanning calorimetry (DSC).[44] In the case where longer chain thiol-stabilised ligands are employed (e.g. tetradecanethiol), sintering was reported to occur at significantly lower temperatures that the main mass loss event.[47]

The sintering event can be monitored using electrical resistance measurements. Prior to sintering, the resistance of AuNPs is generally quite large and dependant on the alkane chain length. Increased distance between gold cores (as result of longer alkane chains) increases resistance across the AuNPs. This is expected for an electron tunnelling mechanism, with studies showing an exponential relationship between the electronic conductivity and the ligand chain length.[48]

A significant drop in electrical resistance occurs upon sintering where a conductive gold film is formed. The electrical conductivity of AuNP films is dependent on the thickness and continuity of the deposited films. The volatility of the stabilising ligand can influence the continuity of the gold films after the sintering event if displaced stabilising ligand does not volatilise upon sintering.[49]

1.3.2 Factors Affecting the Temperature of the Sintering Event

Previous work has examined factors that affect sintering of AuNPs including heating rate,[44] size of the NPs,[50] ligand length[51] and atmosphere.[44] These factors provide a variety of methods to adjust the sintering temperatures of AuNPs.

There is a kinetic component to sintering that is dependent on the activation energy barrier introduced by the stabilising ligand.[44] The rate of heating affects the temperature of the sintering event which implies that there is no specific sintering temperature for a particular AuNP,[52, 53] although many published studies do not consider this aspect. For 1-butanethiol-stabilised AuNPs (BT@AuNPs), slower rates reduced the sintering event

with sintering observed at ~80°C when heated at 2.5°C min^{-1} compared to ~100°C when heated at a rate of 6°C min^{-1}.[54]

The size of AuNPs has been shown to have only a small effect on the thermal stability, with smaller particles exhibiting higher sintering temperatures. AuNPs with diameters of 1.2 nm and 0.9 nm showed sintering temperatures of 147°C and 174°C respectively.[50] This has been attributed to the different surface curvatures of the nanoparticles, with the higher radius of curvature in smaller particles resulting in a larger proportion of Au atoms to be on the surface, which in turn provides a greater coverage of passivating ligands.[2]

Longer thiol-stabilising ligands have been shown to increase AuNPs thermal stability,[15, 47, 51, 52, 55] presumably due to the lower volatility of the longer chain alkanethiols. Investigations using highly thermally stable phthalocyanine molecules to stabilise AuNPs revealed high sintering temperatures (~320°C) as the molecule provided a robust barrier to coalescence.[49]

A shelf life study of AuNPs showed that the surrounding atmosphere can affect Au-S interactions[54] with coalescence observed in ambient conditions over 44 months. It was proposed that the sulfur atom undergoes oxidation from atmospheric oxygen, thus weakening Au-S interactions.[56] This notion was demonstrated using gaseous NO_2 (a strong oxidiser) to sinter AuNPs at room temperature.[44]

Overall, the study of the stability of ligand stabilised AuNPs plays an important role in designing nanomaterials for industrial, biological and engineering applications and manipulation and control the AuNP sintering event.

1.4 Project Aim and Objectives

1.4.1 Project Aim

The aim of the work presented here is to measure and quantify physical and chemical changes that occur before, during, and after the sintering event of thiol-stabilised AuNPs. This work also aims to establish a synthesis for monodisperse AuNPs stabilised only by alkynide ligands.

To achieve these aims, the following objectives have been developed:

1.4.2 Project Objectives

Objective 1. Synthesise and characterise thiol-stabilised AuNPs using ^{1}H nuclear magnetic resonance spectroscopy, transmission electron microscopy, scanning electron microscopy and ultraviolet-visible spectroscopy.

Objective 2. Measure the temperatures of the sintering events of the AuNPs using electrical resistance and differential scanning calorimetry.

Objective 3. Examine changes in physical properties upon heating to temperatures prior to sintering using scanning electron microscopy, small angle x-ray scattering, and electrical resistance measurements.

Objective 4. Analyse changes in the chemical properties of the stabilising ligands upon heating to temperatures up to and beyond sintering.

Objective 5. Measure the effect of various atmospheres upon sintering using electrical resistance measurements.

Objective 6. To investigate current synthetic methods to prepare alkynide-stabilised nanoparticles and develop a synthesis that produces monodisperse AuNPs that are stabilised only by alkynide ligands.

References

1. Falahati, M., Attar, F., Sharifi, M., Saboury, A. A., Salihi, A., Aziz, F. M., Kostova, I., Burda, C., Priecel, P., Lopez-Sanchez, J. A., Laurent, S., Hooshmand, N., El-Sayed, M. A., Gold nanomaterials as key suppliers in biological and chemical sensing, catalysis, and medicine. *Biochimica et Biophysica Acta - General Subjects.* 2019, 129435.
2. Hostetler, M. J., Wingate, J. E., Zhong, C.-J., Harris, J. E., Vachet, R. W., Clark, M. R., Londono, J. D., Green, S. J., Stokes, J. J., Wignall, G. D., Glish, G. L., Porter, M. D., Evans, N. D., Murray, R. W., Alkanethiolate Gold Cluster Molecules with Core Diameters from 1.5 to 5.2 nm: Core and Monolayer Properties as a Function of Core Size. *Langmuir.* 1998, *14* (1), 17-30.
3. Hammami, I., Alabdallah, N. M., jomaa, A. A., kamoun, M., Gold nanoparticles: Synthesis properties and applications. *Journal of King Saud University - Science.* 2021, *33* (7), 101560.
4. Wilton-Ely, J. D. E. T., The surface functionalisation of gold nanoparticles with metal complexes. *Dalton Transactions.* 2008, (1), 25-29.
5. Roux, S., Garcia, B., Bridot, J.-L., Salomé, M., Marquette, C., Lemelle, L., Gillet, P., Blum, L., Perriat, P., Tillement, O., Synthesis, characterization of dihydrolipoic acid capped gold nanoparticles, and functionalization by the electroluminescent luminol. *Langmuir.* 2005, *21* (6), 2526-2536.
6. Ackerson, C. J., Jadzinsky, P. D., Kornberg, R. D., Thiolate ligands for synthesis of water-soluble gold clusters. *Journal of the American Chemical Society.* 2005, *127* (18), 6550-6551.
7. Kadhim, R. J., Karsh, E. H., Taqi, Z. J., Jabir, M. S., Biocompatibility of gold nanoparticles: In-vitro and In-vivo study. *Materials Today: Proceedings.* 2021, *42*, 3041-3045.
8. Zhang, Z., Xin, L., Li, W., Supported gold nanoparticles as anode catalyst for anion-exchange membrane-direct glycerol fuel cell (AEM-DGFC). *International Journal of Hydrogen Energy.* 2012, *37* (11), 9393-9401.
9. Atjayutpokin, T., Eaimsumang, S., Smith, S. M., Boonyuen, S., Luengnaruemitchai, A., Gold nanoparticles-assisted sodium borohydride supported on titania as a catalyst for the oxidative steam reforming of methanol and CO oxidation. *Materials Today Communications.* 2022, *33*, 105019.
10. Rassaei, L., Marken, F., Sillanpää, M., Amiri, M., Cirtiu, C. M., Sillanpää, M., Nanoparticles in electrochemical sensors for environmental monitoring. *TrAC Trends in Analytical Chemistry.* 2011, *30* (11), 1704-1715.
11. Zahra, Z., Habib, Z., Chung, S., Badshah, M. A., Exposure route of TiO2 NPs from industrial applications to wastewater treatment and their impacts on the agro-environment. *Nanomaterials.* 2020, *10* (8), 1469.
12. Wu, J., Liu, B., Wu, H., Wu, Y., Zhang, W., Zhao, S., Zhang, L., Pan, X., Gao, W., Wang, X., Yuan, Y., Zhang, Y., A gold nanoparticle platform for the delivery of functional TGF-β1 siRNA into cancer cells. *Journal of Biomedical Nanotechnology.* 2016, *12* (4), 800-810.
13. Islam, F., Shohag, S., Uddin, M. J., Islam, M. R., Nafady, M. H., Akter, A., Mitra, S., Roy, A., Emran, T. B., Cavalu, S., Exploring the journey of zinc oxide nanoparticles (ZnO-NPs) toward biomedical applications. *Materials.* 2022, *15* (6), 2160.
14. Chen, J., Guo, Y., Zhang, X., Liu, J., Gong, P., Su, Z., Fan, L., Li, G., Emerging nanoparticles in food: Sources, application, and safety. *Journal of Agricultural and Food Chemistry.* 2023, *71* (8), 3564-3582.

15. Wu, Y., Li, Y., Liu, P., Gardner, S., Ong, B. S., Studies of Gold Nanoparticles as Precursors to Printed Conductive Features for Thin-Film Transistors. *Chemistry of Materials.* 2006, *18*, 4627-4632.
16. Hardy, N. J., Hanwell, M. D., Richardson, T. H., Temperature effects on the electrical conductivity of thiol encapsulated gold nanoparticle thin films. *Journal of Materials Science: Materials in Electronics.* 2007, *18* (9), 943-949.
17. Khan, Y., Pavinatto, F. J., Lin, M. C., Liao, A., Swisher, S. L., Mann, K., Subramanian, V., Maharbiz, M. M., Arias, A. C., Inkjet-Printed Flexible Gold Electrode Arrays for Bioelectronic Interfaces. *Advanced Functional Materials.* 2016, *26* (7), 1004-1013.
18. Prakash, A., Ouyang, J., Lin, J.-L., Yang, Y., Polymer memory device based on conjugated polymer and gold nanoparticles. *Journal of Applied Physics.* 2006, *100* (5).
19. Papavassiliou, G. C., Optical properties of small inorganic and organic metal particles. *Progress in Solid State Chemistry.* 1979, *12* (3), 185-271.
20. Logunov, S. L., Ahmadi, T. S., El-Sayed, M. A., Khoury, J. T., Whetten, R. L., Electron Dynamics of Passivated Gold Nanocrystals Probed by Subpicosecond Transient Absorption Spectroscopy. *The Journal of Physical Chemistry B.* 1997, *101* (19), 3713-3719.
21. Ito, E., Kang, H., Lee, D., Park, J. B., Hara, M., Noh, J., Spontaneous desorption and phase transitions of self-assembled alkanethiol and alicyclic thiol monolayers chemisorbed on Au(111) in ultrahigh vacuum at room temperature. *Journal of Colloid and Interface Science.* 2013, *394*, 522-529.
22. Schaaff, T. G., Shafigullin, M. N., Khoury, J. T., Vezmar, I., Whetten, R. L., Cullen, W. G., First, P. N., Gutiérrez-Wing, C., Ascensio, J., Jose-Yacamán, M. J., Isolation of Smaller Nanocrystal Au Molecules: Robust Quantum Effects in Optical Spectra. *The Journal of Physical Chemistry B.* 1997, *101* (40), 7885-7891.
23. Zaitoun, M. A., Mason, W. R., Lin, C. T., Magnetic Circular Dichroism Spectra for Colloidal Gold Nanoparticles in Xerogels at 5.5 K. *The Journal of Physical Chemistry B.* 2001, *105* (29), 6780-6784.
24. Melinger, J. S., Kleiman, V. D., McMorrow, D., Gröhn, F., Bauer, B. J., Amis, E., Ultrafast Dynamics of Gold-Based Nanocomposite Materials. *The Journal of Physical Chemistry A.* 2003, *107* (18), 3424-3431.
25. Urban, M. A.-O. X., Rosati, G., Maroli, G., Pelle, F. D., Bonini, A., Sajti, L., Fedel, M., Merkoçi, A. A.-O., Nanostructure Tuning of Gold Nanoparticles Films via Click Sintering. *Small.* 2024, *20* (13).
26. Im, J., Heaton, C., Putri, N. R. E., Liu, C., Usuba, J., Butler, K., Fay, M., Han, G. G. D., Hooshmand, H., Thompson, A., Wildman, R., Hague, R., Turyanska, L., Tuck, C., On-Demand Sintering of Gold Nanoparticles via Controlled Removal of o-Nitrobenzyl Thiol Ligands Under Record-Low Power for Conductive Patterns. *Advanced Science.* 2025.
27. Wu, Y., Li, Y., Ong, B. S., Liu, P., Gardner, S., Chiang, B., High-Performance Organic Thin-Film Transistors with Solution-Printed Gold Contacts. *Advanced Materials.* 2005, *17* (2), 184-187.
28. Ko, S. H., Park, I., Pan, H., Grigoropoulos, C. P., Pisano, A. P., Luscombe, C. K., Fréchet, J. M. J., Direct nanoimprinting of metal nanoparticles for nanoscale electronics fabrication. *Nano Letters.* 2007, *7* (7), 1869-1877.
29. Basarir, F., Yoon, T.-H., Preparation of highly conductive gold patterns on polyimide via shaking-assisted layer-by-layer deposition of gold nanoparticles. *Colloids and Surfaces A: Physicochemical and Engineering Aspects.* 2012, *393*, 27-31.

30. Huang, R., Fedeli, S., Hirschbiegel, C.-M., Zhang, X., Rotello, V. M., Modulation of Gold Nanoparticle Ligand Structure–Dynamic Relationships Probed Using Solution NMR. *Nanoscience Au.* 2024, *4* (1), 62-68.
31. Reimers, J. R., Ford, M. J., Halder, A., Ulstrup, J., Hush, N. S., Gold surfaces and nanoparticles are protected by Au(0)-thiyl species and are destroyed when Au(I)-thiolates form. *Proceedings of the National Academy of Sciences of the United States of America.* 2016, *113*, E1424-E1433.
32. Brust, M., Walker, M., Bethell, D., Schiffrin, D. J., Whyman, R., Synthesis of thiol-derivatised gold nanoparticles in a two-phase Liquid–Liquid system. *Chemical Communications.* 1994, (7), 801-802.
33. Chai, O. J. H., Xie, J., Unraveling the Mechanism of the Brust-Schiffrin Formation of Au25(SR)18 through Mass Spectrometry. *The Journal of Physical Chemistry Letters.* 2024, *15* (19), 5137-5142.
34. Yang, Z., Pujari, S. P., Armstrong, R., Mathwig, K., Rutjes, F. P. J. T., Smulders, M. M. J., Zuilhof, H., Hydrolytic, Thermal, and Electrochemical Stability of Thiol- and Terminal Alkyne-Based Monolayers on Gold: A Comparative Study. *Langmuir.* 2025, *41* (9), 6197-6207.
35. Zhang, S., Chandra, K. L., Gorman, C. B., Self-Assembled Monolayers of Terminal Alkynes on Gold. *Journal of the American Chemical Society.* 2007, *129* (16), 4876-4877.
36. Maity, P., Takano, S., Yamazoe, S., Wakabayashi, T., Tsukuda, T., Binding Motif of Terminal Alkynes on Gold Clusters. *Journal of the American Chemical Society.* 2013, *135* (25), 9450-9457.
37. Zhang, C., Liu, Z., Zhang, L., Zhu, A., Liao, F., Wan, J., Zhou, J., Tian, Y., A Robust Au−C≡C Functionalized Surface: Toward Real-Time Mapping and Accurate Quantification of Fe2+ in the Brains of Live AD Mouse Models. *Angewandte Chemie International Edition.* 2020, *59* (46), 20499-20507.
38. Tang, Q., Jiang, D.-e., Comprehensive View of the Ligand–Gold Interface from First Principles. *Chemistry of Materials.* 2017, *29* (16), 6908-6915.
39. Weston, R. P., Chen, Y., Dzwonczyk, T. J., Veras, J. A., Sevigny, A. M., Landis, E. C., Electrically Transmissive and Stable Alkyne-Derived Molecular Layers on Nanoporous Gold. *The Journal of Physical Chemistry C.* 2022, *126* (23), 9673-9682.
40. Liu, Y.-Q., Chao, Y.-C., Xu, S.-Q., Peng, Y.-R., Syu, J.-J., Yang, X.-H., Pan, Y.-K., Lin, P.-C., Weng, L.-L., Chen, I. C., Tan, K.-T., Surface Functionalization of Gold Nanoparticles Using Alkyne Derivatives: Applications in Chemical Sensing. *Applied Materials & Interfaces.* 2024.
41. Ando, J., Asanuma, M., Dodo, K., Yamakoshi, H., Kawata, S., Fujita, K., Sodeoka, M., Alkyne-Tag SERS Screening and Identification of Small-Molecule-Binding Sites in Protein. *Journal of the American Chemical Society.* 2016, *138* (42), 13901-13910.
42. Koike, K., Bando, K., Ando, J., Yamakoshi, H., Terayama, N., Dodo, K., Smith, N. I., Sodeoka, M., Fujita, K., Quantitative Drug Dynamics Visualized by Alkyne-Tagged Plasmonic-Enhanced Raman Microscopy. *Nano.* 2020, *14* (11), 15032-15041.
43. Alemán, J. V., Chadwick, A. V., He, J., Hess, M., Horie, K., Jones, R. G., Kratochvíl, P., Meisel, I., Mita, I., Moad, G., Penczek, S., Stepto, R. F. T., Definitions of terms relating to the structure and processing of sols, gels, networks, and inorganic-organic hybrid materials (IUPAC Recommendations 2007). *Pure and Applied Chemistry.* 2007, *79* (10), 1801-1829.
44. Coutts, M. J., Cortie, M. B., Ford, M. J., McDonagh, A. M., Rapid and Controllable Sintering of Gold Nanoparticle Inks at Room Temperature Using a Chemical Agent. *The Journal of Physical Chemistry C.* 2009, *113*, 1325-1328.

45. Lehtinen, K., Zachariah, M., Energy Accumulation in Nanoparticle Collision and Coalescence Processes. *Journal of Aerosol Science.* 2002, *33*, 357-368.
46. Lehtinen, K. E. J., Zachariah, M. R., Effect of coalescence energy release on the temporal shape evolution of nanoparticles. *Physical Review B.* 2001, *63* (20), 205402.
47. Martin, J. E., Odinek, J., Wilcoxon, J. P., Anderson, R. A., Provencio, P., Sintering of alkanethiol-capped gold and platinum nanoclusters. *Journal of Physical Chemistry B.* 2003, *107*, 430-434.
48. Wuelfing, W. P., Green, S. J., Pietron, J. J., Cliffel, D. E., Murray, R. W., Electronic Conductivity of Solid-State, Mixed-Valent, Monolayer-Protected Au Clusters. *Journal of the American Chemical Society.* 2000, *122* (46), 11465-11472.
49. King, S. R., Shimmon, S., Gentle, A. R., Westerhausen, M. T., Dowd, A., McDonagh, A. M., Remarkable thermal stability of gold nanoparticles functionalised with ruthenium phthalocyanine complexes. *Nanotechnology.* 2016, *27* (21), 215702.
50. Smith, B. L., Hutchison, J. E., Transformations during sintering of small (D core < 2 nm) ligand-stabilized gold nanoparticles: Influence of ligand functionality and core size. *Journal of Physical Chemistry C.* 2013, *117*, 25127-25137.
51. King, S. R., Shimmon, S., Totonjian, D. D., McDonagh, A. M., Influence of Bound versus Non-Bound Stabilizing Molecules on the Thermal Stability of Gold Nanoparticles. *Journal of Physical Chemistry C.* 2017, *121*, 13944-13951.
52. Gupta, A., Mandal, S., Katiyar, M., Mohapatra, Y. N., Film processing characteristics of nano gold suitable for conductive application on flexible substrates. *Thin Solid Films.* 2012, *520*, 5664-5670.
53. Martin, J. E., Odinek, J., Wilcoxon, J. P., Anderson, R. A., Provencio, P., Sintering of Alkanethiol-Capped Gold and Platinum Nanoclusters. *The Journal of Physical Chemistry B.* 2003, *107* (2), 430-434.
54. Cortie, M. B., Coutts, M. J., Ton-That, C., Dowd, A., Keast, V. J., McDonagh, A. M., On the Coalescence of Nanoparticulate Gold Sinter Ink. *The Journal of Physical Chemistry C.* 2013, *117* (21), 11377-11384.
55. Huang, D., Liao, F., Molesa, S., Redinger, D., Subramanian, V., Plastic-Compatible Low Resistance Printable Gold Nanoparticle Conductors for Flexible Electronics. *Journal of The Electrochemical Society.* 2003, *150*, G412-G417.
56. Joseph, Y., Guse, B., Nelles, G., Aging of 1,ω-Alkyldithiol Interlinked Au Nanoparticle Networks. *Chemistry of Materials.* 2009, *21* (8), 1670-1676.

Chapter 2

The Fate of Organic Species Upon Sintering of Thiol-Stabilised Gold Nanoparticles Under Different Atmospheric Conditions

2.1 Preamble

Thiol-stabilised AuNPs are extensively used as a nanomaterial, work addressing the impact of the ligand during the formation of gold films has been lacking. There are limited studies reporting the chemical properties of the ligand and the influence of the surrounding atmosphere has upon thermal sintering. The formation of organic residue from the thiol-stabilising ligand after the sintering event will heavily influence the conductivity and stability of the gold film.

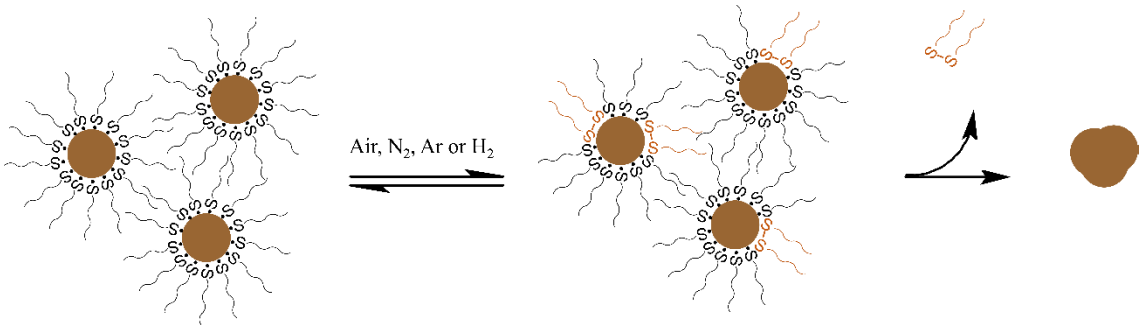

Figure 2.1 Schematic depicting the removal thiyl bound ligands in various atmosphere leaving the vicinity of the AuNPs as a disulfide species.

This chapter shows that upon sintering, surface-bound thiyl ligands exclusively form the corresponding disulfide species when released from AuNP surfaces (Figure 2.1). The volatility of the released disulfide significantly impacts the temperature of the sintering events.

2.2 Certificate of Authorship

The paper entitled "The fate of organic species upon sintering of thiol-stabilized gold nanoparticles under different atmospheric conditions" was published in *Physical Chemistry Chemical Physics*. The following chapter is based on the published work.

I, Paige Summers, certify that the work in Chapter 2 has not been submitted as part of any other documents required for a degree

2.3 Authorship Contributions

Author	Contribution	Signature
Paige K Summers	Conceptualisation, experimental design, performed experiments, analysed data, original manuscript writing, manuscript editing	Production Note: Signature removed prior to publication.
Alexander Angeloski	Experimental design, Technical assistance, conceptualisation, manuscript editing	Production Note: Signature removed prior to publication.
Richard Wuhrer	Technical assistance, manuscript editing	Production Note: Signature removed prior to publication.
Michael B. Cortie	Conceptualisation, manuscript editing	Production Note: Signature removed prior to publication.
M. McDonagh	Conceptualisation, manuscript editing, manuscript writing	Production Note: Signature removed prior to publication.

2.4 The Fate of Organic Species Upon Sintering of Thiol-Stabilised Gold Nanoparticles Under Different Atmospheric Conditions

Abstract

Understanding and controlling the sintering behaviour of gold nanoparticles is important for applications such as printed electronics, catalysis and sensing that utilise these materials. Here we examine the processes by which thiol-protected gold nanoparticles thermally sinter under a variety of atmospheres. We find that upon sintering, the surface-bound thiyl ligands exclusively form the corresponding disulfide species when released from the gold surface. Experiments conducted using air, hydrogen, nitrogen, or argon atmospheres revealed no significant differences between the temperatures of the sintering event nor on the composition of released organic species. When conducted under high vacuum, the sintering event occurred at lower temperatures compared to ambient pressures in cases where the resulting disulfide had relatively high volatility (dibutyl disulfide). Hexadecylthiol-stabilised particles exhibited no significant differences in the temperatures of the sintering event under ambient pressures compared to high vacuum conditions. We attribute this to the relatively low volatility of the resultant dihexadecyl disulfide product.

Introduction

AuNPs have attracted significant attention due to their unique properties and diverse applications.[1, 2] AuNPs may be sintered to form continuous, electrically conducting gold films at moderate to low temperatures.[3, 4] In contrast, for many sensing and catalysis applications it is crucial to prevent sintering and thereby maintain the size and shape of the nanoparticles.[5-7] Understanding the mechanism of the sintering process as well as the influence of atmosphere and ligands on the thermal stability of AuNPs can provide strategies to prevent, control or induce sintering for various applications such as sensors, radio frequency identification tags and in bioimaging.[8-10]

Sintering may be defined as "*temperature-induced coalescence and densification of porous solid particles below the melting points of their major components*"[11] and for AuNPs with diameters >1.5 nm, the temperatures applied to induce sintering are generally significantly lower than the NP melting points.[12] However, a thin molten surface layer

between actively coalescing particles has been described.[13] Coalescence (the disappearance of the boundaries between particles) of organic molecule-stabilised AuNPs generally starts with contact between the NPs and subsequent neck formation.[14] As the surface area of the merging nanoparticles decreases, surface energy is transformed into thermal energy, thus increasing the temperature of the particles.[15, 16]

There remains considerable debate about whether stabilising ligands should first be released from the gold surface[17-19] or if sintering can proceed with the surface layer intact.[20-23] Although the thermal stability and desorption of thiol-based monolayers on flat gold surfaces has been reasonably well investigated, few reports have examined this behaviour on the surfaces of AuNPs.[24-30] Such knowledge is important as the desorption behaviour directly affects the sintering temperatures of AuNPs.[31] In the context of SAMs, Reimers et al. describe an equilibrium between surface-bound thiyl species (that is, Au(0)-·SR species bonded via strong van der Waals attractions, polarisation effects and s–d hybridisation) and unbound disulfide compounds.[32] This model improves upon the more classical Au(I)-thiolate model for Au-SR compounds (such AuNPs). Considering the model of Reimers et al, one might predict that species of the type RS-SR might predominate when released from gold surfaces. Desorption studies on SAMs using hexanethiol on Au(111) under high vacuum at room temperature support this equilibrium model[29] and the disulfide derived from the stabilising thiol has been found to be the major species desorbed from SAMs on gold surfaces upon heating under particular conditions.[33]

In gold clusters of ~ 1.3 nm stabilised using thiols, Au-S bonds can be cleaved at temperatures where the ligands remain in the vicinity of the particle prior to the sintering event.[34] Smith and Hutchison provided evidence that disulfide compounds (formed from the stabilising thiol compound) exist on the surface of AuNPs at room temperature and that their concentration increased upon heating.[35] Disulfide species have also been identified in the core of thiolate stabilised Au130 clusters.[36] These observations are not inconsistent with the concept of an equilibrium between bound thiyl and disulfide species. We hypothesised that such an equilibrium would be disrupted when the disulfide leaves the vicinity of the particle surface, which will be a function of the disulfide volatility.

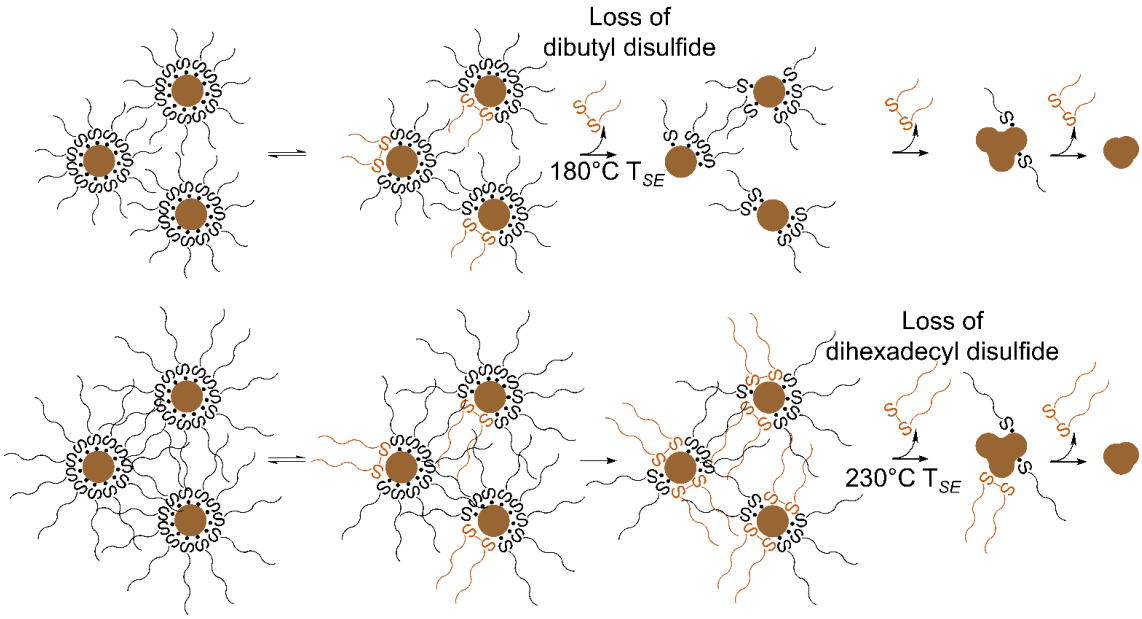

Figure 2.2 Schematic depicting the removal of short (a) and long (b) chain thiyl ligands from the surface of gold nanoparticles under ambient pressures. Initially, an equilibrium exists between bound thiyl and disulfide. (a) Short chain butanethiyl produces volatile dibutyl disulfide that leave the vicinity of the particle surface at moderate temperatures. (b) Long chained hexadecanethiyl ligands produce dihexadecyl disulfide with relatively low volatility that leave the surface at significantly higher temperatures.

Ligands have a significant role in the stability of AuNPs, with longer chain alkanethiol ligands (thus lower volatility) generally exhibiting a greater T_{SE} compared to shorter chain (higher volatility) ligands.[9, 31, 35, 37, 38] Here we show that the sintering of thiol-stabilised AuNPs is critically controlled by the equilibrium between thiyl and disulfide species and describe the influence of ligand volatility and atmosphere (Figure 2.2). We explore the sintering of thiol-stabilised AuNPs using ^{1}H nuclear magnetic resonance (NMR), TGA, DSC, electrical conductivity measurements, and mass spectroscopy to elucidate the processes that occur under different atmospheric conditions during the thermal sintering event, and examine the nature of the residual material upon sintering. These findings shed new light on the processes involved in sintering alkanethiol-stablised AuNPs.

Experimental

General

1-Butanethiol (Sigma-Aldrich), 1-hexadecanethiol (Fluka), and deuterated chloroform ($CDCl_3$) were used as received. Tetrachloroauric acid,[39] BT@AuNPs, and 1-hexadecanethiol-capped AuNPS (HDT@AuNPs) were prepared using literature procedures.[40] Dihexadecyl disulfide and dibutyl disulfide were synthesised using literature procedures.[41] ^{1}H NMR data are as follows: dihexadecyl disulfide: 0.88 (6H, t, J

= 9 Hz, -CH_3), 1.33-1.19 (4H, m, -CH_2*CH_2*CH_3), 1.42-1.34 (4H, m, -CH_2-), 1.72-1.62 (4H, quin, J = 9 Hz -CH_2-), 2.68 (4H, t, J = 9 Hz, -CH_2*CH_2*S), dibutyl disulfide: 0.92 (6H, t, J = 9 Hz, -CH_3), 1.47-1.36 (4H, sex, J = 9 Hz, -CH_2*CH_2*CH_3), 1.71-1.62 (4H, quin, J = 9 Hz, -CH_2-), 2.68 (4H, t, J = 9 Hz , -CH_2*CH_2*S).

^{1}H NMR spectra were recorded using an Agilent NMR spectrometer operating at 500.13 MHz ($CDCl_3$, δ7.26). Thermogravimetric analysis-mass spectroscopy (TGA-MS) analysis was performed using a Netzsch STA 449 F5 Jupiter TGA instrument coupled to an Agilent 5977B mass spectrometer. The heating rate was 10°C min^{-1} under a 30:70 helium: air gas flow rate of 50 ml min^{-1}, using 5-6 mg of the sample in an alumina oxide crucible. TGA was performed using a TA Instruments SDT Q600 with a heating rate of 10°C min^{-1} under an air atmosphere and flow rate of 50 ml/min with 5-6 mg of sample used. DSC was completed using a TA Instruments Q2000 with a heating rate of 10°C min^{-1}. Samples were prepared in air in a Tzero pan with Tzero hermetic lid, which could be punctured using a steel pin.

Transmission electron microscope (TEM) images were taken using a FEI Tecnai T20 TWIN microscope (LaB6) operating at 200 keV and fitted with a Gatan 894 2k x 2k camera. The TEM samples were prepared by evaporating diluted nanoparticle solution on the carbon-coated copper grid. The images were analysed using ImageJ software (https://imagej.nih.gov/ij/). Scanning electron microscope (SEM) was performed at facilities at Western Sydney University. A Zeiss Merlin field emission gun scanning electron microscope (FEGSEM) was utilised for imaging samples prepared on stubs. The FEGSEM was operated at 10kV accelerating voltage in Hivac mode at a working distance of approximately 3 mm. Both secondary and in-lens secondary detectors were utilised for imaging.

Resistance Measurements of AuNP Films

Films of AuNPs were formed by drop casting 10 mg/mL suspensions of AuNPs in chloroform onto DropSens (Metrohm) interdigitated gold electrodes and heated within a modified Linkam THMS600 temperature control stage. A heating rate of 10°C min^{-1} from room temperature to 350°C was maintained using a Linkam TMS 94 controller. The temperature was measured using a Rigol DM3058E digital multimeter and a PT100 (RS PRO) RTD sensor, 2mm x 5mm Class B thermocouple placed within 2 mm of the gold electrodes and held in contact with the heating block surface using a small clamp. We note that temperature measurements using a thermocouple in vacuo can be problematic

and so data were verified using certified melting standards (acetanilide, saccharin, dicyandiamide, benzanilide, acetaminosalol, phenacetin, benzil, azobenzene and benzoic acid).

Electrical resistance was measured with a Rigol DM3068 digital multimeter (maximum resistance of 100 MΩ). A LabView program was used to interface with and control the multimeters, and to acquire the temperature and electrical resistance. The flow rate of gases was controlled using an Apex mass flow controller with a rate of 25 ml min^{-1}. High vacuum measurements were recorded using a highly modified Linkam heating stage mounted within a purpose-built vacuum chamber operating at ~8 x 10^{-6} mbar. Data were analysed using Jamovi software (https://www.jamovi.org/) with Kruskal-Wallis One-Way ANOVA (non-parametic) and Dwass-Steel-Critchlow-Fligner pairwise comparisons to calculate p-values.

Analysis of Heated AuNPs

AuNPs were heated in gastight conical reaction vials to 300°C under atmospheres of air, nitrogen or hydrogen. The organic residues were collected by rinsing the interior of the cooled vials with deuterated chloroform and then filtering through cellulose fibre (Kimwipe) to remove elemental gold. The resultant solutions were analysed using ^{1}H NMR spectroscopy.

Results and Discussion

AuNPs were synthesised using variations of the two-phase Brust-Schiffrin method.[32] BT@AuNPs (synthesised using 1-butanethiol as stabilising ligand) had diameters of 3.2 (± 0.1) nm (measured using TEM, Figure 2.7, Section 2.5, Supplementary Information). HDT@AuNPs (synthesised using 1- hexadecanethiol as stabilising ligand) had diameters of 2.7 (± 0.05) nm (Figure 2.7, Section 2.5, Supplementary Information). The ^{1}H NMR spectra of BT@AuNPs and HDT@AuNPs in $CDCl_3$ (Figure 2.8, Section 2.5, Supplementary Information) are similar to previously reported spectra of octanethiol-stabilised AuNPs.[35] In the ^{1}H NMR spectrum of BT@AuNPs, no signals arising from the protons attached to C1 were observed. This is typical for thiol-stabilised AuNPs with diameters of ~3 nm.[42-44] However, in small clusters ~1 nm NMR signals arising from the alpha protons were observed .[45, 46] This was attributed to fewer types of binding sites on the small clusters, thus diminishing spectral broadening created from chemical shift distributions. Furthermore, methylene groups close to the Au surface are more densely

packed relative to those further from the surface and therefore experience faster spin relaxation from dipolar interactions[42] resulting in broader signals,[43]as shown in Figure 2.8 (Section 2.5, Supplementary Information). The resonances for the protons attached to C2 to C3 are observed as a broad peak from 1.45-1.10 ppm, and C4 as a triplet at 0.88 ppm. The ^{1}H NMR spectrum of HDT@AuNPs contains a signal at 1.60 ppm assigned to the protons attached to C2, a broad peak at 1.26 ppm assigned to protons attached to C3-15, and a triplet at 0.88 ppm assigned to the protons on C16. No signal arising from unbound thiol or the protons attached to C1 were observed.

A drop-cast film of AuNPs was heated at a rate of 10°C min^{-1} in air to 350°C to facilitate sintering. Figure 2.9 (Section 2.5, Supplementary Information) shows representative SEM images of (a) as-prepared BT@AuNPs and (b) sintered BT@AuNPs. Prior to sintering (Figure 2.9 a/c, Section 2.5, Supplementary Information), the nanoparticulate nature of the samples is apparent whereas after sintering (Figure 2.9 b/d, Section 2.5, Supplementary Information), no nanoparticles are evident but larger gold structures separated by grain boundaries are observed. It has been reported that there is a kinetic component to the thermal sintering of the AuNPs, with slower heating rates leading to lower temperatures of sintering events.[47] Thus, a heating rate of 10°C min^{-1} was maintained for all experiments to allow for meaningful comparisons to be made.

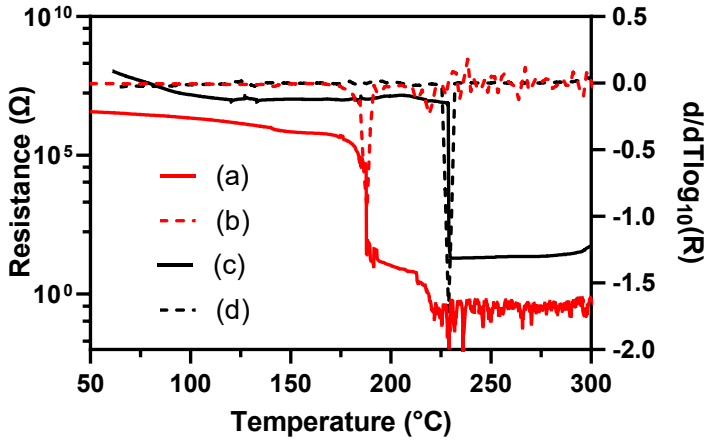

Figure 2.3 Resistance data of (a) BT@AuNPs and (c) HDT@AuNP, and the corresponding derivatives of the resistance vs temperature curves (b) BT@AuNPs d/dT $\log_{10}$(R), s, (d) HDT@AuNPs d/dT $\log_{10}$(R).

The resistances of drop-cast films of AuNPs were measured as a function of temperature using interdigitated gold electrodes heated at a rate of 10°C min^{-1}. The sintering event is characterised by a drop in resistance from values >1 MΩ to values <100

Ω. We use the definition of the T_{SE} as the temperature at the maximum rate of change in resistance.[10] Figure 2.3 shows representative data recorded while heating BT@AuNPs and HDT@AuNPs. Resistance at room temperature was significantly lower for films of BT@AuNPs compared to those of HDT@AuNPs. The greater T_{SE} for the longer chain length HDT@AuNPs compared to BT@AuNPs is consistent with previous reports (230°C and 180°C respectively).[31]

TGA-MS data (see Figure 2.10, Section 2.5, Supplementary Information) were collected for BT@AuNPs at temperatures between 40°C and 1300°C. Upon heating BT@AuNPs under He or air atmospheres, no species were detected prior to the main mass loss event. A mass loss of ~10 % was observed and occurred at the T_{SE}, which is consistent with previous reports.[35] In He or air atmospheres, the mass spectrometry data revealed a single peak in the extracted ion chromatogram. Analysis of the chromatogram showed mass spectra that corresponded to only dibutyl disulfide. No other products were detected. Products formed from heating HDT@AuNPs were not detected due to their low volatility and thus precluded analysis.

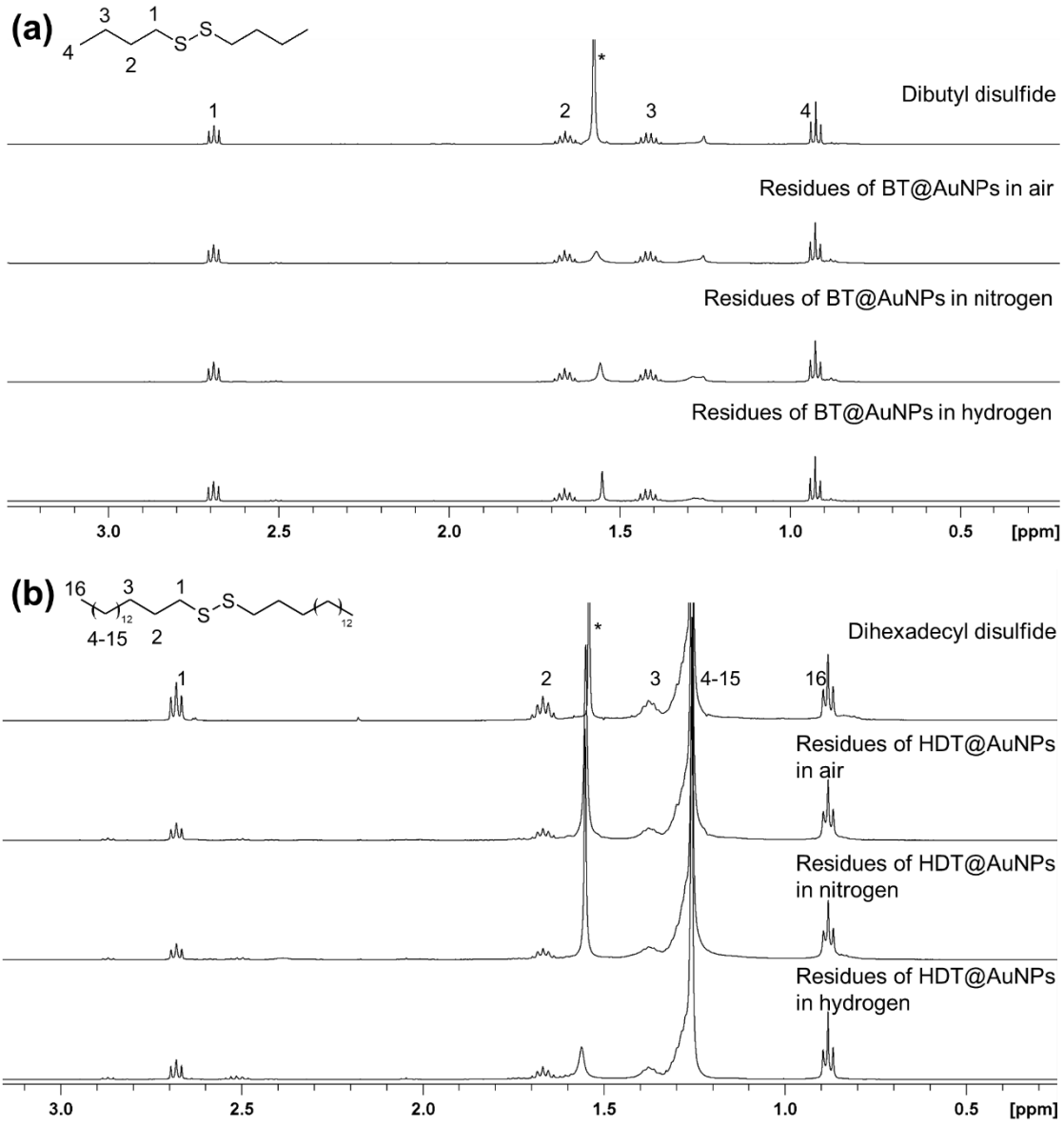

Figure 2.4 ^{1}H NMR spectra of sintering residue of (a) BT@AuNP in hydrogen and nitrogen and (b) HDT@AuNP in hydrogen and nitrogen (* denotes H_2O at 1.58 ppm).

The nature of the compound(s) released from the surface before and during the sintering event is crucial to the understanding of the processes involved with sintering of thiol-stabilised AuNPs. To obtain this data, ^{1}H NMR spectra were collected of the residues of AuNPs heated at 10°C min^{-1} beyond the T_{SE} in airtight reaction vessels (Figure 2.4). After cooling to room temperature, solvent ($CDCl_3$) was added to the reaction vessels, filtered to remove the sintered gold, and ^{1}H NMR spectra recorded immediately. Figure 2.4a shows the ^{1}H NMR spectrum of BT@AuNP residue post-sintering. Comparison with an authentic sample of dibutyl disulfide reveals that the major reaction product is dibutyl disulfide. HDT@AuNPs exhibited the same behavior (Figure 2.4b). This is in agreement

with previous reports that describe the mechanism of the removal of thiol-based ligands from SAMS by oxidation of the surface-bound thiyls to the corresponding disulfide compounds.[29] The ^{1}H NMR spectra of other possible sulfur-containing compounds 1-butanethiol and di-n-butylsulfide differ from those shown in Figure 2.4 as (in $CDCl_3$) the signals of the protons bonded to α-carbon atoms have chemical shifts at ~2.5 ppm[48] while peaks at for the dialkyl disulfide compounds are observed at ~2.7 ppm (Figure 2.11, Section 2.5, Supplementary Information).

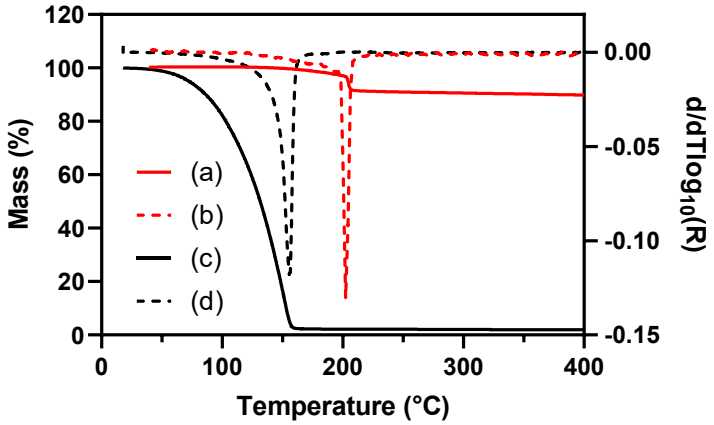

Figure 2.5 Thermogravimetric analysis data of (a) BT@AuNPs, (b) BT@AuNPs d/dT $\log_{10}(R)$, (c) dibutyl disulfide, (d) dibutyl disulfide d/dT $\log_{10}(R)$.

Comparison of TGA data for the AuNPs with data for dibutyl disulfides (Figure 2.5) and dihexadecyl disulfide (Figure 2.6) is informative. Thermogravimetry with a heating rate of 10°C min^{-1} from room temperature to 450°C, shows mass losses of 8 % and 33 % for BT@AuNPs (Figure 2.5) and HDT@AuNPs (Figure 2.6), respectively, which is in agreement with previously reported literature.[10] Interestingly, total mass loss of neat dibutyl disulfide occurs at a temperature ~50°C lower than the temperature of mass loss from BT@AuNPs.

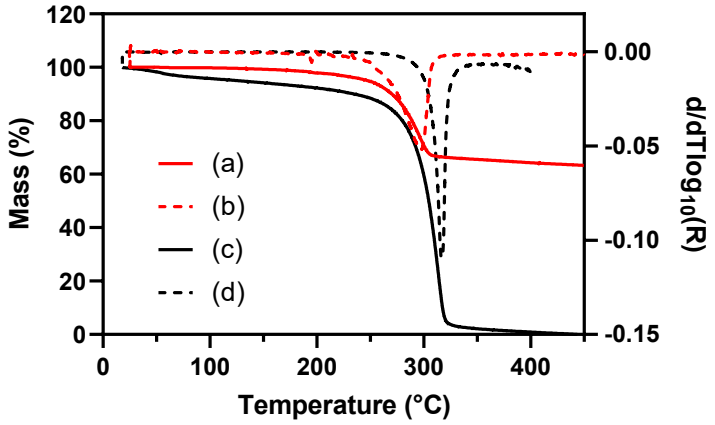

Figure 2.6 Thermogravimetric analysis data of (a) HDT@AuNPs, (b) HDT@AuNPs d/dT $\log_{10}(R)$, (c) dihexadecyl disulfide, (d) dihexadecyl disulfide d/dT $\log_{10}(R)$.

In contrast, mass loss for neat dihexadecyl disulfide (max. rate of mass loss ~305°C) occurs at similar temperatures to that of HDT@AuNPs (max. rate of mass loss ~298°C) (Figure 2.6). That is, for BT@AuNPs, the ligands remain in the vicinity of the AuNPs at temperatures beyond those where neat dibutyl disulfide vaporises. On the other hand, dihexadecyl disulfide vaporises at a temperature more than 100°C greater than that of dibutyl disulfide (significantly greater van der Waals interactions due to longer chain lengths) and so for the HDT@AuNPs, the long-chain intermolecular interactions between the ligands have a more dominant effect on T_{SE}. In general, it is apparent that the volatility of the disulfide has a significant effect on the temperatures at which ligands are removed from the particle environment.

The thermal behaviour of the AuNPs was also examined using DSC (Figure 2.12, Section 2.5, Supplementary Information). Samples were placed in DSC pans where the hermetic seals were either intact (closed pan) or punctured (open pan). Figure 2.12 (Section 2.5, Supplementary Information) shows a difference of ~20°C in the temperatures of maximum heat flow (associated with the sintering event) for BT@AuNP in open pan (200°C) and closed pan (220°C) experiments. For HDT@AuNPs, the open and closed pan experiments showed no difference in the temperature of maximum heat flow with sharp peaks at 233°C for both.

The DSC results suggest that when BT@AuNPs are heated in an environment where the disulfide product can readily escape, the equilibrium (as depicted in Figure 2.2) is shifted to the right environment, and the disulfide is prevented from escaping. In contrast, the different pan environments have minimal effect on HDT@AuNPs sintering event, as

the dihexadecyl disulfide has relatively low volatility, as shown in Figure 2.12 (Section 2.5, Supplementary Information), and thus the amount that remains in the vicinity of the NPs is unaltered.

AuNPs were sintered under different gaseous atmospheres and electrical resistance data were used to determine the T_{SE} (Table 2.1). These data are consistent with the TGA data. The Kruskal-Wallis (non-parametric) method was used to compare T_{SE} data obtained under different gaseous environments (Tables 2.2 and 2.3, Section 2.5, Supplementary Information). No significant differences ($p>0.05$) in T_{SE} were observed for the different gaseous environments for BT@AuNPs or HDT@AuNPs, respectively. That is, oxygen-containing, hydrogen, or inert atmospheres exert no influence on the sintering event or the temperature-induced ligand reaction.

Coupled with the TGA data (Figure 2.6), it is apparent that, at the T_{SE} for HDT@AuNPs, significant amounts of dihexadecyl disulfide remain in the vicinity of the sintered gold up until ~320°C. In the case of BT@AuNPs, removal of dibutyl disulfide at the T_{SE} was rapid as this species volatilises at temperatures less than the T_{SE} .

Table 2.1 Summary of T_{SE} (°C) of BT@AuNP and HDT@AuNP determined using electrical resistance measurements in different atmospheres the T_{SE}.

AuNPs	Air	Nitrogen	Argon	Hydrogen	Vacuum
BT@AuNPs	184 (±4)	190 (±1)	187 (±7)	192 (±12)	152 (±4)
HDT@AuNPs	215 (±9)	218 (±9)	218 (±18)	213 (±12)	206 (±4)

Visual observation of the HDT@AuNPs during sintering revealed that the gold becomes lustrous only above the temperature of complete volatilisation of the dihexadecyl disulfide, whilst BT@AuNPs formed lustrous films at the T_{SE}. Comparison of T_{SE} data for HDT@AuNPs sintered under gaseous atmospheres compared to in vacuo (~8 x 10^{-6} mbar) also showed no significant differences ($p>0.05$). In contrast, T_{SE} data for BT@AuNPs sintered *in vacuo* were significantly lower ($p<0.05$) compared to T_{SE} under the gaseous environments. BT@AuNPs sintered ~30°C lower under high vacuum compared to BT@AuNPs under the gaseous environmental conditions. We attribute this difference to the greater volatility of the dibutyl disulfide in vacuo compared to atmospheric pressure, which has the effect of moving the equilibrium (shown in Figure 2.2) to the right.

This effect was also observed in the open/closed DSC measurements. This effect is not evident in the T_{SE} data for the HDT@AuNPs because of the much lower volatility of the dihexadecyl disulfide (compared to dibutyl disulfide). These observations are consistent with those from open/closed pan DSC and TGA data.

We have also considered the possibility that the transport of detached species to the gas phase may be more efficient in the presence of gas flux than in vacuum. However, this effect would show the opposite trend to that observed. Processes involved with sintering of BT@AuNPs and HDT@AuNPs were investigated under different atmospheric conditions. The organic residue obtained upon sintering thiol-stabilised AuNPs was unambiguously identified as the dialkyl disulfide and was formed consistently regardless of the atmospheric conditions. Furthermore, the various gaseous atmospheres had no significant effect on T_{SE} for either the BT@AuNPs or HDT@AuNPs.

Conclusions

TGA data showed that neat dibutyl disulfide evaporated well before the T_{SE} of BT@AuNP, however TGA-MS of BT@AuNP. showed no loss of dibutyl disulfide before T_{SE}. If the Au-S interaction was the dominant factor that influenced the T_{SE}, then applying high vacuum should result in no change the T_{SE}. We showed that this is not the case and that sintering under high vacuum conditions resulted in significantly lower T_{SE}. This can be explained by considering an equilibrium between dibutyl disulfide (the only detected volatile species) and the bound thiyl. Increasing the rate of removal of disulfide (by increasing its volatility under high vacuum) shifts the equilibrium to the right and thus lowers T_{SE}. In contrast, neat dihexadecyl disulfide and HDT@AuNPs exhibited similar mass loss behavior when analysed using TGA. Furthermore, under high vacuum, the T_{SE} of HDT@AuNP was not notably different to that of particles under ambient pressure. These results are a consequence of the much lower volatility of the dihexadecyl disulfide (compared to dibutyl disulfide). These findings, along with the observations made by DSC, indicate that the T_{SE} of AuNPs stabilised using alkanethiols is controlled primarily by the volatility of the resultant disulfide species.

Acknowledgements

This research is supported by an Australian Government Research Training Program Scholarship. We acknowledge the Advanced Materials Characterisation Facility of Western Sydney University for access to its instrumentation and staff. In particular, we

thank Dr Laurel George and Dr Daniel Fanna. We acknowledge Professor James Brown, University of Technology Sydney, for assistance with statistical analysis and Mr Greg Delsanto, University of Technology Sydney science workshop, for access to equipment. Dr Angus Gentle is acknowledged for assistance with LabView software.

2.5 Supplementary Information

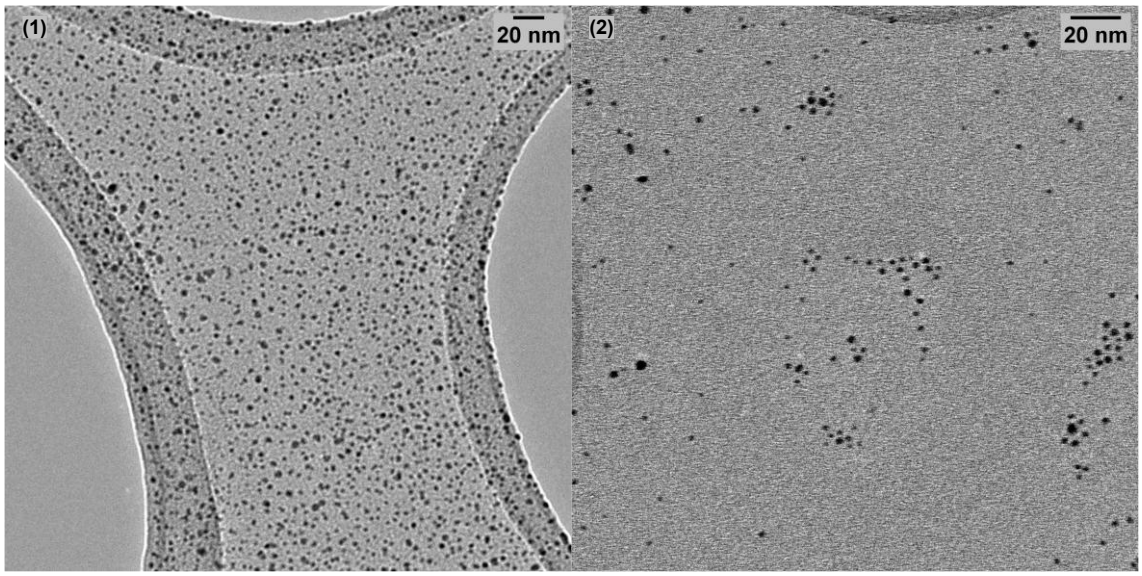

Figure 2.7 TEM images of (1) BT@AuNP and (2) HDT@AuNP.

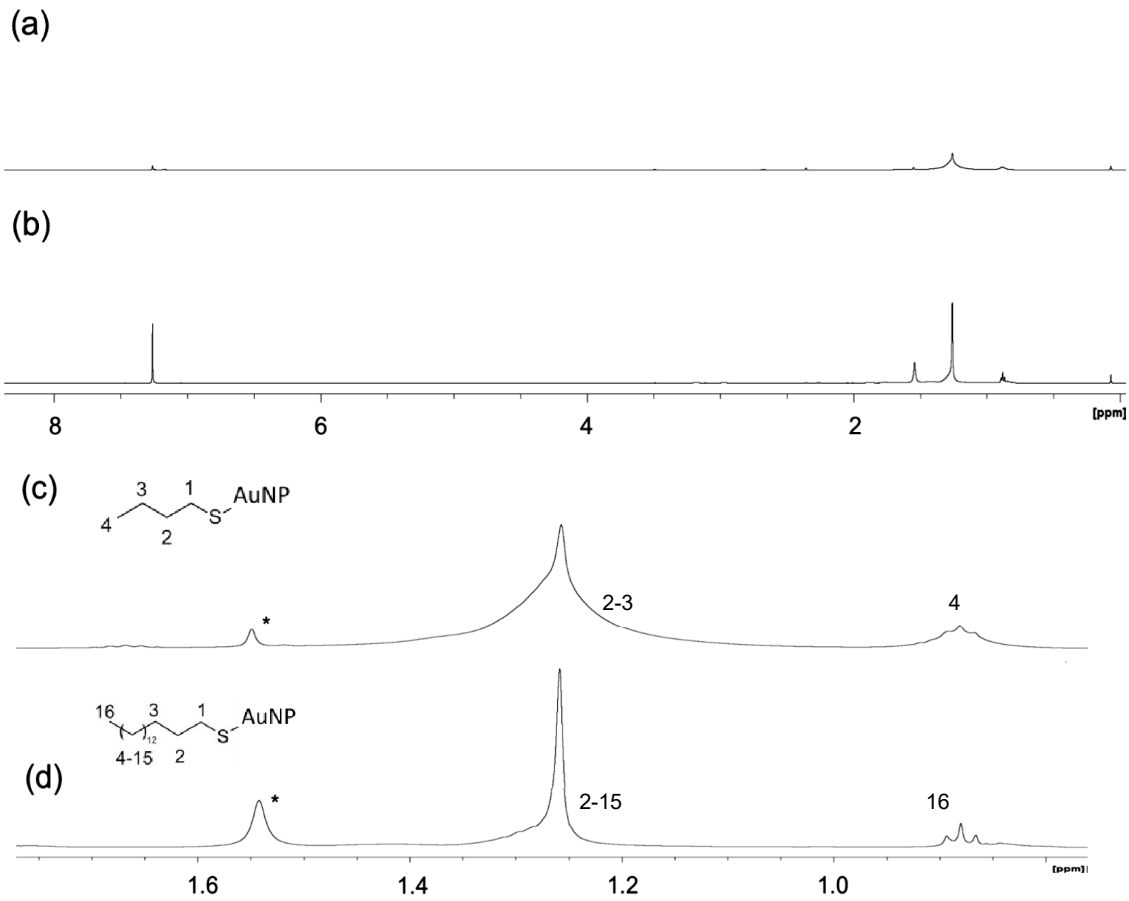

Figure 2.8 ^{1}H NMR spectra of (a)/(c) BT@AuNP and (b)/(d) HDT@AuNP in $CDCl_3$. * indicates water (1.58 ppm).

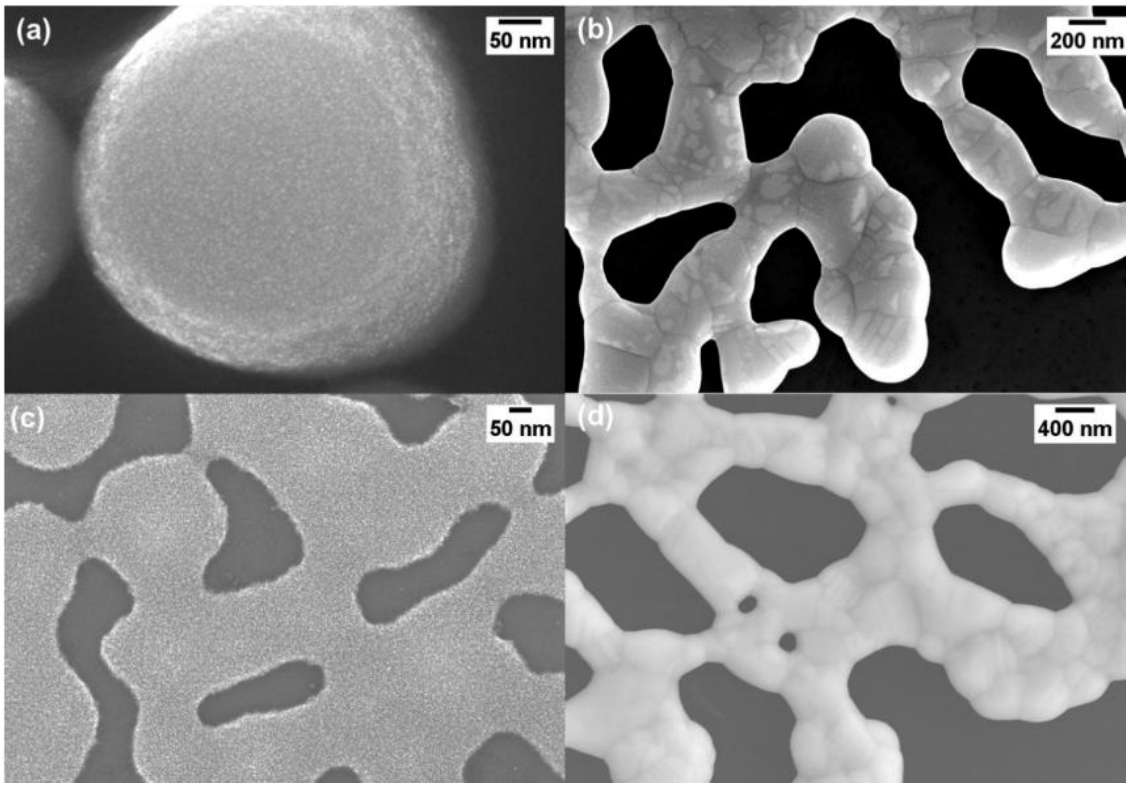

Figure 2.9 SEM images of (a) BT@AuNPs and (c) HDT@AuNPs deposited using chloroform before heating and (b/d) after heating 10°C min^{-1} in air to 350°C.

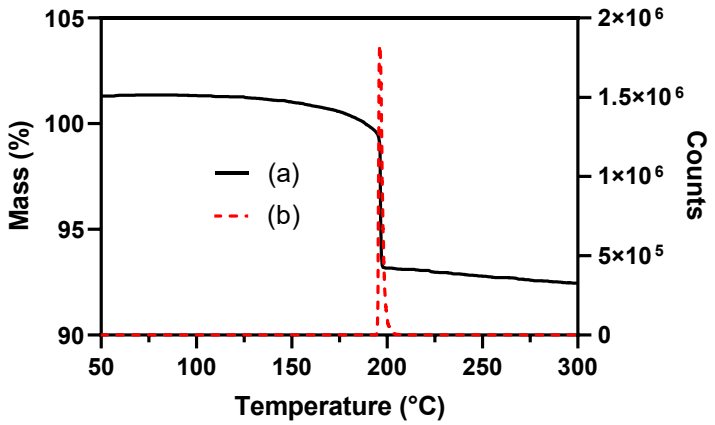

Figure 2.10 TGA-MS data for BT@AuNPs (a) mass loss and (b) counts under a helium atmosphere.

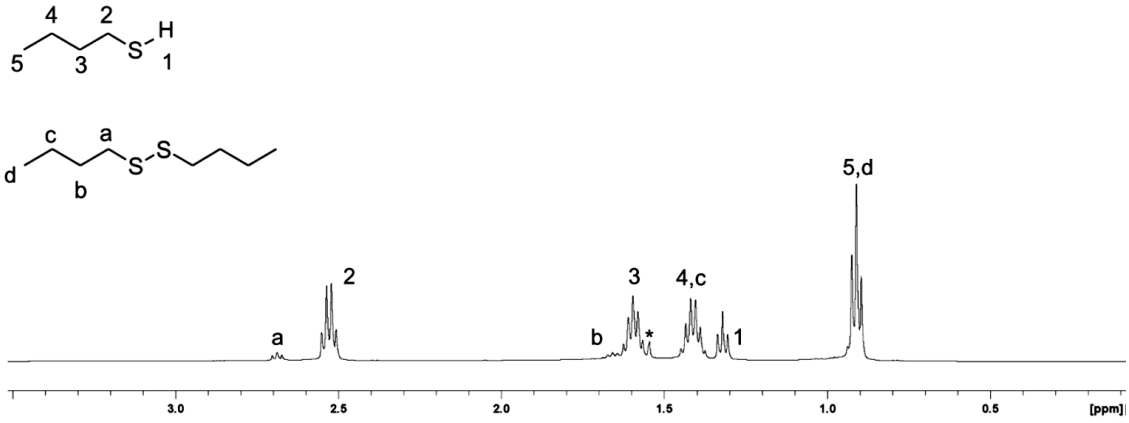

Figure 2.11 ^{1}H NMR spectra of 1-butanethiol spiked with dibutyl disulfide.

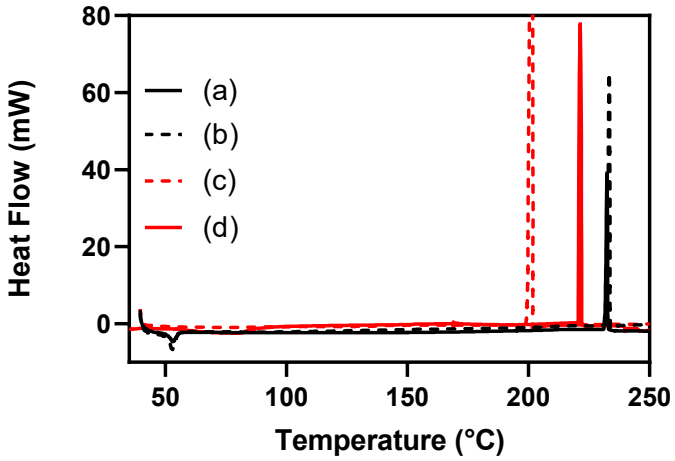

Figure 2.12 Heat flow peaks (exothermic) under open and closed environments for HDT@AuNP(a/b) and BT@AuNP(c/d) respectively.

Table 2.2.HDT@AuNPs Kruskal-Wallis test comparing gases argon, hydrogen and air (gases) and gases with high vacuum (atmospheres) T_{SE}.

	X^2	df	p
Gases	0.651	3	0.885
Atmospheres	2.34	1	0.126

Table 2.3 BT@AuNPs Kruskal-Wallis test comparing gases argon, hydrogen and air (gases), and between gases with high vacuum (atmospheres) T_{SE}.

	X^2	df	p
Gases	3.14	3	0.371
Atmospheres	10	1	0.002

References

1. D'Acunto, M., Cioni, P., Gabellieri, E., Presciuttini, G., Exploiting gold nanoparticles for diagnosis and cancer treatments. *Nanotechnology.* 2021, *32*, 192001.
2. Saha, K., Agasti, S. S., Kim, C., Li, X., Rotello, V. M., Gold Nanoparticles in Chemical and Biological Sensing. *Chemical Reviews.* 2012, *112*, 2739-2779.
3. Bishop, P. T., Ashfield, L. J., Berzins, A., Boardman, A., Buche, V., Cookson, J., Gordon, R. J., Salcianu, C., Sutton, P. A., Printed gold for electronic applications. *Gold Bulletin.* 2010, *43*, 181-188.
4. Wu, Y., Li, Y., Liu, P., Gardner, S., Ong, B. S., Studies of Gold Nanoparticles as Precursors to Printed Conductive Features for Thin-Film Transistors. *Chemistry of Materials.* 2006, *18*, 4627-4632.
5. Korotcenkov, G., Brinzari, V., Cho, B. K., Conductometric gas sensors based on metal oxides modified with gold nanoparticles: a review. *Microchimica Acta.* 2016, *183*, 1033-1054.
6. Peng, X., Wan, G., Wu, L., Zeng, M., Lin, S., Wang, G., Peroxidase-like activity of Au@TiO2 yolk-shell nanostructure and its application for colorimetric detection of H2O2 and glucose. *Sensors and Actuators B: Chemical.* 2018, *257*, 166-177.
7. Buonerba, A., Grassi, A., Trends in Sustainable Synthesis of Organics by Gold Nanoparticles Embedded in Polymer Matrices. *Catalysts.* 2021, *11*, 714.
8. Jin, R., Zeng, C., Zhou, M., Chen, Y., Atomically Precise Colloidal Metal Nanoclusters and Nanoparticles: Fundamentals and Opportunities. *Chemical Reviews.* 2016, *116* (18), 10346-10413.
9. Huang, D., Liao, F., Molesa, S., Redinger, D., Subramanian, V., Plastic-Compatible Low Resistance Printable Gold Nanoparticle Conductors for Flexible Electronics. *Journal of The Electrochemical Society.* 2003, *150*, G412-G417.
10. Falahati, M., Attar, F., Sharifi, M., Saboury, A. A., Salihi, A., Aziz, F. M., Kostova, I., Burda, C., Priecel, P., Lopez-Sanchez, J. A., Laurent, S., Hooshmand, N., El-Sayed, M. A., Gold nanomaterials as key suppliers in biological and chemical sensing, catalysis, and medicine. *Biochimica et Biophysica Acta - General Subjects.* 2019, 129435.
11. Alemán, J. V., Chadwick, A. V., He, J., Hess, M., Horie, K., Jones, R. G., Kratochvíl, P., Meisel, I., Mita, I., Moad, G., Penczek, S., Stepto, R. F. T., Definitions of terms relating to the structure and processing of sols, gels, networks, and inorganic-organic hybrid materials (IUPAC Recommendations 2007). *Pure and Applied Chemistry.* 2007, *79* (10), 1801-1829.
12. Arcidiacono, S., Bieri, N. R., Poulikakos, D., Grigoropoulos, C. P., On the coalescence of gold nanoparticles. *International Journal of Multiphase Flow.* 2004, *30* (7), 979-994.
13. José-Yacamán, M., Gutierrez-Wing, C., Miki, M., Yang, D. Q., Piyakis, K. N., Sacher, E., Surface Diffusion and Coalescence of Mobile Metal Nanoparticles. *The Journal of Physical Chemistry B.* 2005, *109* (19), 9703-9711.
14. Chen, Y., Palmer, R. E., Wilcoxon, J. P., Sintering of Passivated Gold Nanoparticles under the Electron Beam. *Langmuir.* 2006, *22* (6), 2851-2855.
15. Ruffino, F., Torrisi, V., Grimaldi, M. G., Experimental study on the coalescence process of SiO2 supported colloidal Au nanoparticles. *Physica E: Low-dimensional Systems and Nanostructures.* 2015, *74*, 388-399.
16. Lehtinen, K., Zachariah, M., Energy Accumulation in Nanoparticle Collision and Coalescence Processes. *Journal of Aerosol Science.* 2002, *33*, 357-368.
17. Zhu, C., Liang, S., Song, E., Zhou, Y., Wang, W., Shan, F., Shi, Y., Hao, C., Yin, K., Zhang, T., Liu, J., Zheng, H., Sun, L., In-situ liquid cell transmission electron microscopy

investigation on oriented attachment of gold nanoparticles. *Nature Communications.* 2018, *9* (1), 421.
18. van Huis, M. A., Kunneman, L. T., Overgaag, K., Xu, Q., Pandraud, G., Zandbergen, H. W., Vanmaekelbergh, D., Low-Temperature Nanocrystal Unification through Rotations and Relaxations Probed by in Situ Transmission Electron Microscopy. *Nano Letters.* 2008, *8* (11), 3959-3963.
19. Liao, H.-G., Cui, L., Whitelam, S., Zheng, H., Real-Time Imaging of Pt3Fe Nanorod Growth in Solution. *Science.* 2012, *336* (6084), 1011-1014.
20. Guo, P., Gao, Y., Coalescence of Au Nanoparticles without Ligand Detachment. *Physical Review Letters.* 2020, *124* (6), 066101.
21. Yao, Q., Yuan, X., Fung, V., Yu, Y., Leong, D. T., Jiang, D.-e., Xie, J., Understanding seed-mediated growth of gold nanoclusters at molecular level. *Nature Communications.* 2017, *8* (1), 927.
22. Kundu, S., Das, K., Konovalov, O., Prolonged reorganization of thiol-capped Au nanoparticles layered structures. *American Institute of Physics Advances.* 2013, *3* (9), 092130.
23. Ristau, R., Tiruvalam, R., Clasen, P. L., Gorskowski, E. P., Harmer, M. P., Kiely, C. J., Hussain, I., Brust, M., Electron microscopy studies of the thermal stability of gold nanoparticle arrays. *Gold Bulletin.* 2009, *42* (2), 133-143.
24. Hayashi, T., Wakamatsu, K., Ito, E., Hara, M., Effect of steric hindrance on desorption processes of alkanethiols on Au(111). *Journal of Physical Chemistry C.* 2009, *113*, 18795-18799.
25. Yan, B., Zhu, Z. J., Miranda, O. R., Chompoosor, A., Rotello, V. M., Vachet, R. W., Laser desorption/ionization mass spectrometry analysis of monolayer-protected gold nanoparticles. *Analytical and Bioanalytical Chemistry.* 2010, *396*, 1025-1035.
26. Casanova-Moreno, J. R., Bizzotto, D., What happens to the thiolates created by reductively desorbing SAMs? An in situ study using fluorescence microscopy and electrochemistry. *Langmuir.* 2013, *29*, 2065-2074.
27. Mulder, W. H., Calvente, J. J., Andreu, R., A kinetic model for the reductive desorption of self-assembled thiol monolayers. *Langmuir.* 2001, *17*, 3273-3280.
28. Aagaard, N. D., Azcárate, J. C., Olmos-Asar, J., Mariscal, M. M., Solla-Gullón, J., Zelaya, E., Fonticelli, M. H., Mechanistic Framework for the Formation of Different Sulfur Species by Electron Irradiation of n -Dodecanethiol Self-Assembled Monolayers on Au(111) and Au(100). *The Journal of Physical Chemistry C.* 2020, *124*, 22591-22600.
29. Cristina, L. J., Ruano, G., Salvarezza, R., Ferrón, J., Thermal Stability of Self-Assembled Monolayers of n-Hexanethiol on Au(111)-(1 × 1) and Au(001)-(1 × 1). *Journal of Physical Chemistry C.* 2017, *121*, 27894-27904.
30. Ito, E., Kang, H., Lee, D., Park, J. B., Hara, M., Noh, J., Spontaneous desorption and phase transitions of self-assembled alkanethiol and alicyclic thiol monolayers chemisorbed on Au(111) in ultrahigh vacuum at room temperature. *Journal of Colloid and Interface Science.* 2013, *394*, 522-529.
31. King, S. R., Shimmon, S., Totonjian, D. D., McDonagh, A. M., Influence of Bound versus Non-Bound Stabilizing Molecules on the Thermal Stability of Gold Nanoparticles. *Journal of Physical Chemistry C.* 2017, *121*, 13944-13951.
32. Reimers, J. R., Ford, M. J., Halder, A., Ulstrup, J., Hush, N. S., Gold surfaces and nanoparticles are protected by Au(0)-thiyl species and are destroyed when Au(I)-thiolates form. *Proceedings of the National Academy of Sciences of the United States of America.* 2016, *113*, E1424-E1433.

33. Ito, E., Noh, J., Hara, M., Steric effects on adsorption and desorption behaviors of alkanethiol self-assembled monolayers on Au(111). *Chemical Physics Letters.* 2008, *462*, 209-212.
34. Shivhare, A., Chevrier, D. M., Purves, R. W., Scott, R. W. J., Following the thermal activation of Au25(SR)18 clusters for catalysis by X-ray absorption spectroscopy. *Journal of Physical Chemistry C.* 2013, *117*, 20007-20016.
35. Smith, B. L., Hutchison, J. E., Transformations during sintering of small (D core < 2 nm) ligand-stabilized gold nanoparticles: Influence of ligand functionality and core size. *Journal of Physical Chemistry C.* 2013, *117*, 25127-25137.
36. Tlahuice-Flores, A., Santiago, U., Bahena, D., Vinogradova, E., Conroy, C. V., Ahuja, T., Bach, S. B. H., Ponce, A., Wang, G., José-Yacamán, M., Whetten, R. L., Structure of the Thiolated Au130 Cluster. *The Journal of Physical Chemistry A.* 2013, *117* (40), 10470-10476.
37. Martin, J. E., Odinek, J., Wilcoxon, J. P., Anderson, R. A., Provencio, P., Sintering of alkanethiol-capped gold and platinum nanoclusters. *Journal of Physical Chemistry B.* 2003, *107*, 430-434.
38. Gupta, A., Mandal, S., Katiyar, M., Mohapatra, Y. N., Film processing characteristics of nano gold suitable for conductive application on flexible substrates. *Thin Solid Films.* 2012, *520*, 5664-5670.
39. King, S.-R., Massicot, J., McDonagh, A., A Straightforward Route to Tetrachloroauric Acid from Gold Metal and Molecular Chlorine for Nanoparticle Synthesis. *Metals.* 2015, *5*, 1454-1461.
40. Brust, M., Walker, M., Bethell, D., Schiffrin, D. J., Whyman, R., Synthesis of thiol-derivatised gold nanoparticles in a two-phase Liquid–Liquid system. *Journal of the Chemical Society, Chemical Communications.* 1994, (7), 801-802.
41. Noureldin, N. A., Caldwell, M., Hendry, J., Lee, D. G., Heterogeneous Permanganate Oxidation of Thiols. *Synthesis.* 1998, *11* (11), 1587-1589.
42. Terrill, R. H., Postlethwaite, T. A., Chen, C.-h., Poon, C.-D., Terzis, A., Chen, A., Hutchison, J. E., Clark, M. R., Wignall, G., Monolayers in Three Dimensions: NMR, SAXS, Thermal, and Electron Hopping Studies of Alkanethiol Stabilized Gold Clusters. *Journal of the American Chemical Society.* 1995, *117* (50), 12537-12548.
43. Hostetler, M. J., Wingate, J. E., Zhong, C.-J., Harris, J. E., Vachet, R. W., Clark, M. R., Londono, J. D., Green, S. J., Stokes, J. J., Wignall, G. D., Glish, G. L., Porter, M. D., Evans, N. D., Murray, R. W., Alkanethiolate Gold Cluster Molecules with Core Diameters from 1.5 to 5.2 nm: Core and Monolayer Properties as a Function of Core Size. *Langmuir.* 1998, *14* (1), 17-30.
44. Badia, A., Gao, W., Singh, S., Demers, L., Cuccia, L., Reven, L., Structure and Chain Dynamics of Alkanethiol-Capped Gold Colloids. *Langmuir.* 1996, *12* (5), 1262-1269.
45. Wu, Z., Gayathri, C., Gil, R. R., Jin, R., Probing the Structure and Charge State of Glutathione-Capped Au25(SG)18 Clusters by NMR and Mass Spectrometry. *Journal of the American Chemical Society.* 2009, *131* (18), 6535-6542.
46. Qian, H., Zhu, M., Gayathri, C., Gil, R. R., Jin, R., Chirality in Gold Nanoclusters Probed by NMR Spectroscopy. *ACS Nano.* 2011, *5* (11), 8935-8942.
47. Coutts, M. J., Cortie, M. B., Ford, M. J., McDonagh, A. M., Rapid and Controllable Sintering of Gold Nanoparticle Inks at Room Temperature Using a Chemical Agent. *The Journal of Physical Chemistry C.* 2009, *113*, 1325-1328.
48. Wang, M.-L., Tseng, Y.-H., Synthesis of thioether using dimethyloctyl(3-sulfopropyl)ammonium betaine and di-active site quaternary ammonium salt as new phase-transfer catalysts. *Reaction Kinetics and Catalysis Letters.* 2004, *82* (1), 81-87.

Chapter 3

Nano to Macro Transition of Gold Nanoparticles Prior to Sintering

3.1 Preamble

Upon heating, thiyl ligands leave the vicinity of the AuNP surface as the corresponding disulfide (as discussed in Chapter 2), and the leaving disulfides are an influence on the T_{SE} for AuNPs. Currently, there are few studies that investigate the electrical behaviour, size and morphology of thiol-stabilised AuNPs at temperatures prior to the T_{SE}. Exploring these properties provides some fundamental understanding of thiol-stabilised AuNPs in this temperature regime. This chapter investigates the stability of butanethiol- and hexadecanethiol-stabilised AuNPs at temperatures prior to sintering.

3.2 Certificate of Authorship

A manuscript entitled "Nano to Macro Transition of Gold nanoparticles Prior to Sintering" was published in *Journal of Material Science, Materials in Electronics.* The following chapter is based on the published work.

I, Paige Summers, certify that the work in Chapter 3 has not been submitted as part of any other documents required for a degree.

3.3 Authorship Contributions

Author	Contribution	Signature
Paige K Summers	Conceptualisation, experimental design, performed experiments, analysed data, original manuscript writing, manuscript editing	Production Note: Signature removed prior to publication.
Alexander Angeloski	Technical assistance, conceptualisation, performed experiments, analysed data, manuscript writing, manuscript editing	Production Note: Signature removed prior to publication.
Michael B. Cortie	Conceptualisation, manuscript editing, performed experiments	Production Note: Signature removed prior to publication.
Richard Wuhrer	Technical assistance, manuscript editing	Production Note: Signature removed prior to publication.
Andrew M. McDonagh	Conceptualisation, manuscript editing, manuscript writing	Production Note: Signature removed prior to publication.

3.4 Nano to Macro Transition of Gold Nanoparticles Prior to Sintering

Abstract

The thermal behaviour of ligand-stabilised AuNPs is an important consideration when using these materials to form gold films via sintering. AuNPs stabilised with butanethiol and hexadecanethiol ligands displayed quite different properties upon heating up to their sintering temperatures. Films of AuNPs bearing the longer chain stabilising ligand hexadecanethiol form become liquid at 56°C. This temperature corresponds to the melting point of dihexadecyl disulfide, a known product that forms when such AuNPs are heated. No liquid phase was observed for BT@AuNPs at any temperature. Films of the HDT@AuNPs had quite high resistances (>100 MΩ) at room temperature and the short-chain BT@AuNPs had resistances in the kΩ range. Small-angle X-ray scattering (SAXS) data showed that the butanethiol-stabilised AuNPs begin to coarsen at ~140°C while the hexadecaenthiol particles began to coarsen ~90°C

Introduction

The sintering of AuNPs is a convenient technique for the formation of electrically conductive gold films and additively manufactured gold-based materials and devices.[1-3] Sintering involves the coalescence of particles at temperatures below their melting point, which in the case of bulk gold is 1064°C.[4] The AuNPs can be formulated as printable inks that can be printed using either contact or non-contact printing techniques, and then sintering at moderate temperatures (usually around 200°C) to form the desired gold structures.[1, 5, 6] Prior to sintering, the AuNPs must be stabilised to prevent unwanted aggregation or coalescence, which would otherwise render printable inks unusable. A number of stabilisers have been investigated including ionic compounds (e.g. citrate),[7, 8] polymers,[9] and of particular relevance to this work, thiol compounds.[10]

Thiol-protected AuNPs have shown to be accessible, reproducible, stable and have a large range of tuneable sintering temperatures.[11-17] The interaction of the sulfur atoms with the gold surface may be described as a thiyl-gold species (where thiyl is the ·SR radical species), which exists in equilibrium with the corresponding disulfide compound (RS-SR).[18] Upon sintering, the stabilising ligands are released as the disulfide species, with the volatility of the disulfide influencing the T_{SE}.[15] However, the properties of such

thiol-stabilised AuNPs have been less studied in the temperature range immediately prior to and during the sintering transition.[19] For amine-stabilised AuNPs, coarsening behaviour prior to sintering has been reported at temperatures approaching the T_{SE}, (by observation of optical properties and SEM).[20] Here we examine the behaviour of thiol-stabilised AuNPs (using a short- and long-chain stabilising alkanethiol) in the temperature regime from room temperature to sintering. The electronic conductivity of films of alkanethiol-stabilised AuNPs offers insights into their structures. Between individual NPs, the conductivity has been shown to occur due to electron tunnelling between the gold cores *via* the alkanethiolate chains.[21] Previously, the electrical conductivity for films of gold nanoparticles was observed to increase irreversibly upon heating to temperatures below those of T_{SE} and the activation energies were found to change dramatically following a single heating cycle.[22]

We build upon our previous investigations that demonstrated the effect of the volatility of dialkyl disulfide compounds that form during heating on the sintering behaviour of thiol-stabilised AuNPs.[12, 15, 23] Here, we use electrical resistance measurements, SAXS and SEM to examine thiol-stabilised AuNPs at temperatures from room temperature up to their T_{SE} to better understand the processes that lead from the nanoscale to macroscale gold films.

Experimental

1-Butanethiol, 1-hexadecanethiol, tetraoctylammonium bromide (TOAB), sodium borohydride, and methanol were purchased from Sigma-Aldrich and used as received. Toluene (ChemSupply Australia) and chloroform (Rowe Scientific) were used as received. Tetrachloroauric acid,[24] BT@AuNPs, and HDT@AuNPs were prepared using literature procedures.[25] The AuNPs were characterised by SEM, TEM, and ultraviolet-visible (UV-vis) absorption spectroscopy.

Resistance measurements; BT@AuNPs suspensions in chloroform (10 mg/ml) were drop cast onto DropSens (Metrohm) interdigitated gold electrodes forming films of AuNPs, which were then heated within a modified Linkam THMS600 temperature control stage as described previously.[15] A heating rate of 10°C min^{-1} from room temperature to 250°C was used. A Rigol DM3068 digital multimeter with a maximum resistance measurement capability of 100 MΩ was to measure electrode resistances. A LabView program was used to acquire the temperature and electrical resistance data.

SEM was performed at facilities at Western Sydney University, Australia. A Zeiss Merlin FEGSEM was utilised for imaging samples prepared on stubs. The FEGSEM was operated at 10kV accelerating voltage in Hivac mode at a working distance of approximately 3 mm. Both secondary and in-lens secondary detectors were utilised for imaging. TEM images were taken using a JEOL JEM-F200 FE-TEM operating at 200 kV and fitted with a Gatan Rio 1816 – 4k x 4k camera. The TEM samples were prepared by evaporating diluted nanoparticle solution on the carbon-coated copper grid. The images were analysed using ImageJ software (https://imagej.nih.gov/ij/).

UV-vis spectra were recorded on an Agilent Cary 60 spectrophotometer. Samples were prepared in a quartz cuvette by dispersing ~0.4 mg of AuNP sample in toluene (8 mL). Variable temperature SAXS measurements were performed at the Australian Synchrotron using the SAXS undulator source. Powders of AuNPs were placed in SiO_2 capillaries. The samples were exposed to 8 x 10^{12} photons per second at an X-ray energy of 11.5 keV, and scattered X-rays were detected using a Pilatus 1M detector with active area of 170 mm x 170 mm at a distance of 1400 mm. Detector images were acquired at a scan rate of 10 Hz and averaged to yield one frame for every ~1°C in temperature between 30 to 160 or 230°C. Detector images were corrected using ScatterBrain IDL and q *vs* T plots were prepared using Python3.

Results and Discussion

Synthesis

BT@AuNPs and HDT@AuNPs were synthesised using the two-phase Brust-Schriffrin method[25] and had diameters of 3.1 (± 0.9) nm and 3.5 (± 1.7) nm respectively (measured using TEM, Figure 3.6, Section 3.5, Supplementary Information). The UV-visible spectra of the nanoparticles (Figure 3.7, Section 3.5, Supplementary Information) contain shoulders at ~517 nm (BT@AuNPs) and ~512 nm (HDT@AuNPs), which is consistent with previous reports.[26, 27] Importantly, no unbound thiol was detected in the ^{1}H NMR spectra of the synthesised AuNPs.

Scanning electron microscopy

Representative SEM images of films of BT@AuNPs on silicon wafer are shown in Figure 3.1. Unheated films are comprised of AuNPs that are uniform in size (within the resolution of the instrument), Figure 3.1 (a) and (b). Images of films that have been heated to 100°C reveal AuNPs of similar size to the unheated particles. After heating to 150°C, coarsening of the AuNPs is apparent but no sintering occurs at this temperature. Figure 3.2 shows SEM images of HDT@AuNPs that have been heated to various temperature. Unheated films contain AuNPs in a uniform layer, and are similar in appearance to those of BT@AuNPs.

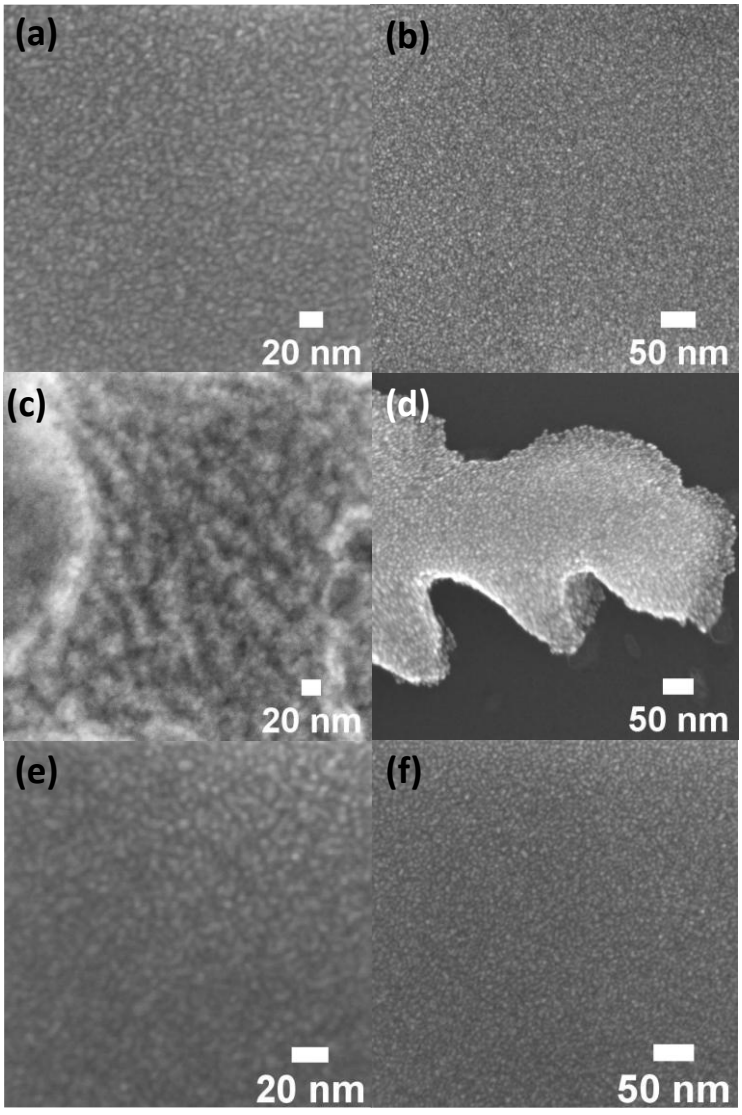

Figure 3.1 SEM images (obtained at 21°C) of BT@AuNPs after exposure to the following temperatures for 2 hours: (a) and (b), room temperature; (c) and (d), 100°C; (e) and (f), 150°C.

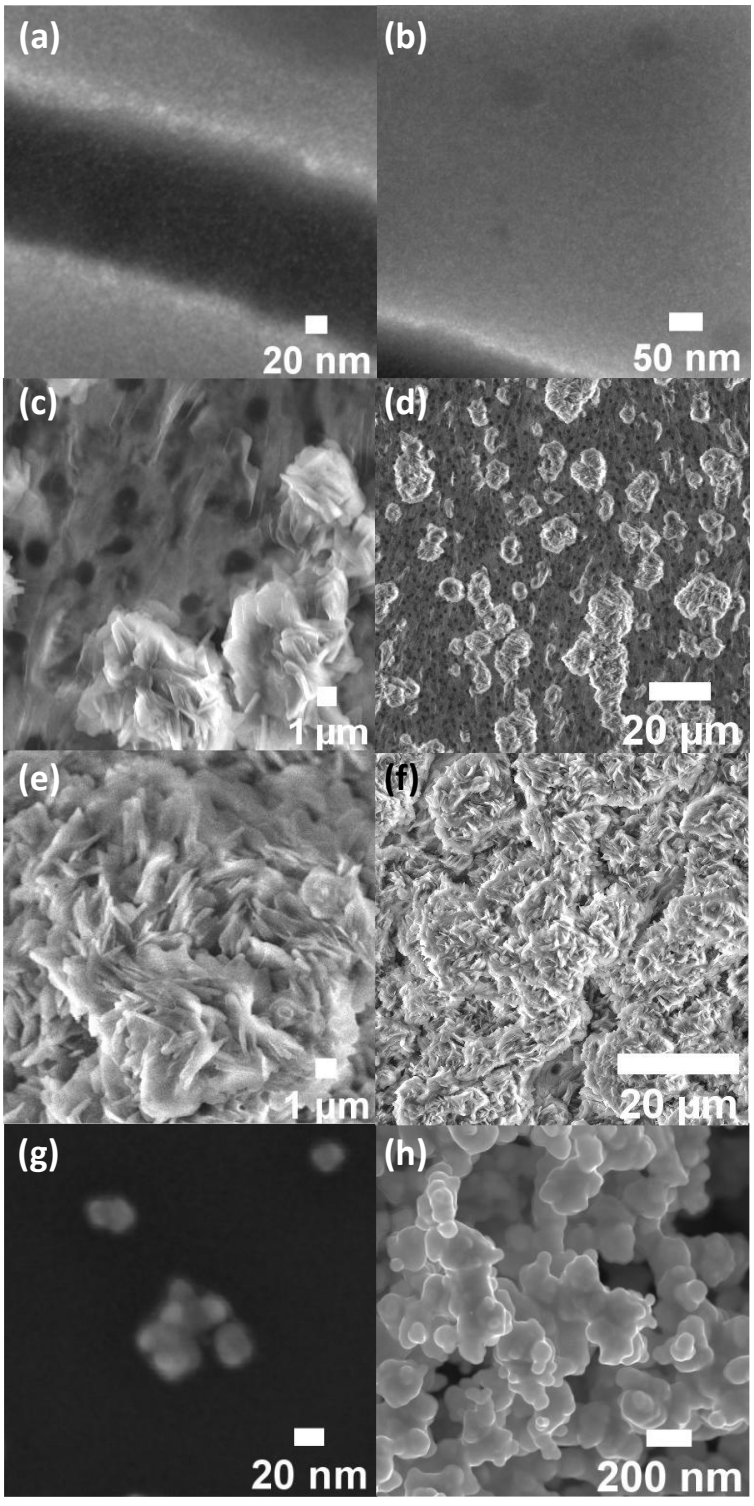

Figure 3.2 SEM images (obtained at 21°C) of HDT@AuNPs after exposure to the following temperatures for 2 hours: (a) and (b), room temperature; (c) and (d), 100°C; (e) and (f), 150°C;(g) and (h), 200°C.

In contrast, films of HDT@AuNPs heated to 100°C and 150°C contain deposits of a crystalline material that obscure the AuNPs. We attribute these deposits to increased formation of dihexadecyl disulfide upon heating,[15] which melts at ~56°C and

subsequently solidifies upon cooling to room temperature prior to imaging. Upon heating to 200°C, coalesced gold material is evident and the organic material observed in Figure 3.2 (c-f) is absent. Previous TGA[15] showed that dihexadecyl disulfide undergoes mass loss at 200°C, and so over the heating period of 2 hours, organic material is removed from the surface. In the case of BT@AuNPs, the formed dibutyl disulfide has significantly greater volatility,[15] and thus evaporates during heating as well as during SEM imaging (in the high vacuum environment) to leave no observable residue upon cooling to room temperature.

In general, the released dihexadecyl disulfide from HDT@AuNPs results in a layer of organic material on the AuNPs that increases with temperature until ~150°C, whereas the more volatile dibutyl disulfide from BT@AuNPs is removed rapidly from the vicinity of the gold surfaces. Thus, the BT@AuNPs could be imaged at each intermediate temperature, with no coarsening evident until temperatures >100°C. Importantly, during these experiments only a small proportion of the total ligand concentration has been removed. If otherwise, the AuNPs would have sintered.[15]

Resistance Measurements of Gold Nanoparticle Films

The electrical resistance of solid films of thiol-stabilised AuNPs is dependent on electron tunnelling between the gold cores *via* the alkanethiyl ligands.[21] The technique is therefore useful to probe changes in interparticle distances changes in the temperature range that precedes sintering, whereupon the resistance is similar to that of bulk gold after sintering. Small changes in core size (1.6 nm vs 2.2 nm diameters) have relatively minor effects on conductivity but increased thiol ligand carbon chain length correlates with decreased conductivity.[21] Dropcast BT@AuNP films had resistances in the range of 3-4 MΩ when maintained at 24°C, which were stable for at least 10 hours (see Figure 3.8, Section 3.5, Supplementary Information). In contrast, the resistances of dropcast HDT@AuNP films were outside the range of our instrumentation (>100 MΩ) at 24°C. The increased resistances of AuNPs bearing longer chain stabilising groups has been investigated by others[21, 28, 29] and is a consequence of electrons of the gold atoms having to tunnel over greater distances.

Upon increasing the temperature to 100°C, the resistance of BT@AuNPs decreased by several orders of magnitude (from 3-4 MΩ range to 40-50 kΩ) where it remained stable for at least 5 hours (Figure 3.9, Section 3.5, Supplementary Information). The HDT@AuNP films also exhibit a drop in resistance upon heating to 100°C with the

resistance changing from off-scale to ~80 MΩ (Figure 3.3). In contrast to the BT@AuNPs, we observed that the HDT@AuNP films become molten at ~56°C. This phenomenon has been investigated previously using differential scanning calorimetry.[30] Alkylthiolate-stabilised AuNPs with carbon chain lengths of 12 to 20 displayed phase transitions at temperatures similar to those observed here and with enthalpies that increased with increasing chain lengths.[29-31] A melting event was associated with the interdigitation of CH_2 units located ~10-12 units from the Au core.[31] In light of more recent findings,[15] we propose that the transition to liquid phase is a consequence of the melting of the corresponding dialkyl disulfide that has been released from the NP surface. We also note that a small increase in resistance (from ~70 to ~90 MΩ) over 6 hours was observed for the HDT@AuNPs and is attributed to the fluid film expanding and thinning across the electrode surface, which was observed visually to occur.

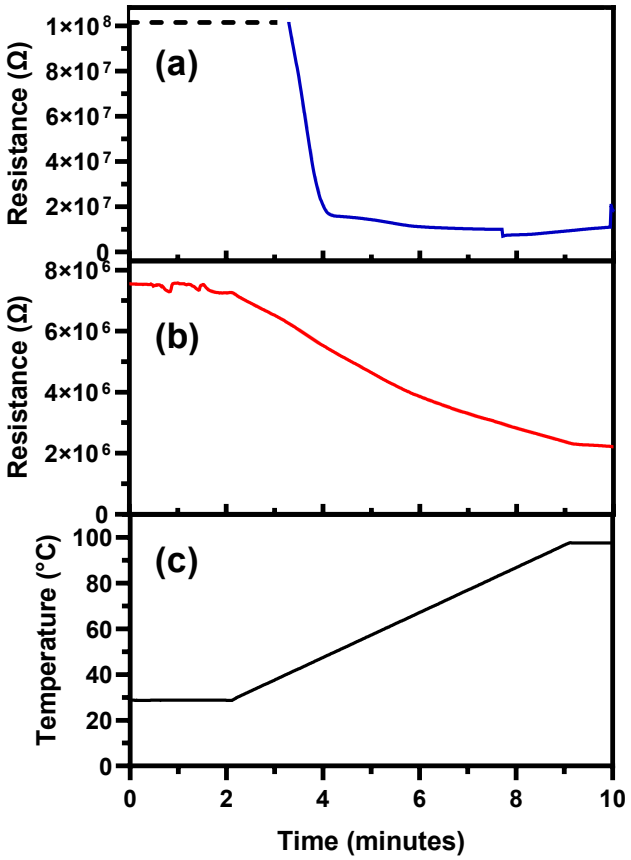

Figure 3.3 Graph showing the resistances of HDT@AuNP films (a) and BT@AuNP films (b) from room temperature to 100°C.

Upon cooling the films from 100°C to room temperature, the resistances of films of BT@AuNPs did not return to the original MΩ range but increased to ~20 kΩ (Figure 3.9, Section 3.5, Supplementary Information) and remained stable for several hours. Re-heating the AuNP films to 180°C induced sintering at a temperature similar to that of BT@AuNP films heated directly from room temperature (T_{SE} ~180°C). Our experiments indicate that changes to the AuNP film that occur upon heating to do not influence the eventual sintering process but nor do the films return to their original as-formed state, an idea proposed by others based on optical measurements.[22] This phenomenon may have electronic applications as many AuNPs films are hindered by very high resistances at room temperature.

The resistance of HDT@AuNP films also increased upon cooling from 100°C to room temperature to a value that was, again, out of range of our instruments (Figure 3.9, Section 3.5, Supplementary Information), and was associated with the solidification of the films at ~56°C. Re-heating to ~210°C induced sintering of the HDT@AuNPs at a similar temperature to that observed for films of HDT@AuNPs heated directly (T_{SE} ~220°C). The electrical resistance of films not returning to the original resistance and their changes with temperature have been reported previously[22] and it was speculated that a chemical change occurred on the particle surface. In this work, these chemical changes are discussed in the Scanning Electron Microscopy section above.

The resistance data acquired in this work shows decreases in resistance at temperatures corresponding to an increase in the gold particle size (as shown in SAXS data below). This observation suggests a shift in conductance mechanism from tunnelling (common in smaller particles) towards bulk conductance as the effective cross section of conductive gold increases.[15, 21]

Small-angle X-ray Scattering

AuNPs have been previously investigated using SAXS to probe suspensions of AuNPs in a variety of solvents.[32-35] Here we present data acquired using variable-temperature synchrotron SAXS experiments on AuNP powders heated at 3°C min^{-1}. The size of scattering elements probed was between 1 to 9 nm.

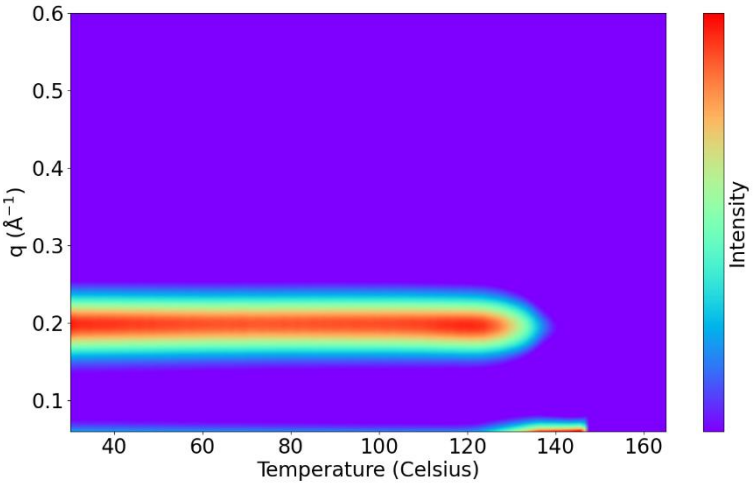

Figure 3.4 Heat map of SAXS data for BT@AuNPs heated to 165°C at 3°C min^{-1}.

The q dependence *vs* temperature for BT@AuNPs (Figure 3.4) shows a single constant diffraction band at q = 0.2 $Å^{-1}$, corresponding to an average spherical particle diameter of 31 Å (or 3.1 nm), which is in agreement with the measured size obtained using TEM (Figure 3.6, Section 3.5, Supplementary Information) The presence of a single band at q = 0.2 $Å^{-1}$ suggests that the dispersion of the particle sizes is low. The BT@AuNPS scattering band is present with no measurable changes in intensity of FWHM until ~125°C. From 125 to 140°C, the band decreases in intensity, with an associated increase in scattering from species at q < 0.1 $Å^{-1}$, which indicates a coarsening of the BT@AuNPS. Above 140°C, all scattering signals disappear, which we attribute to the formation of particles (or aggregates of particles) > 9 nm in diameter, which subsequently scatter at angles beyond the measurable range of the instrument. As the experiment temperature is less than T_{SE} for BT@AuNPs, the variable temperature SAXS clearly demonstrate the thermal stability until ~125°C, at which point they coarsen into larger particles or aggregates of particles of > 9 nm in diameter. This observation is in agreement with

previous studies showing an increase in the sizes of AuNPs prior to the sintering event[20] and well as the SEM observations discussed above.

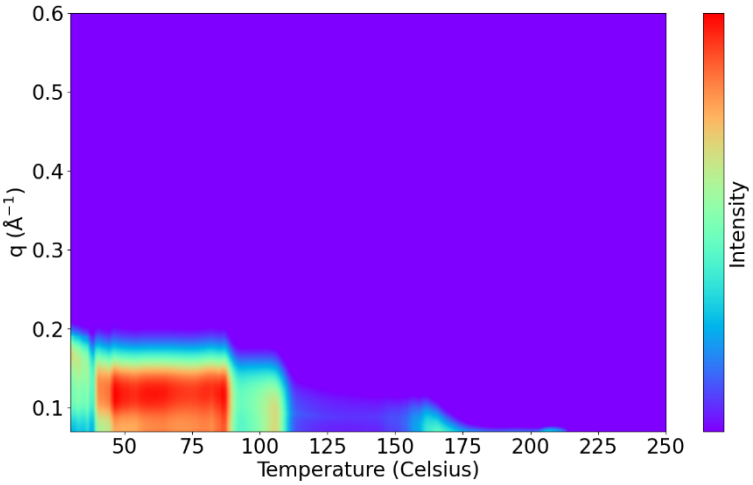

Figure 3.5 Heat map of SAXS data for HDT@AuNPs heated to 250°C at 3°C min^{-1}.

For HDT@AuNPS, the scattering behaviour (Figure 3.5) is different to that observed for the BT@AuNPs. At room temperature, two low intensity diffraction bands are present at q range of 0.19 to 0.1 $Å^{-1}$ indicating a disperse mixture of 3.5 to 6 nm scattering elements. The distributions of these scatterers merge into a single band at q= 0.12 by ~40°C, suggesting a slight coarsening of the HDT@AuNPs to a size of 5.2 nm. In the region where the surface disulfide layer melts (~50°C) the ~5 nm scatterers remain stable until 90°C as indicated by diffraction bands with equal intensities between ~50°C to ~90°C. There is a sharp decrease in intensity between 90-110°C and almost no intensity until ~160°C, where very small amounts of scattering are observed at $q < 0.1$ indicating the presence of larger coarsened AuNPS, similar to those observed in BT@AuNPS. By 225°C (close to the T_{SE}), all particles are larger than the q limit of the experiment. Beyond the T_{SE}, a featureless region is observed. We propose that the lack of diffraction between 110°C and 160°C is attributed to the formation of the liquid films whereby the particles are scattering in a fashion more like a solution (rather than diffraction from a solid AuNPs film). Instead, a low intensity featureless dispersion is observed until ~160°C. At 160°C, an increased intensity of scattering from species at $q < 0.1$ $Å^{-1}$ is observed, attributable to the coarsening of the HDT@AuNPs to form scattering species >9 nm in diameter. That is, sufficient dihexadecyl disulfide is formed from the surface of AuNPs to give a

dispersion of HDT@AuNPs in dihexadecyl disulfide, from which the suspended HDT@AuNPs coarsen.

Conclusions

Films of AuNPs stabilised with butanethiol and hexadecanethiol ligands displayed quite different properties upon heating up to their sintering temperatures. Films of HDT@AuNPs, which form non-volatile dihexadecyl disulfide upon heating, become liquid at 56°C. This temperature corresponds to the melting point of dihexadecyl disulfide. In contrast, no liquid phase was observed for BT@AuNPs at any temperature. The stabilising ligands also had a significant influence on the electrical resistances of the AuNP films. The longer HDT ligands imparted resistances of >100 MΩ at room temperature whilst BT@AuNP films had resistances in the kΩ range. Upon heating, both types of films showed a decrease in resistance. In the case of BT@AuNP films, the resistance did not return to that of the as-formed films. SAXS data showed that the BT@AuNPs do not coarsen until ~140°C while HDT@AuNPs underwent changes at lower temperatures (~90°C) that we ascribe to the liquid phase in which the particles were embedded.

Acknowledgments

We acknowledge the Advanced Materials Characterisation Facility of Western Sydney University for access to its instrumentation and staff. In particular, we thank Dr Laurel George and Dr Daniel Fanna.

3.5 Supplementary Information

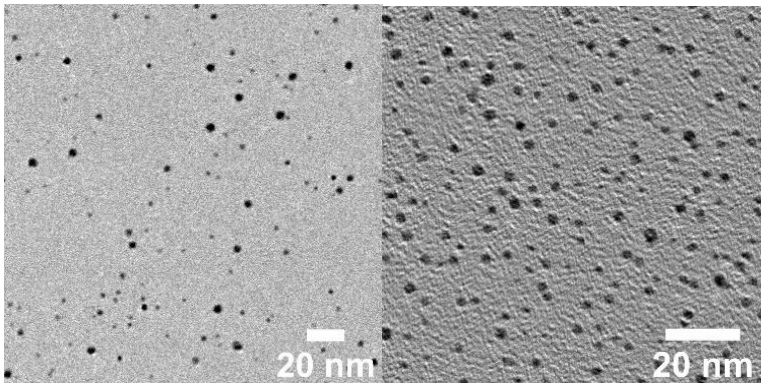

Figure 3.6 TEM images of HDT@AuNPs (left) and BT@AuNPs (right).

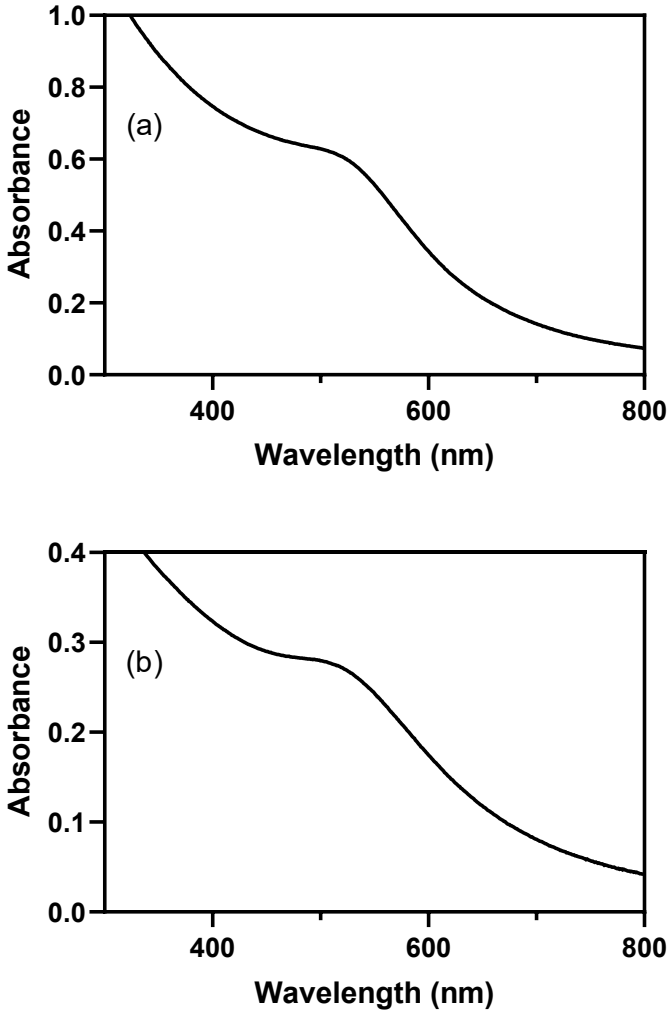

Figure 3.7 UV-vis of (a) BT@AuNPs and (b) HDT@AuNPs.

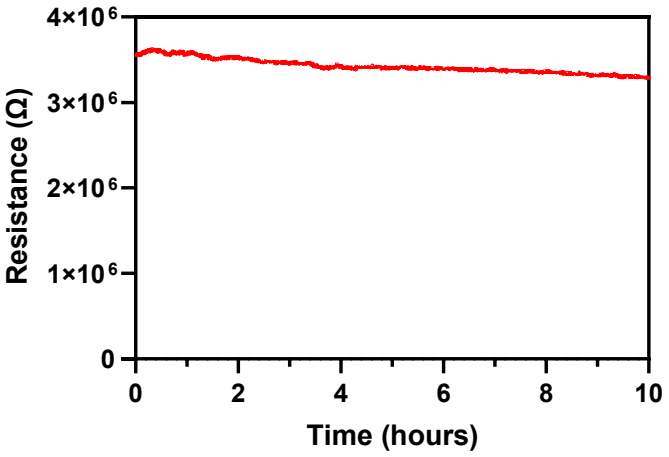

Figure 3.8 Resistance of BT@AuNPs held at 24 for 10 hours.

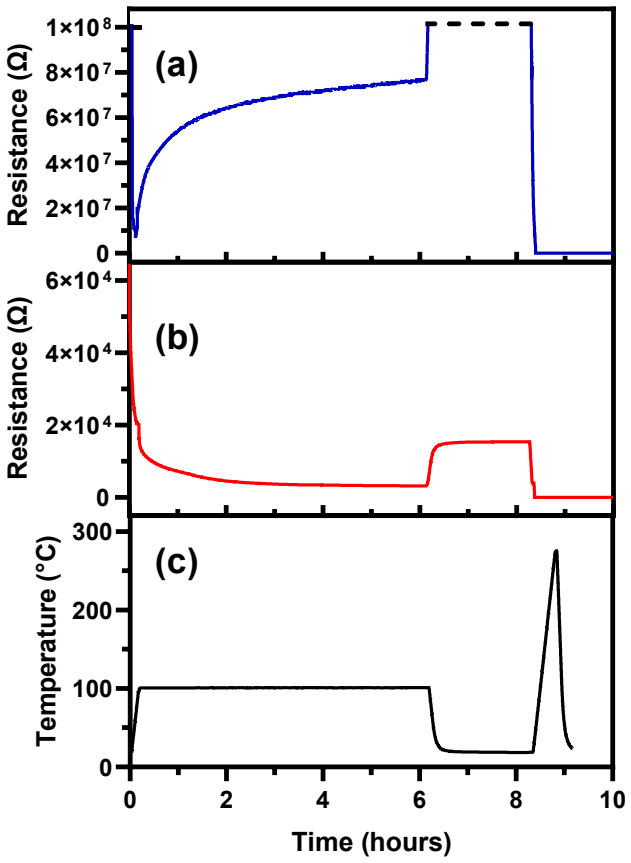

Figure 3.9 Graph showing the resistances of (a) HDT@AuNP films and (b) BT@AuNP films heated at temperatures shown on (c).

References

1. Im, J., Heaton, C., Putri, N. R. E., Liu, C., Usuba, J., Butler, K., Fay, M., Han, G. G. D., Hooshmand, H., Thompson, A., Wildman, R., Hague, R., Turyanska, L., Tuck, C., On-Demand Sintering of Gold Nanoparticles via Controlled Removal of o-Nitrobenzyl Thiol Ligands Under Record-Low Power for Conductive Patterns. *Advanced Science.* 2025.
2. Im, J. A.-O., Trindade, G. A.-O. X., Quach, T. A.-O., Sohaib, A. A.-O., Wang, F. A.-O., Austin, J. A.-O., Turyanska, L. A.-O., Roberts, C. A.-O., Wildman, R. A.-O., Hague, R. A.-O., Tuck, C. A.-O., Functionalized Gold Nanoparticles with a Cohesion Enhancer for Robust Flexible Electrodes. *Applied Nano Materials.* 2022, *5* (5), 6708-6716.
3. Klajn, R., Bishop, K. J. M., Fialkowski, M., Paszewski, M., Campbell, C. J., Gray, T. P., Grzybowski, B. A., Plastic and moldable metals by self-assembly of sticky nanoparticle aggregates. *Science.* 2007, *316* (5822), 261-264.
4. International Union of, P., Applied, C., sintering.
5. Zamani, M., Klapperich, C., Furst, A., Recent advances in gold electrode fabrication for low-resource setting biosensing. *Lab on a Chip.* 2023, *23*.
6. Huang, D., Liao, F., Molesa, S., Redinger, D., Subramanian, V., Plastic-Compatible Low Resistance Printable Gold Nanoparticle Conductors for Flexible Electronics. *Journal of The Electrochemical Society.* 2003, *150*, G412-G417.
7. Tirkey, A., Babu, P. J., Synthesis and characterization of citrate-capped gold nanoparticles and their application in selective detection of creatinine (A kidney biomarker). *Sensors International.* 2024, *5*, 100252.
8. Grys, D.-B., de Nijs, B., Salmon, A. R., Huang, J., Wang, W., Chen, W.-H., Scherman, O. A., Baumberg, J. J., Citrate Coordination and Bridging of Gold Nanoparticles: The Role of Gold Adatoms in AuNP Aging. *Nano.* 2020, *14* (7), 8689-8696.
9. Ortega-Córdova, R., Sánchez-Carillo, K., Carrasco-Saavedra, S., Ramírez-García, G., Pérez-García, M. G., Soltero-Martínez, J. F. A., Mota-Morales, J. D., Polyvinylpyrrolidone-mediated synthesis of ultra-stable gold nanoparticles in a nonaqueous choline chloride–urea deep eutectic solvent. *The Royal Society of Chemistry Applied Interfaces.* 2024, *1* (3), 600-611.
10. Ngernpimai, S., Puangmali, T., Kopwitthaya, A., Tippayawat, P., Chompoosor, A., Teerasong, S., Enhanced Stability of Gold Nanoparticles with Thioalkylated Carboxyl-Terminated Ligands for Applications in Biosensing. *Applied Nano Materials.* 2024, *7* (11), 13124-13133.
11. King, S. R., Shimmon, S., Totonjian, D. D., McDonagh, A. M., Influence of Bound versus Non-Bound Stabilizing Molecules on the Thermal Stability of Gold Nanoparticles. *Journal of Physical Chemistry C.* 2017, *121*, 13944-13951.
12. King, S. R., Shimmon, S., Gentle, A. R., Westerhausen, M. T., Dowd, A., McDonagh, A. M., Remarkable thermal stability of gold nanoparticles functionalised with ruthenium phthalocyanine complexes. *Nanotechnology.* 2016, *27* (21), 215702.
13. Coutts, M. J., Cortie, M. B., Ford, M. J., McDonagh, A. M., Rapid and Controllable Sintering of Gold Nanoparticle Inks at Room Temperature Using a Chemical Agent. *The Journal of Physical Chemistry C.* 2009, *113*, 1325-1328.
14. Cortie, M. B., Coutts, M. J., Ton-That, C., Dowd, A., Keast, V. J., McDonagh, A. M., On the Coalescence of Nanoparticulate Gold Sinter Ink. *The Journal of Physical Chemistry C.* 2013, *117* (21), 11377-11384.
15. Summers, P. K., Angeloski, A., Wuhrer, R., Cortie, M. B., McDonagh, A. M., The fate of organic species upon sintering of thiol-stabilised gold nanoparticles under different atmospheric conditions. *Physical Chemistry Chemical Physics.* 2023, *25* (10), 7170-7175.

16. Summers, P., Wuhrer, R., McDonagh, A., Electrically conductive gold films formed by sintering of gold nanoparticles at room temperature initiated by ozone. *Journal of Nanoparticle Research.* 2024, *26*.
17. Martin, J. E., Odinek, J., Wilcoxon, J. P., Anderson, R. A., Provencio, P., Sintering of alkanethiol-capped gold and platinum nanoclusters. *Journal of Physical Chemistry B.* 2003, *107*, 430-434.
18. Reimers, J. R., Ford, M. J., Halder, A., Ulstrup, J., Hush, N. S., Gold surfaces and nanoparticles are protected by Au(0)-thiyl species and are destroyed when Au(I)-thiolates form. *Proceedings of the National Academy of Sciences of the United States of America.* 2016, *113*, E1424-E1433.
19. Smith, B. L., Hutchison, J. E., Transformations during sintering of small (D core < 2 nm) ligand-stabilized gold nanoparticles: Influence of ligand functionality and core size. *Journal of Physical Chemistry C.* 2013, *117*, 25127-25137.
20. King, S. R., Gentle, A. R., Cortie, M. B., McDonagh, A. M., On the Development of Optical Properties during Thermal Coarsening of Gold Nanoparticle Composites. *The Journal of Physical Chemistry C.* 2018, *122* (22), 12098-12105.
21. Wuelfing, W. P., Green, S. J., Pietron, J. J., Cliffel, D. E., Murray, R. W., Electronic Conductivity of Solid-State, Mixed-Valent, Monolayer-Protected Au Clusters. *Journal of the American Chemical Society.* 2000, *122* (46), 11465-11472.
22. Hardy, N. J., Hanwell, M. D., Richardson, T. H., Temperature effects on the electrical conductivity of thiol encapsulated gold nanoparticle thin films. *Journal of Materials Science: Materials in Electronics.* 2007, *18* (9), 943-949.
23. Summers, P. K., Wuhrer, R., McDonagh, A. M., Electrically conductive gold films formed by sintering of gold nanoparticles at room temperature initiated by ozone. *Journal of Nanoparticle Research.* 2024, *26* (5), 97.
24. King, S. R., Massicot, J., McDonagh, A. M., A Straightforward Route to Tetrachloroauric Acid from Gold Metal and Molecular Chlorine for Nanoparticle Synthesis. *Metals.* 2015, *5* (3), 1454-1461.
25. Wu, Y., Li, Y., Liu, P., Gardner, S., Ong, B. S., Studies of Gold Nanoparticles as Precursors to Printed Conductive Features for Thin-Film Transistors. *Chemistry of Materials.* 2006, *18* (19), 4627-4632.
26. Link, S., El-Sayed, M. A., Size and Temperature Dependence of the Plasmon Absorption of Colloidal Gold Nanoparticles. *The Journal of Physical Chemistry B.* 1999, *103* (21), 4212-4217.
27. Philip, D., Synthesis and spectroscopic characterization of gold nanoparticles. *Spectrochimica Acta Part A: Molecular and Biomolecular Spectroscopy.* 2008, *71* (1), 80-85.
28. Brust, M., Bethell, D., Kiely, C. J., Schiffrin, D. J., Self-Assembled Gold Nanoparticle Thin Films with Nonmetallic Optical and Electronic Properties. *Langmuir.* 1998, *14* (19), 5425-5429.
29. Terrill, R. H., Postlethwaite, T. A., Chen, C.-h., Poon, C.-D., Terzis, A., Chen, A., Hutchison, J. E., Clark, M. R., Wignall, G., Monolayers in Three Dimensions: NMR, SAXS, Thermal, and Electron Hopping Studies of Alkanethiol Stabilized Gold Clusters. *Journal of the American Chemical Society.* 1995, *117* (50), 12537-12548.
30. Badia, A., Singh, S., Demers, L., Cuccia, L., Brown, G. R., Lennox, R. B., Self-Assembled Monolayers on Gold Nanoparticles. *Chemistry – A European Journal.* 1996, *2* (3), 359-363.
31. Badia, A., Cuccia, L., Demers, L., Morin, F., Lennox, R. B., Structure and Dynamics in Alkanethiolate Monolayers Self-Assembled on Gold Nanoparticles: A DSC, FT-IR,

and Deuterium NMR Study. *Journal of the American Chemical Society.* 1997, *119* (11), 2682-2692.
32. Chen, X., Schröder, J., Hauschild, S., Rosenfeldt, S., Dulle, M., Förster, S., Simultaneous SAXS/WAXS/UV–Vis Study of the Nucleation and Growth of Nanoparticles: A Test of Classical Nucleation Theory. *Langmuir.* 2015, *31* (42), 11678-11691.
33. Chen, X., Wang, J., Pan, R., Roth, S., Förster, S., Insights into Growth Kinetics of Colloidal Gold Nanoparticles: In Situ SAXS and UV–Vis Evaluation. *The Journal of Physical Chemistry C.* 2021, *125* (1), 1087-1095.
34. Chen, X., Wei, M., Jiang, S., Förster, S., Two Growth Mechanisms of Thiol-Capped Gold Nanoparticles Controlled by Ligand Chemistry. *Langmuir.* 2019, *35* (37), 12130-12138.
35. Rattanawongwiboon, T., Soontaranon, S., Hemvichian, K., Lertsarawut, P., Laksee, S., Picha, R., Study on particle size and size distribution of gold nanoparticles by TEM and SAXS. *Radiation Physics and Chemistry.* 2022, *191*, 109842.

Chapter 4

Electrically Conductive Gold Films Formed by Sintering of Gold Nanoparticles at Room Temperature Initiated by Ozone

4.1 Preamble

In Chapter 2, it was shown that reducing, inert and air atmospheres had no influence on the leaving disulfide compounds and sintering temperatures. Previous work showed that a strong oxidising agent (nitrogen dioxide) reduces the temperatures at which thiol-stabilised AuNPs sinter although no examination of the chemical impact of the strong oxidiser was reported. Here, the effect of ozone on the thermal stability of thiol-stabilised gold nanoparticles is examined using the experimental methods discussed in the previous chapters. Upon sintering in an ozone-containing atmosphere, surface-bound butanethiyl ligands exclusively form 1-butanesulfonate species when released from AuNP surfaces, which leads to sintering at significantly lower temperatures than those in non-oxidising atmospheres.

4.2 Certificate of Authorship

The paper entitled "Electrically conductive gold films formed by sintering of gold nanoparticles at room temperature initiated by ozone" was published in *Journal of Nanoparticle Research.* The following chapter is based on the published work.

I, Paige Summers, certify that the work in Chapter 4 has not been submitted as part of any other documents required for a degree.

4.3 Authorship Contributions

Author	Contribution	Signature
Paige K. Summers	Conceptualisation, experimental design, performed experiments, analysed data, original manuscript writing, manuscript editing	Production Note: Signature removed prior to publication.
Richard Wuhrer	Technical assistance, manuscript editing	Production Note: Signature removed prior to publication.
Andrew M. McDonagh	Conceptualisation, manuscript editing	Production Note: Signature removed prior to publication.

4.4 Electrically Conductive Gold Films Formed By Sintering of Gold Nanoparticles At Room Temperature Initiated By Ozone

Abstract

Understanding and controlling the sintering behaviour of gold nanoparticles is important in the field of ligand-protected nanoparticles for their use as precursors for thin film fabrication. Lowering the temperature of the sintering event of gold nanoparticles by facilitating desorption of the ligand through oxidation can provide compatibility of sintered gold nanoparticle thin films onto heat sensitive substrates. Here we examine the processes by which 1-butanethiol-protected gold nanoparticles sinter under an ozone-rich environment. Upon heating, an ozone-rich environment significantly reduces the temperature of the sintering event when compared to sintering under ambient conditions. At room temperature, exposure to an ozone-rich environment induces sintering over a period of 2.5 hours. Upon exposure to ozone, the surface-bound butanethiol ligands are oxidised to 1-butanesulfonic acid which facilitates sintering.

Introduction

Sintering of AuNPs is an attractive technique to form continuous, electrically conducting thin films.[1, 2] Using this method, low cost printable electronic devices such as thin-film transistors,[2] field effect transistors,[3] and contacts[2, 4] can be fabricated. Formulations that sinter AuNPs at relatively low temperatures provide great flexibility and enable AuNP films to be applied to low melting point polymers or other heat-sensitive substrates. AuNPs can sinter if there is sufficient energy to overcome the activation energy barrier provided by the stabilising ligands.[5] One method to lower the activation energy barrier, and thus the T_{SE}, is to oxidise the capping ligands, which facilitates desorption from the gold surface.

The bond between gold and the thiolate stabilising ligand may be described as a gold-thiyl interaction (where thiyls are species with the RS· structure).[6] These interactions can be degraded upon exposure to an oxidiser, to UV light, or at elevated temperatures.[7-12] Alkanethiolate SAMs on gold have been shown to oxidise to alkanesulfinates and alkanesulfides under ambient conditions.[10, 13-15] Scanning tunnelling microscope images of air-oxidised decanethiol SAMs on Au(111) shows that after a two-week exposure to ambient conditions, some conversion to decanesulfonate occurs.[16] Density functional

theory calculations revealed that under oxidising conditions (surface oxide or ozone) thiolate groups on Au (111) surfaces might form sulfoxide derivatives (R2S=O), with sulfinate ($RS(=O)O^-$) and sulfonate ($RS(=O)2O^-$) derivatives formed if active oxygens are further supplied.[17]

Of particular relevance to the current work, exposure of thiol-bound SAMs on gold to ozone has been shown to oxidise the sulfur atoms.[11, 18, 19] With regard to AuNPs, ozone can reduce the affinity of thiol-based ligands to the gold core in supported AuNPs, allowing for removal of the ligands by washing with water.[20] X-ray photoelectron spectroscopy analysis of the ozone treated AuNPs revealed that the sulfur atoms had been oxidised upon exposure.[20] Previous work has also utilised nitrogen dioxide to oxidise the thiolate stabilising ligands of AuNPs which subsequently sintered at room temperature.[5] In this work, we examine the sintering of thiol-stabilised AuNPs using ozone, a common and readily generated gas. We show that in an ozone-rich environment, the ligands surrounding AuNPs are oxidised and significantly reduce T_{SE} to produce gold films. Importantly, we investigate the organic profile of the desorbed ligand to determine the processes that occur upon sintering. These findings shed a new light on advancing the use of gold films for heat sensitive substrates.

Experimental

General

1-Butanethiol, sodium 1-butanesulfonate, TOAB, sodium borohydride, methanol, acetonitrile, $CDCl_3$ and deuterated dimethyl sulfoxide (DMSO-d_6) were purchased from Sigma-Aldrich and used as received. Toluene (ChemSupplyAustralia), chloroform (Rowe Scientific) were used as received. 1-Butanesulfonic acid[21] and dibutyl disulfide[22] were prepared by literature procedures. Tetrachloroauric acid,[23] and BT@AuNPs[2] were prepared using literature procedures. The AuNPs were characterised by SEM, TEM and ^{1}H NMR. ^{1}H NMR spectra were recorded using a Bruker NMR spectrometer operating at 400 MHz. Spectra were referenced using residual non-deuterated signals: DMSO-d_6 (1H δ 2.49), $CDCl_3$ (1H δ 7.26). TEM images were taken using a JEOL JEM-F200 FE-TEM operating at 200 kV and fitted with a Gatan Rio 1816 – 4k x 4k camera. The TEM samples were prepared by evaporating diluted nanoparticle solution on the carbon-coated copper grid. The images were analysed using ImageJ software (https://imagej.nih.gov/ij/). SEM was performed at facilities at Western Sydney University. A Zeiss Merlin FEGSEM was

utilised for imaging samples prepared on stubs. The FEGSEM was operated at 10kV accelerating voltage in Hivac mode at a working distance of approximately 3 mm. Both secondary and in-lens secondary detectors were utilised for imaging. High-resolution mass-spectrometry (HRMS) was performed using an Agilent 6510 Q-TOF using flow injection and in positive ion mode for $[M+H]^+$, or negative ion mode $[M-H]^-$ where specified.

Resistance Measurements of AuNP Films

Suspensions of BT@AuNPs in chloroform (0.5 mL of 10 mg/ml) were drop cast onto DropSens (Metrohm) interdigitated gold electrodes forming films of AuNPs of ~5 mm diameter, which were then heated within a modified Linkam THMS600 temperature control stage. A Linkam TMS 94 controller maintained a heating rate of 10°C min^{-1} from room temperature to 250°C. A Rigol DM3058E digital multimeter and a PT100 (RS PRO) RTD sensor, 2mm x 5mm Class B thermocouple measured the temperature on the gold electrode. A Rigol DM3068 digital multimeter (maximum resistance of 100 MΩ) measured the Electrical resistance of the electrode. A LabView program was used to interface with and control the multimeters, and to acquire the temperature and electrical resistance. Ozone was generated using a Hailea HLO-300 Ozonizer at 300 mg/h in a flow of 3.5 L/min. *Warning. Ozone was destructive to several electronic components including thermocouples when exposed for extended periods (up to 20 hours).*

Analysis of Ozone Treated AuNPs

BT@AuNPs were placed in a 5 mL side arm tube attached to a condenser cooled to -0.5°C and fitted with a drying tube. The outflow from an ozone generator was passed through dry silica gel beads tightly packed in a condenser cooled to -0.5°C to remove moisture and then directed into the side arm tube for 48 hrs. Organic residues were then collected by rinsing the interior of the condenser and reaction tube first with $CDCl_3$ (with sonication) and then DMSO-d_6. The solutions were filtered through cellulose fibre (Kimwipe) to remove elemental gold and analysed using ^1H NMR spectroscopy and HRMS.

Results and Discussion

BT@AuNPs (as shown in Figure 4.7, Section 4.5, Supplementary Information) were synthesised using a two-phase Brust-Schiffrin method and had diameters of 3.4 (± 1.4) nm (measured using TEM, Figure 4.6, Section 4.5, Supplementary Information).

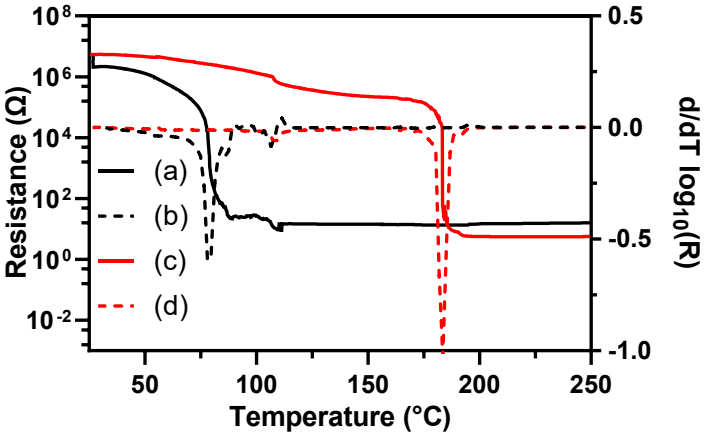

Figure 4.1 Resistance data obtained from films of BT@AuNPs during heating. Conditions: (a) ozone-rich environment, (c) air. (b) and (d) are the corresponding derivatives of the resistance vs temperature curves.

Films of AuNPs were prepared by drop-casting a suspension of BT@AuNPs in chloroform onto interdigitated gold electrodes. Upon heating at 10°C min^{-1} in air, the films sintered at ~190°C to form a conductive gold film. The sintering event is associated with a change in resistance from >1 MΩ to <100 Ω (Figure 4.1). These results are consistent with our earlier studies on BT@AuNPs.[24] In contrast, heating of the films in an ozone-rich atmosphere caused the films to sinter at ~80°C, which is significantly lower than the T_{SE} of the AuNPs sintered in air.

Figure 4.2 BT@AuNP ink film (left) before and (right) after exposure to a stream of ozone for 3 hours.

The significant decrease in the T_{SE} observed upon heating at 10°C min^{-1} prompted experiments to examine the effect of exposure to ozone at room temperature. Films of metallic gold were formed from AuNP films exposed to a stream of ozone (Figure 4.2). To probe this behaviour further, films of AuNPs were formed by dropcasting AuNP

suspensions onto interdigitated electrodes and the resistance measured upon exposure to ozone. Figure 4.3 shows the resistance of BT@AuNPs at room temperature upon exposure to air and an ozone rich environment over 15 h. In our hands, and as reported by others such AuNPs are stable and do not sinter over periods of at least months. Under an atmosphere of air, the resistance remained stable at 2.5 MΩ. In contrast, under an ozone atmosphere the resistance of the BT@AuNPs decreased markedly to ~300 Ω after ~2.5 h. The slightly greater resistance of the room temperature sintered AuNPs (300 Ω) compared to the thermally sintered AuNPs (~15 Ω) may be attributed to residual organic material remaining after the decomposition of butanethiol (see below), leading to a less dense film.[25]

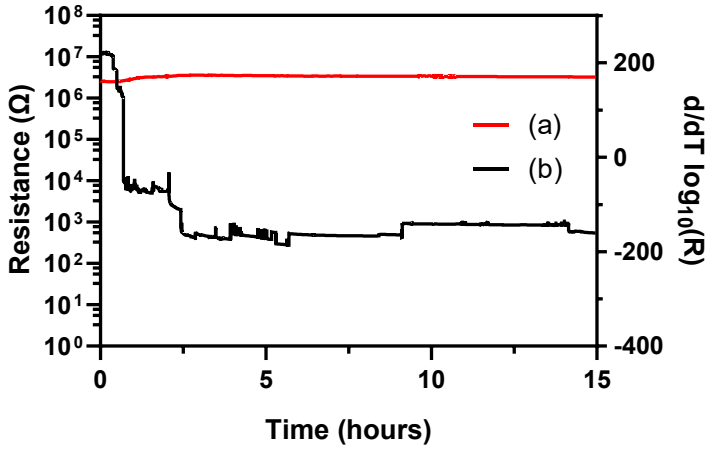

Figure 4.3 Resistance data of BT@AuNPs at (a) room temperature in air and (b) an ozone rich environment over 15h.

Low temperature sintering has been reported in our earlier work using a chemically synthesised oxidant but the nature of the reactions leading to the sintering event was not explored.[5] Here we examine the residue surrounding the gold film formed after exposure to the ozone atmosphere using ^{1}H NMR spectroscopy and HRMS data. After reaction with ozone, which induced sintering, the reaction vessel was rinsed with $CDCl_3$ and then DMSO-d_6. The $CDCl_3$ fraction contained very little material of which none could be characterised by ^{1}H NMR spectroscopy. The DMSO-d_6 fraction contained a significant amount of organic material.

The ^{1}H NMR spectrum of the DMSO-d_6 fraction contained signals that are consistent with the spectrum of 1-butanesulfonic acid (Figures 4.8 and 4.9, Section 4.5, Supplementary Information). A triplet at 0.85 ppm is assigned to the CH_3 group, a sextet and a quintet at 1.31 and 1.54 ppm, respectively, are assigned to the two central CH_2

groups. A triplet at 2.43 ppm is assigned to the CH_2 group adjacent to the SO_3H group. However, the origin of the proton attached to the sulfonate group from the NP residue is not apparent. It is likely that it arises from the solvent used to gather the ^1H NMR spectrum. Importantly, we found no evidence of dibutyl disulfide formation upon ozone-induced sintering in either the ^1H NMR spectrum (Figure 4.9, Section 4.5, Supplementary Information) or HRMS. Upon sintering in air, hydrogen, nitrogen or argon atmospheres, surface-bound thiyl ligands leave exclusively as their corresponding disulfide compounds.[24] Other possible sulfur-containing compounds such as 1-butanethiol were excluded by comparison of the ^1H NMR spectra (Figure 4.9, Section 4.5, Supplementary Information).

The $CDCl_3$ and DMSO-d_6 fractions were both examined by mass spectrometry in positive and negative ion modes. In negative ion mode, the major peak was observed at m/z 137.027 (Figure 4.10, Section 4.5, Supplementary Information), which corresponds to the sulfonate ion with formula $CH_3(CH_2)_3SO^{3-}$. Other oxygen- and sulfur-containing compounds such as sulfoxide and sulfinates (105 and 121 m/z respectively) were not detected. These findings are consistent with work examining UV-induced photooxidation of thiol SAMs on gold (over various time periods) using X-ray photoelectron spectroscopy where only the corresponding sulfonate ions were detected.[26]

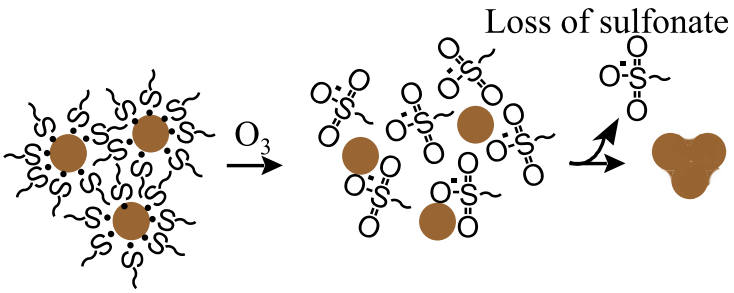

Figure 4.4 Schematic depicting the removal of butanethiyl ligands from the surface of gold nanoparticles in an ozone rich environment.

Considering the resistance data together with post-sintering analysis, it is apparent that when the BT@AuNPs are exposed to an ozone-rich environment, the butanethiol ligands undergo oxidation to butanesulfonic acid thus facilitating desorption of the ligand from the gold surface and inducing the sintering event (Figure 4.4)

SEM images were collected of thermally-induced and ozone-induced sintered BT@AuNPs, as well as pristine BT@AuNPs (Figure 4.5). The SEM images of the thermally-induced, sintered gold films are consistent with previous reports, showing

densification and large grain barriers.[24] SEM images of the room temperature ozone-induced sintered gold films show finer grain size with agglomeration of particles and some residual material. Grains ranging from 600-1000 nm are apparent in the thermally-induced sintered structures while the ozone-induced films have smaller grains ≤ 200 nm.

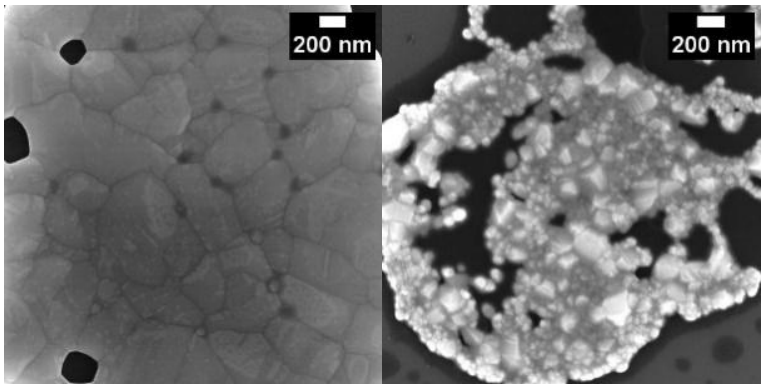

Figure 4.5 SEM images of gold films obtained by (left) heating BT@AuNPs in to 250°C at 10°C min^{-1}, and (right) exposing BT@AuNPs to an ozone-rich atmosphere for 6 h at room temperature.

Conclusion

Conductive gold films have been prepared by sintering BT@AuNPs under an ozone-rich atmosphere. Resistance measurements of BT@AuNPs showed that exposure to the ozone-containing atmosphere during heating significantly reduced the T_{SE} compared to sintering under ambient conditions by ~80°C. Furthermore, electrically conductive gold films were formed at room temperature when BT@AuNPs were exposed to ozone for ~2.5 hours.

Examination of the AuNPs post-sintering revealed that the butanethiyl ligands undergo oxidation to form the corresponding butanesulfonic acid, which is a poor stabilising ligand. We found no evidence for dibutyl disulfide (the major product of sintering under ambient conditions) in the post-sintering residue, indicating that the oxidation process is further promoted by ozone. The gold films prepared by the new room temperature ozone-induced sintering process showed a different morphology to those sintered by thermal activation under ambient conditions (observed by SEM) with the former producing finer grain sizes.

Acknowledgements

We acknowledge the Advanced Materials Characterisation Facility of Western Sydney University for access to its instrumentation and staff. In particular, we thank Dr. Laurel

George and Dr. Daniel Fanna. We thank Dr Thomas Lockwood (University of Technology Sydney) for assistance with mass spectrometry and the microstructural analysis unit (University of Technology Sydney) for assistance with TEM.

4.5 Supplementary Information

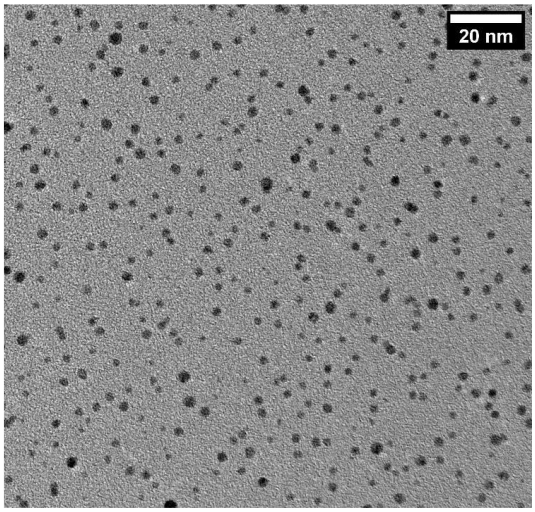

Figure 4.6 TEM image of drop cast BT@AuNPs.

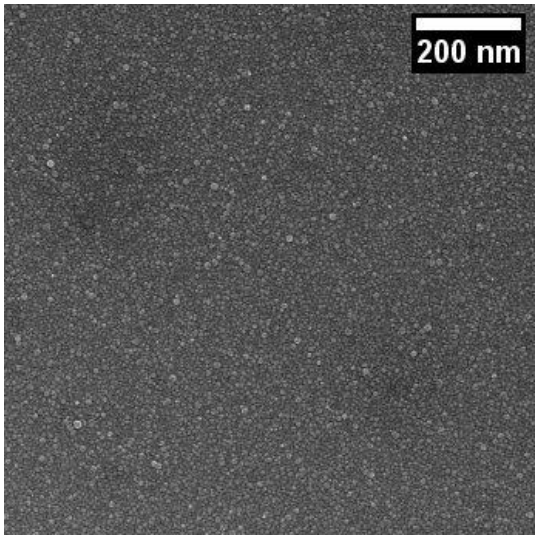

Figure 4.7 SEM image of drop cast BT@AuNPs (on silicon wafer).

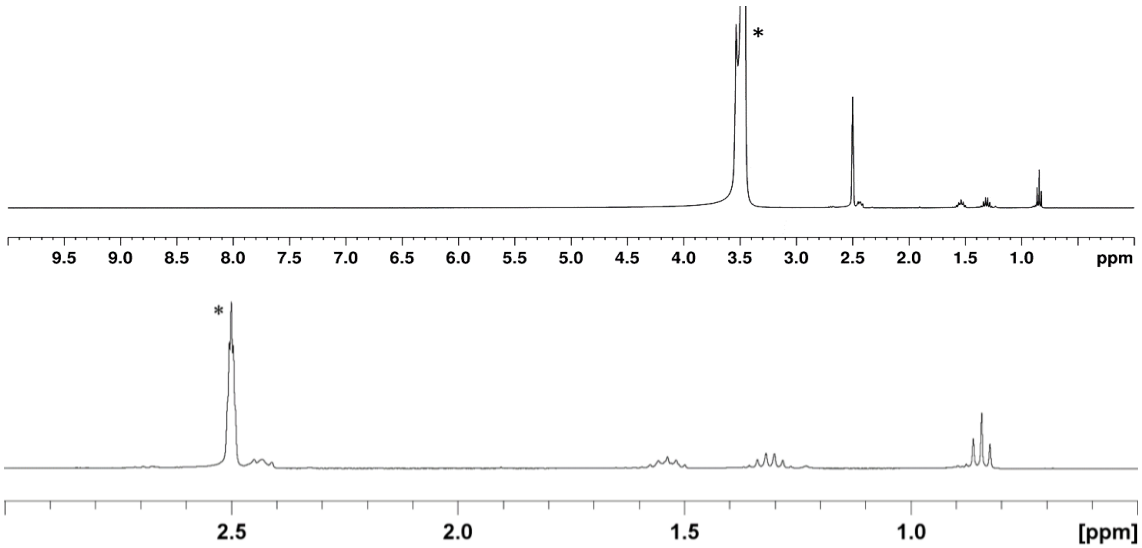

Figure 4.8 ^{1}H NMR spectra of the DMSO-soluble residue from ozone-induced sintered BT@AuNPs. Top: full range spectrum, Bottom: Signals in the range 0 – 3 ppm (* denotes residual DMSO at δ 2.49).

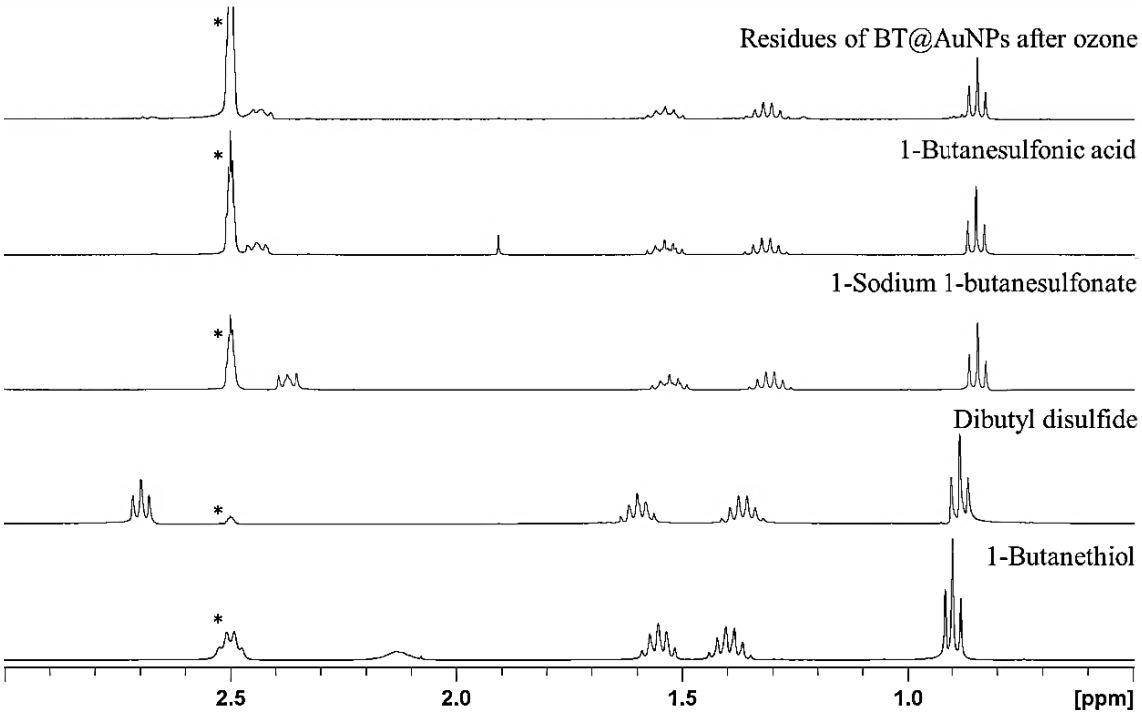

Figure 4.9 ^{1}H NMR spectra of the residue from ozone-induced sintered BT@AuNPs as well as spectra for 1-butanesulfonic acid, 1-sodium 1-butanesulfonate, dibutyl disulfide and 1-butanethiol (* denotes residual DMSO at δ 2.49).

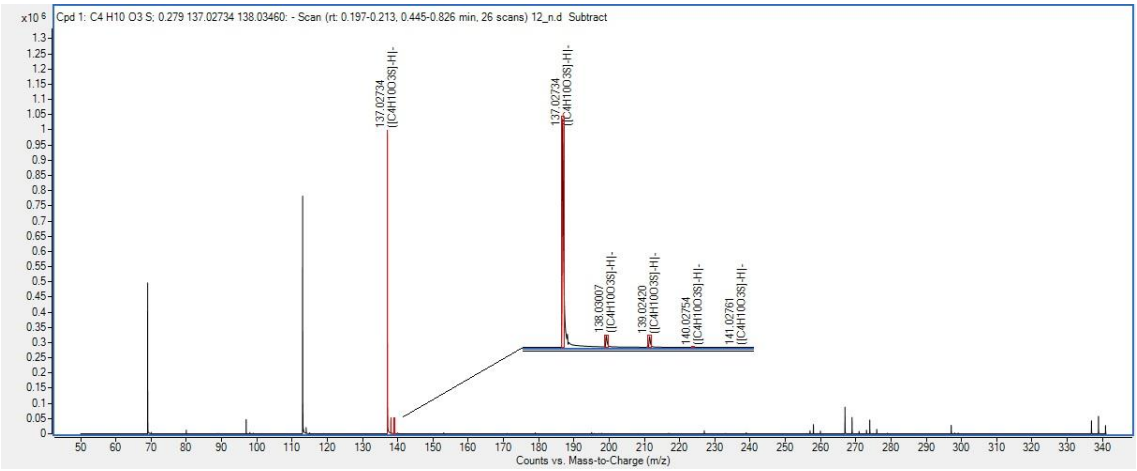

Figure 4.10 Mass spectrum of residue from ozone-induced sintered BT@AuNPs (Relative Mass Difference: -3.35 ppm)

References

1. Bishop, P. T., Ashfield, L. J., Berzins, A., Boardman, A., Buche, V., Cookson, J., Gordon, R. J., Salcianu, C., Sutton, P. A., Printed gold for electronic applications. *Gold Bulletin.* 2010, *43*, 181-188.
2. Wu, Y., Li, Y., Liu, P., Gardner, S., Ong, B. S., Studies of Gold Nanoparticles as Precursors to Printed Conductive Features for Thin-Film Transistors. *Chemistry of Materials.* 2006, *18*, 4627-4632.
3. Presnova, G., Presnov, D., Krupenin, V., Grigorenko, V., Trifonov, A., Andreeva, I., Ignatenko, O., Egorov, A., Rubtsova, M., Biosensor based on a silicon nanowire field-effect transistor functionalized by gold nanoparticles for the highly sensitive determination of prostate specific antigen. *Biosensors and Bioelectronics.* 2017, *88*, 283-289.
4. Huang, D., Liao, F., Molesa, S., Redinger, D., Subramanian, V., Plastic-Compatible Low Resistance Printable Gold Nanoparticle Conductors for Flexible Electronics. *Journal of The Electrochemical Society.* 2003, *150*, G412-G417.
5. Coutts, M. J., Cortie, M. B., Ford, M. J., McDonagh, A. M., Rapid and Controllable Sintering of Gold Nanoparticle Inks at Room Temperature Using a Chemical Agent. *The Journal of Physical Chemistry C.* 2009, *113*, 1325-1328.
6. Reimers, J. R., Ford, M. J., Halder, A., Ulstrup, J., Hush, N. S., Gold surfaces and nanoparticles are protected by Au(0)-thiyl species and are destroyed when Au(I)-thiolates form. *Proceedings of the National Academy of Sciences of the United States of America.* 2016, *113*, E1424-E1433.
7. Sotthewes, K., Kap, Ö., Wu, H., Thompson, D., Huskens, J., Zandvliet, H. J. W., Ordering of Air-Oxidized Decanethiols on Au(111). *The Journal of Physical Chemistry C.* 2018, *122* (15), 8430-8436.
8. Garrell, R. L., Chadwick, J. E., Severance, D. L., McDonald, N. A., Myles, D. C., Adsorption of Sulfur Containing Molecules on Gold: The Effect of Oxidation on Monolayer Formation and Stability Characterized by Experiments and Theory. *Journal of the American Chemical Society.* 1995, *117* (46), 11563-11571.
9. Horn, A. B., Russell, D. A., Shorthouse, L. J., Simpson, T. R. E., Ageing of alkanethiol self-assembled monolayers. *Journal of the Chemical Society, Faraday Transactions.* 1996, *92* (23), 4759-4762.
10. Scott, J. R., Baker, L. S., Everett, W. R., Wilkins, C. L., Fritsch, I., Laser Desorption Fourier Transform Mass Spectrometry Exchange Studies of Air-Oxidized Alkanethiol Self-Assembled Monolayers on Gold. *Analytical Chemistry.* 1997, *69* (14), 2636-2639.
11. Schoenfisch, M. H., Pemberton, J. E., Air Stability of Alkanethiol Self-Assembled Monolayers on Silver and Gold Surfaces. *Journal of the American Chemical Society.* 1998, *120* (18), 4502-4513.
12. Willey, T. M., Vance, A. L., van Buuren, T., Bostedt, C., Terminello, L. J., Fadley, C. S., Rapid degradation of alkanethiol-based self-assembled monolayers on gold in ambient laboratory conditions. *Surface Science.* 2005, *576* (1), 188-196.
13. Tarlov, M. J., Newman, J. G., Static secondary ion mass spectrometry of self-assembled alkanethiol monolayers on gold. *Langmuir.* 1992, *8* (5), 1398-1405.
14. Li, Y., Huang, J., McIver, R. T., Jr., Hemminger, J. C., Characterization of thiol self-assembled films by laser desorption Fourier transform mass spectrometry. *Journal of the American Chemical Society.* 1992, *114* (7), 2428-2432.

15. Burroughs, J. A., Hanley, L., Laser desorption ion trap mass spectrometry of self-assembled monolayers. *Journal of the American Society for Mass Spectrometry.* 1993, *4* (12), 968-970.
16. Kap, Ö., Kabanov, N., Tsvetanova, M., Varlikli, C., Klavsyuk, A. L., Zandvliet, H. J. W., Sotthewes, K., Structural Stability of Physisorbed Air-Oxidized Decanethiols on Au(111). *The Journal of Physical Chemistry C.* 2020, *124* (22), 11977-11984.
17. Jang, Y. H., Goddard, W. A., III, Oxidation of Thiol Anchor Groups in Molecular Junction Devices: A Density Functional Theory Study. *The Journal of Physical Chemistry C.* 2010, *114* (10), 4646-4651.
18. Poirier, G. E., Herne, T. M., Miller, C. C., Tarlov, M. J., Molecular-Scale Characterization of the Reaction of Ozone with Decanethiol Monolayers on Au(111). *Journal of the American Chemical Society.* 1999, *121* (41), 9703-9711.
19. Zhang, Y., Terrill, R. H., Tanzer, T. A., Bohn, P. W., Ozonolysis Is the Primary Cause of UV Photooxidation of Alkanethiolate Monolayers at Low Irradiance. *Journal of the American Chemical Society.* 1998, *120* (11), 2654-2655.
20. Elliott, E. W., III, Glover, R. D., Hutchison, J. E., Removal of Thiol Ligands from Surface-Confined Nanoparticles without Particle Growth or Desorption. *Nano.* 2015, *9* (3), 3050-3059.
21. Smith, K., Hou, D., A General and Efficient Method for the Preparation of Organic Sulfonic Acids by Insertion of Sulfur Trioxide into the Metal−Carbon Bond of Organolithiums. *The Journal of Organic Chemistry.* 1996, *61* (4), 1530-1532.
22. Shaabani, A., Tavasoli-Rad, F., Lee, D. G., Potassium Permanganate Oxidation of Organic Compounds. *Synthetic Communications.* 2005, *35* (4), 571-580.
23. King, S. R., Massicot, J., McDonagh, A., A Straightforward Route to Tetrachloroauric Acid from Gold Metal and Molecular Chlorine for Nanoparticle Synthesis. *Metals.* 2015, *5*, 1454-1461.
24. Summers, P. K., Angeloski, A., Wuhrer, R., Cortie, M. B., McDonagh, A. M., The fate of organic species upon sintering of thiol-stabilised gold nanoparticles under different atmospheric conditions. *Physical Chemistry Chemical Physics.* 2023, *25* (10), 7170-7175.
25. Brust, M., Fink, J., Bethell, D., Schiffrin, D. J., Kiely, C., Synthesis and reactions of functionalised gold nanoparticles. *Journal of the Chemical Society, Chemical Communications.* 1995, (16), 1655-1656.
26. Hutt, D. A., Leggett, G. J., Influence of Adsorbate Ordering on Rates of UV Photooxidation of Self-Assembled Monolayers. *The Journal of Physical Chemistry.* 1996, *100* (16), 6657-6662.

Chapter 5

Alkynide-stabilised Gold Nanoparticles: A Synthetic Investigation

5.1 Preamble

Thiol-stabilised AuNPs have been shown to be useful materials for the formation of gold films by sintering. AuNPs with other stabilising ligands have been less explored and so the techniques applied in Chapters 2-4 may be meaningfully applied to AuNPs bearing other stabilising ligands such as alkynes. As discussed in Chapter 1, the Au-C bond (see Figure 5.1) is stronger than the Au-S bond in analogous AuNPs[1]. To assess the behaviour of AuNPs stabilised with alkyne compounds during the sintering process, it is important to have AuNPs of known composition. While methods have been reported for the synthesis of alkynide-stabilised AuNPs, many include additional stabilising compounds in varying amount. In this chapter, a synthesis of AuNPs that are stabilised solely with alkyne compounds is presented (Figure 5.1b) together with an assessment of their stability in solvent.

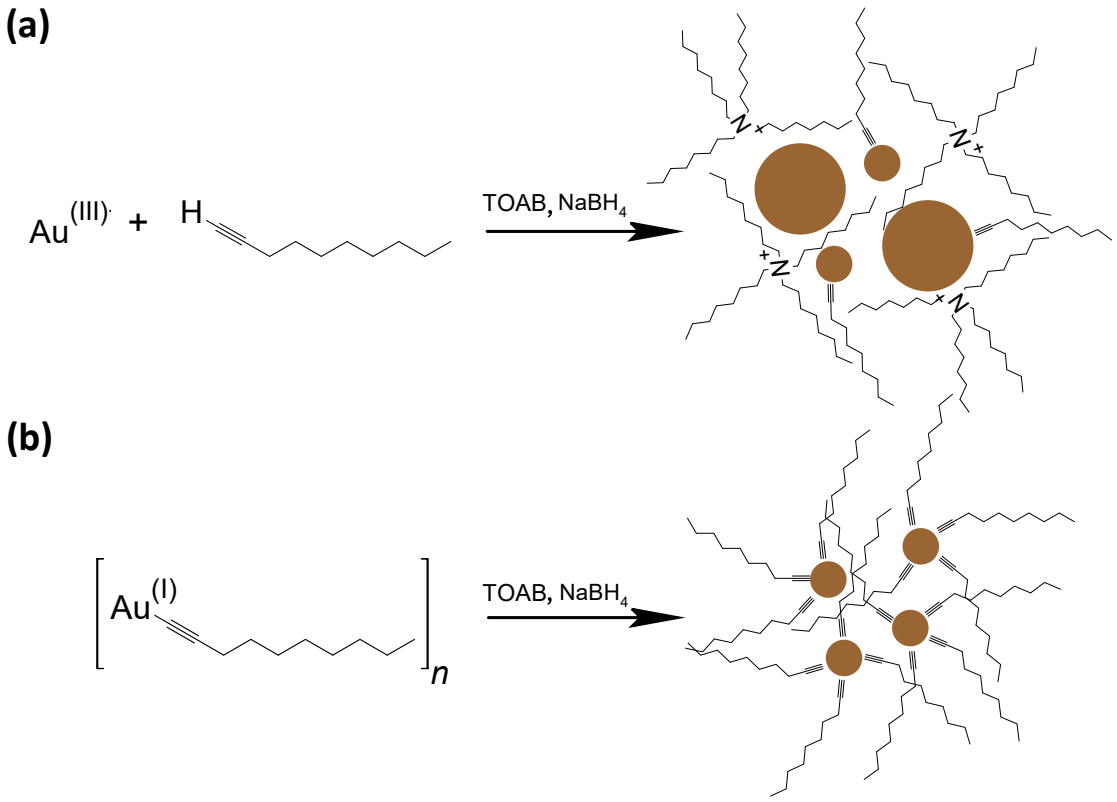

Figure 5.1 Schematic showing new insights of (a) current synthetic technique of stabilising alkynides on AuNPs and (b) the synthetic technique developed in Chapter 5.

5.2 Certificate of Authorship

A manuscript entitled "Alkynide-stabilised Gold Nanoparticles: A Synthetic Investigation" was published in *Nano Futures*. The following chapter is based on the published work.

I, Paige Summers, certify that the work in Chapter 5 has not been submitted as part of any other documents required for a degree.

5.3 Authorship Contributions

Author	Contribution	Signature
Paige K Summers	Conceptualisation, experimental design, performed experiments, analysed data, original manuscript writing, manuscript editing	Production Note: Signature removed prior to publication.
Andrew M. McDonagh	Conceptualisation, manuscript editing	Production Note: Signature removed prior to publication.

5.4 Alkynide-Stabilised Gold Nanoparticles: A Synthetic Investigation

Abstract

Alkyne compounds have emerged as promising stabilising ligands for gold nanoparticles, with potential applications in sensing, catalysis and biological imaging. Several examples of alkynide-stabilised gold nanoparticles have been reported although most use a mixed-ligand system that requires additional stabilising agents. Thus, a facile and size controllable synthesis of gold nanoparticles stabilised exclusively with alkyne compounds is highly desirable. Here we report dec-1-ynide@AuNPs that were synthesised by reduction of a Au(I) dec-1-ynide complex to give nanoparticles with diameter of ~3.4 nm and are stable in air for up to 2 months. ^{1}H NMR spectra indicate that the particles have a shell that contains gold(I) species surrounding a core of gold(0) atoms. Methods that utilised reduction of Au(III) chloride with the phase transfer agent TOAB resulted in bidisperse AuNPs with diameters of ~9 nm and ~3 nm. Variation of the synthesis conditions did not have a significant effect on the particle sizes and residual TOAB was required to maintain particle stability.

Introduction

AuNPs are typically stabilised by ligands where molecular composition and conformation play a critical role in electronic and optical characteristics, stability and reactivity.[2-4] Ligands that have been used to stabilise AuNPs include citrate,[5] thiol, phosphine, and amine ligands,[2] polymers,[6] N-heterocyclic carbenes,[7] and of particular relevance to the current work, alkynes.[8-10]

Alkynes have emerged as an important class of ligands to stabilise AuNPs[8, 9] as well as gold nanoclusters (AuNCs)[11-14] (we use the terminology[15] that nanoclusters have diameters ≤2nm). Alkynide ligands provide additional opportunities to tune the optical[16, 17] and catalytic properties[8, 18] of AuNPs and afford a strong Au-ligand bond.[19, 20]

Alkyne compounds are useful to covalently bond biological molecules gold surfaces to avoid interference from biological thiols[21] and impart high electrochemical transmittance to improve signal transmission during sensing processes.[1, 22, 23] AuNPs functionalised with alkynes are sensitive detectors of hydrogen peroxide and streptavidin proteins, showing long term stability and resistance to decomposition under harsh

conditions.[9] They exhibit stability in high salt conditions, a range of pH values, allowing reliable detection in biological applications.[24] They have also demonstrated some excellent catalytic properties.[8, 25]

Alkynide-stabilised AuNPs can be synthesised by a variety of methods. Ligand exchange reactions have been used where the particle core is formed using another stabilising group and then exchanged for the alkynide ligand. For example, polyvinylpyrrolidone (PVP) stabilised AuNCs can undergo ligand exchange to give phenylacetylene, 1-octyne, or 9-ethynyl-phenanthrene stabilised particles.[12, 13] Interestingly, acetylide stabilised particles were unable to be synthesised from PVP@AuNPs with diameters >4 nm. Recently, acetylide stabilised AuNPs with diameters greater than 4 nm were synthesised in the presence of PVP,[8] although in this case the PVP stabiliser was not entirely displaced by the incoming alkynide ligands. Citrate-stabilised AuNPs have been shown to undergo ligand exchange with alkynide ligands to produce phenylacetylene-polyethylene glycol (PEG) stabilised NPs[25] or alkynylated biotin stabilised particles.[9] Thiolate-stabilised AuNPs can exchange thiol ligands for alkynide ligands under certain conditions.[9] Using alkynide anions (either lithium- or gold(I)-phenylacetylide) resulted in either partial and full ligand exchange on (Au_{25}) NCs.[26]

Direct synthesis methods have also been explored. A one-pot method involving synchronous nucleation and passivation added all reagents (metal salt, ligand, and reductant) simultaneously albeit with less kinetic and yield control.[27, 28] The popular Brust-Schiffrin method[29] (used to prepare thiol-stabilised AuNPs) has been modified to use 1-dodecyne as a stabiliser and yielded particles with diameters of 4.5 and 2.6 nm.[10]

Direct reduction of Au(I)-alkynide complexes has been used to synthesise alkynide-protected AuNCs with well-defined sizes and structures[11, 14, 28, 30-33] albeit with low yields although a recent synchronous nucleation and passivation strategy has been applied to give AuNCs in up to 70% yield.[34]

As part of our investigations into the sintering behaviour of AuNPs[35-41] that include alkynide-stabilised AuNPs (to probe the effect of the strong Au–C bond), we required syntheses that produce alkynide-stabilised AuNPs in reasonable yield and quantities, with well-defined ligand environments. We found that several existing synthetic methods were not suitable for this task, or that they resulted in AuNPs that retained additional stabilising agents. With only a few reported methods for the synthesis of alkynide-stabilised AuNPs, a facile synthesis that produces AuNPs stabilised only with alkyne ligands and with a

reasonably narrow size distribution was critical to ensure reproducible behaviour. Such a method would also be valuable in applications such as sensors and catalysis (although not the focus of the current work) where activity can be dependent on NP sizes and distributions.[42-45]

Here we report our investigations into the synthesis of alkynide-stabilised AuNPs using methods based on the Brust-Schiffrin synthesis as well as via an Au(I)-alkynide precursor. We show that syntheses that use Brust-Schiffrin conditions adapted for alkynes do not yield AuNPs stabilised solely with alkynide ligands. However, when Au(I)dec-1-ynide was used as a precursor, we obtained AuNPs with diameters 2-4 nm that are stabilised with only alkynide ligands.

Results and Discussion

A synthesis of AuNPs was conducted using a TOAB-assisted phase transfer reduction method (Method A) and 1-decyne. This general method is commonly used to prepare thiol-stabilised AuNPs (the Brust-Schiffrin method).[29] As we show below, this method requires that the phase transfer agent (in this case TOAB) not be removed for the particles to remain stable when alkyne was used as a stabilising ligand.

AuNPs were synthesised by first transferring $AuCl_4^-$ into toluene from water using TOAB as phase-transfer agent. 1-Decyne was added and the Au(III) was reduced using $NaBH_4$ to give a deep red dispersion of AuNPs. The resultant AuNPs were characterised by UV-vis absorption spectroscopy, TEM, and ^1H NMR.

The UV-vis spectrum (see Figure 5.2a) contains a plasmon resonance band with a peak at 525 nm, consistent with previous reports.[10] TEM (Figure. 5.3a and Figure 5.8a, Section 5.5, Supplementary Information) showed nanoparticles with size ranges of 9.4 (±3) nm and 4.0 (±1) nm (Figure 5.9a, Section 5.5, Supplementary Information). These were stable as powders for up to two months. After two months, when the powders were dispersed in chloroform, a deep blue colour was observed, indicating the formation of large and irreversible aggregates that precipitated within 12 hours.

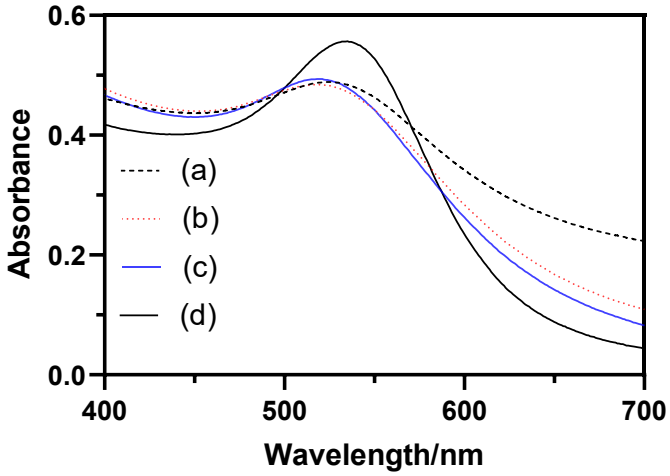

Figure 5.2 UV-visible spectra of (a) AuNPs synthesised using Method A, (b) AuNPs synthesised using Method B, (c) AuNPs synthesised using Method C (washed with water only), (d) AuNPs synthesised using Method E.

The ^{1}H NMR spectrum of the AuNPs prepared by Method A (Figure 5.10, Section 5.5, Supplementary Information) contains signals arising from TOAB (assigned by comparison with the spectrum of pure TOAB, Figure 5.10, Section 5.5, Supplementary Information). Signals associated with the alkynide ligand are not apparent. ^{1}H NMR spectra also revealed that after multiple (up to 16) washes with acetonitrile, as well as mechanical agitation, residual TOAB could not be removed. Interestingly, previous research that used ligand exchange methods (PVP or PEG exchanged for acetylide ligands) to form acetylide-protected AuNPs with diameters >4 nm reported residual PVP or PEG in the resultant nanoparticles.[8, 25] However, smaller nanoparticles (diameter <2 nm) have been stabilised solely by acetylide ligands via a ligand exchange with PVP.[12] We therefore investigated modifications to Method A in an effort to synthesise smaller AuNPs (i.e. diameters <4 nm). Several variations to reaction conditions of the Brust-Schiffrin method have been shown to yield thiolate-stabilised AuNPs with diameters as small as ~1.5 nm.[46, 47] We applied these variations to the synthesis of alkynide-stabilised AuNPs such that the 1-decyne:$HAuCl_4$ mole ratio was increased from 1:1 to 64:1, the reaction temperature reduced to ~-10°C, and the time period for $NaBH_4$ addition was decreased from 30 seconds to ~1 second (Method B).

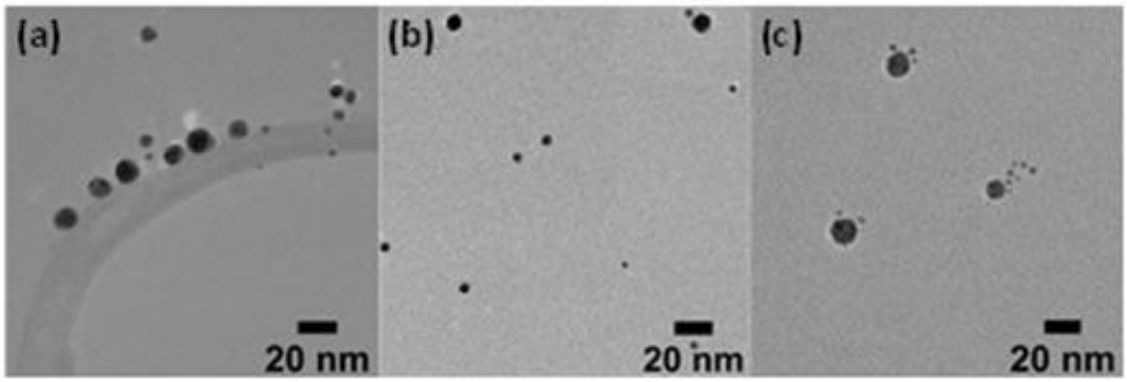

Figure 5.3 TEM of (a) Dec-1-ynide/TOAB-stabilised AuNPs (Method A); (b) Dec-1-ynide/TOAB-stabilised AuNPs (Method B); (c) TOAB-stabilised AuNPs (Method C).

The UV-vis spectrum (Figure 5.2b) of AuNPs obtained using Method B contains a plasmon resonance band with a maximum at 517 nm, suggesting only a small reduction in particle size (compared to 525 nm for Method A).[2] TEM images (5.3b and Figure 5.8b, Section 5.5, Supplementary Information) showed that the size of the gold core for Method B have two distinct sizes of 9.1 (±0.5) nm and 3.5 (±0.7) nm (Figure 5.9b, Section 5.5, Supplementary Information), which are also similar to those prepared using Method A. Likewise, the ^{1}H NMR spectrum of AuNPs synthesised using Method B was similar to that of particles prepared by Method A. Thus, the modifications to the synthetic method did not yield smaller nor TOAB-free AuNPs.

To explore whether the addition of alkyne was at all necessary in these methods, AuNPs were synthesised using a similar procedure except the addition of 1-decyne was omitted (Method C).[48] This reaction yielded similar deep red dispersions of AuNPs but were significantly less stable than the alkynide-containing dispersions. The as-synthesised dispersions precipitated within 24 hours, indicating aggregation. Washing the particles resulted in rapid aggregation and solvent removal gave a solid material that could not be re-dispersed. The UV-vis spectrum (Figure 5.2c) of the as-synthesised TOAB@AuNPs, contains a plasmon resonance band at 519 nm and TEM images (Figure 5.3c and Figure 5.8c, Section 5.5, Supplementary Information) show two distinct size ranges of 10.8 (±2) nm and 3.1 (±0.6) nm (Figure 5.8c, Section 5.5, Supplementary Information), similar to the AuNPs synthesised by Methods A and B. The ^{1}H NMR spectrum of the TOAB@AuNPs (Figure 5.10, Section 5.5, Supplementary Information) was also similar to those of particles prepared by Methods A and B. Thus, we conclude that stable AuNPs synthesised by this modified Brust-Schiffrin method must contain both

alkynide and TOAB stabilising ligands and that monodisperse particles with d<5 nm are not readily accessible by this route.

In our quest for alkynide-stabilised AuNPs with diameters <4 nm, we reasoned that one factor that influenced the larger particles that result from Methods A-C (compared to thiolate-stabilised analogues) involves the pathway of reactions that lead from Au(III) to Au(0).[49] When $HAuCl_4$ is reacted with thiol, there is an immediate reduction of Au(III) to Au(I) and an associated oxidation of the thiol, Equation (1). Upon introduction of $NaBH_4$, there is then rapid reduction of Au(I) to Au(0) to form NPs, Equation (2). In contrast, addition of $HAuCl_4$ to a terminal acetylene does not facilate reduction of the Au(III) to Au(I). Thus, when $NaBH_4$ is added to the $HAuCl_4$ and alkyne mixture, a three-electron process must occur to give Au(0) NPs, Equation (3), as well as breaking the quite stable (relative to the thiol H-S bond) H-C alkyne bond.[50] To mimic the reduction process utilised in thiol-stabilised AuNPs, a Au(I)-alkynide complex was synthesised and subsequently reduced to form AuNPs. This strategy has been utilised in synthesis of alkynide-protected NCs stabilised using a range of alkynes.[14, 31]

$$HAu(III)Cl_4 + 3HSR \rightarrow (Au(I)SR)_n + RS\text{-}SR + 4HCl \quad (1)$$

$$(Au(I)SR)_n \xrightarrow{NaBH_4} RS@Au(0)NPs \quad (2)$$

$$HAu^{III}Cl_4 + HC \equiv CR \xrightarrow{NaBH_4} RC \equiv C@Au^0NPs \quad (3)$$

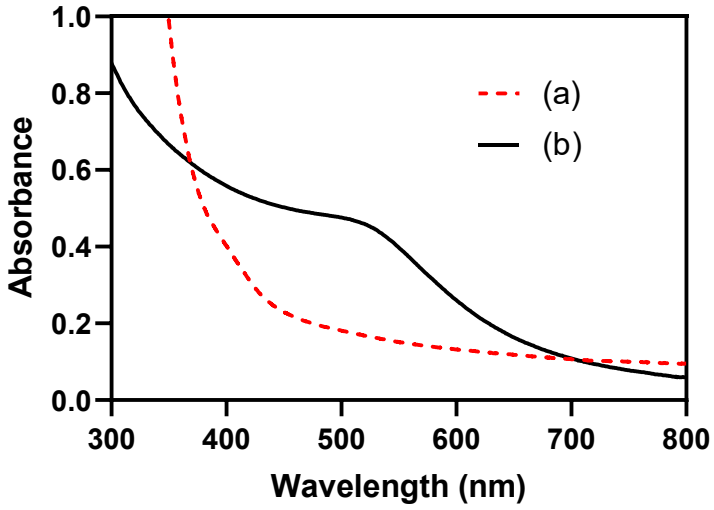

Figure 5.4 UV-visible spectrum of (a) gold(I)dec-1-ynide; (b) dec-1-ynide@AuNPs (Method D).

In this work, dec-1-ynide-stabilised AuNPs were synthesised using the gold(I)dec-1-ynide complex. The gold(I)-complex was dissolved in toluene together with the phase-transfer agent, TOAB. Aqueous $NaBH_4$ was added and the organic phase became brown in colour, indicating the formation of AuNPs (Method D). The resultant AuNPs were cleaned by precipitation with methanol and washed twice with additional acetonitrile. The washed nanoparticles could be re-suspended in chloroform or toluene without aggregation, unlike those prepared by Methods A-C. The NPs were stable for up to two months as powders, as evidenced by their ability to be re-suspended in chloroform or toluene without colour change.

The UV-vis spectrum (Figure 5.4b) contains an absorbance shoulder at ~520 nm and is similar to the spectrum of octyn-1-ide stabilised AuNPs with diameters of ~3.2 nm (prepared via ligand exchange with PVP).[12] The surface plasmon band indicates that the diameters of the AuNPs are smaller than those synthesised by Methods A-C. The spectrum of the dec-1-ynide@AuNPs is markedly different to that of the gold(I)dec-1-yne complex (Figure 5.4a). SEM (Figure 5.5a and Figure 5.8d, Section 5.5, Supplementary Information) of AuNPs synthesised using Method D revealed average diameters of ~4 nm. TEM images (Figure 5.5b) indicate a size range of 3.4 (±0.4) nm, (Figure 5.9d, Section 5.5, Supplementary Information).

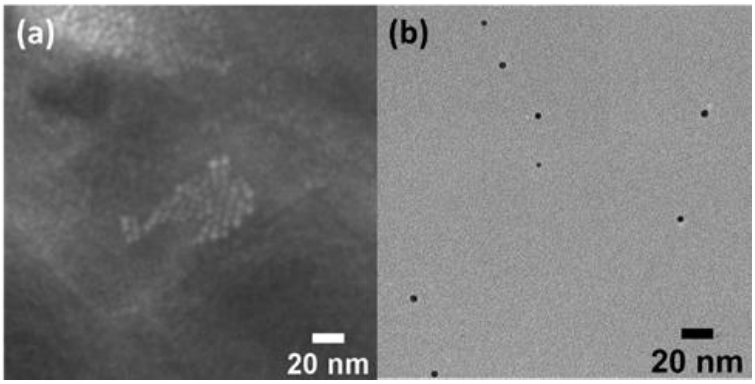

Figure 5.5 (a) SEM and (b) TEM of Dec-1-ynide-stabilised AuNPs via Method D.

^{1}H NMR spectra, (Figure 5.6b), contain no signals from residual TOAB nor from 1-decyne. Interestingly, the ^{1}H NMR spectrum of dec-1-ynide@AuNPs is very similar to that of the gold(I)dec-1-ynide complex (Figure 5.6a). In both spectra, Figure 5.6 (a and b), a triplet at 2.62 ppm is assigned to the protons at the C2 positions (the position adjacent to the C≡C), a quintet at 1.62 ppm is assigned to the protons at C3, and a multiplet at 1.42 ppm is assigned to the C4 protons.

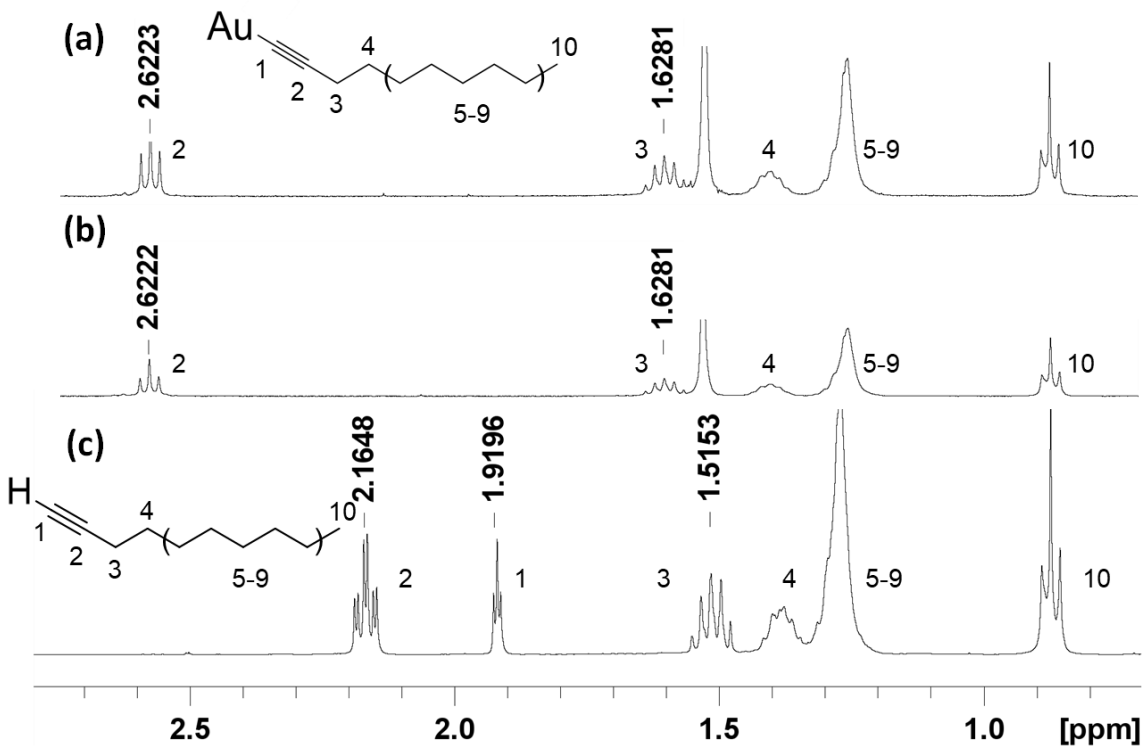

Figure 5.6 ^{1}H NMR spectra of (a) gold(I)dec-1-yn-1-ide; (b) dec-1-ynide@AuNPS (Method D); (c) 1-decyne.

Peak broadening of signals assigned to protons close to the gold surface has been reported for thiol-stabilised AuNCs,[47, 51, 52] unlike the spectrum shown in Figure 5.6b. Previous work investigating phenylacetylide-stabilised AuNCs, formed from a gold(I)phenylacetylide compound, proposed (based on X-ray photoelectron spectroscopy data) an Au(0) core surrounded by Au(I) species but no NMR were reported.[14] ^{1}H NMR spectra of AuNPs stabilised with N-heterocyclic carbenes showed remarkable similarly to that of the precursor Au(I) carbene complex, suggesting also an Au(0) core with an Au(I) shell.[53] In contrast, 4-pentyl phenylacetylene-protected gold clusters of ~1.5 nm prepared via ligand exchange with PVP-stabilised AuNCs show peak broadening on the phenyl and methylene peaks.[13] We therefore propose that the dec-1-ynide@AuNPs synthesised in the current work are of similar composition. That is, they contain a significant amount of Au(I) species at the particle surface. However, future work involving X-ray photoelectron spectroscopy would provide further clarification of this aspect.

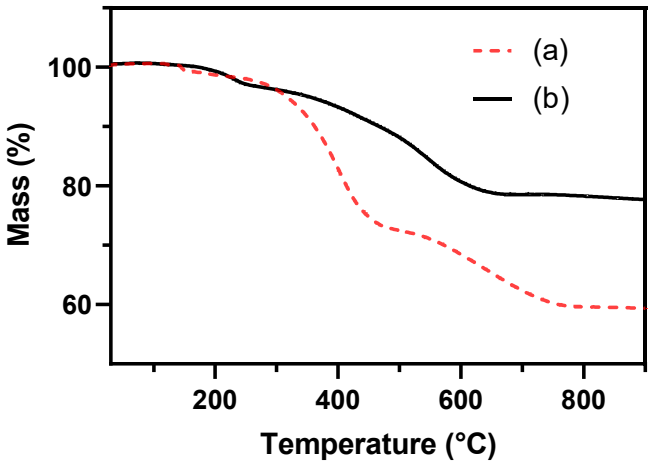

Figure 5.7 TGA for (a) gold(I)dec-1-ynide; (b) dec-1-ynide@AuNPs (Method D).

TGA data for gold(I)dec-1-ynide and dec-1-ynide@AuNPs are shown in Figure 5.7. A mass loss of 42% was observed for gold(I)dec-1-ynide upon heating to 1100°C. This agrees with the calculated value of 41%. For the dec-1-ynide@AuNPs, a mass loss of a 22% was measured. For particles with radii of 1.7 nm (and thus a mass of gold of 3.98 x 10^{-19} g) this implies 1.12 x 10^{-19} g of ligand per NP, or 491 ligands per nanoparticle. Thus, the surface coverage of ligands on the NPs is calculated to be 13.5 ligands/nm^2. This number is similar that of AuNPs stabilised by N-heterocyclic carbenes with a reported Au(I) shell over an a Au(0) core,[54]with a surface density of 13.1 ligands nm^{-2}.

The dec-1-ynide@AuNPs showed ligand loss over two distinct steps commencing at ~190°C and ~247°C. A similar pattern was reported for AuNCs stabilised with phenylacetylene-stabilised AuNCs[14] as well as N-heterocyclic carbene-stabilised AuNPs.[53]

Having developed a synthesis of decyn-1-ide@AuNPs with diameters of < 4nm, a synthesis of dec-1-ynide@AuNPs with diameters > 4 nm was explored. Based on variations to reaction conditions of the Brust-Schiffrin method that affect particle diameter,[46, 47] a modified version of Method D was performed using the following parameters; the amount of reducing agent was halved compared that of Method D, the time for addition of the reducing agent was increased to 60 seconds, and the temperature was maintained at 23°C (Method E). The ^{1}H NMR spectrum of the AuNPs prepared by Method E (Figure 5.10, Section 5.5, Supplementary Information) contains signals similar to the spectra of AuNPs prepared using Methods A-C, that is, signals from only TOAB

were observed. Method E also resulted in a deep purple-red solution, with UV-vis spectrum containing a plasmon resonance band with a maximum at 535 nm (Figure 5.2d). These data indicate that modifying Method D in this fashion results in mostly TOAB stabilised nanoparticles in contrast to the decyn-1-ide@AuNPs formed by Method D. A summary of the properties of AuNPs obtained by Method A-D is given in Table 4.1.

Table 4.1 Summary of AuNP properties

Method	Size (nm)	Plasmon resonance wavelength (nm)	Ligand Profile	Remarks
A	9.4 (±3) / 4.0 (±1)	525	1-Decyne/TOAB	Stable as powders for up to two months
B	9.1 (±0.5) / 3.5 (±0.7)	517	1-Decyne/TOAB	
C	10.8 (±2) / 3.1 (±0.6)	519	TOAB	Precipitated within 24 hours from toluene. Aggregated upon washing.
D	3.4 (±0.4)	520	1-Decyne	Stable as powders for up to two months.

Conclusion

Several pathways into alkynide-stabilised AuNPs have been explored. Stable dec-1-ynide@AuNPs have been synthesised by reduction of a Au(I)dec-1-ynide complex to give monodisperse NPs with diameter of ~3.4 nm (Method D). ^{1}H NMR spectra indicate that the particles have a shell that contains gold(I) species. However, Method E gave AuNPs stabilised predominantly by TOAB.

Methods that utilised reduction of Au(III) chloride with the phase transfer agent TOAB (Methods A-C) resulted in bidisperse AuNPs with diameters of ~9 nm and ~3 nm. Variation of the synthesis conditions did not have a significant effect on the particle sizes. All of the AuNPs prepared by Methods A-C had similar organic profiles with TOAB required to maintain particle stability. AuNPs prepared using only TOAB as stabiliser (Method C) yielded NPs with lower stability than those that also utilised 1-decyne (Methods A-B).

Experimental

Materials and Methods

1-Decyne, TOAB, sodium borohydride, triethylamine, dimethylsulfide, methanol, acetonitrile, $CDCl_3$ were purchased from Sigma-Aldrich and used as received. Toluene and diethyl ether (ChemSupplyAustralia), chloroform (Rowe Scientific) and ethanol (POCD Scientific) were used as received. Tetrachloroauric acid,[55] Dec-1-ynide/TOAB stabilised AuNPs[10] and TOAB stabilised AuNPs[48] were prepared using literature procedures. Synthesis of chloro(dimethylsulfide)gold(I) was prepared from a previously published report.[56] All glassware and stir bars were cleaned with Aqua Regia (HCI:HNO_3).

TGA measurements were carried out using a TA Instruments SDT Q600 with a heating rate of 10°C min^{-1} under a nitrogen atmosphere (flow rate of 100 mL min^{-1}). UV-Vis spectra were recorded on an Agilent Cary 60 spectrophotometer. Samples were prepared in a quartz cuvette by dissolving ~ 0.4 mg of AuNP sample in toluene (8 mL). ^{1}H NMR spectra were recorded using a Bruker NMR spectrometer operating at 400 MHz. Spectra were referenced using residual non-deuterated signals $CDCl_3$ (1H δ 7.26). TEM images were taken using a JEOL JEM-F200 FE-TEM operating at 200 kV and fitted with a Gatan Rio 1816 – 4k x 4k camera. The TEM samples were prepared by evaporating diluted nanoparticle solution on the carbon-coated copper grid. The images were analysed using ImageJ software (https://imagej.nih.gov/ij/). SEM was performed at facilities at Western Sydney University. A Zeiss Merlin FEGSEM was utilised for imaging samples prepared on stubs. The FEGSEM was operated at 10kV accelerating voltage in Hivac mode at a working distance of approximately 3 mm. Both secondary and in-lens secondary detectors were utilised for imaging.

Synthetic Procedures

Synthesis of dec-1-ynide/TOAB-stabilised AuNPs - Method A. Dec-1-ynide/TOAB-stabilised AuNPs was synthesised using a modified literature method.[10] A aqueous solution of tetrachloroauric acid (5 mL, 0.14 mmol, 0.027 M) was mixed with TOAB (0.29 g, 0.56 mmol,) in toluene (10 mL). After 15 minutes, decyne (3.3 mg, 0.42 mmol) in toluene (5 ml) was added to the solution then cooled in an ice bath. After 15 min, an ice-cold, freshly made aqueous solution of $NaBH_4$ (3.5 mL, 1.4 mmol, 0.4 M) was added dropwise over 30s. After further stirring for 12 h, the organic layer was separated and

evaporated under a stream of dry nitrogen gas. Acetonitrile was added to the residue to precipitate a black solid. The acetonitrile was removed using a pipette, and the solid was washed with acetonitrile a further five times. ^{1}H NMR ($CDCl_3$, 400 MHz): 3.36 (8H, t, J= 8 Hz), 1.72-1.62 (8H, m), 1.45-1.33 (16H, m), 1.33-1.19 (24H, m), 0.88 (12H, t, J= 7 Hz).

Synthesis of dec-1-ynide/TOAB-stabilised AuNPs - Method B. Dec-1-ynide/TOAB-stabilised AuNPs were using a modified literature method.[10] An aqueous solution of tetrachloroauric acid (5 mL, 0.027 M, mmol) was cooled to - 10°C then mixed with TOAB (0.29 g, 0.56 mmol,) in toluene (10 mL). After 15 minutes, decyne (0.63 g, 4.5 mmol) in toluene (53 ml) was added to the solution. After 15 min an ice-cold, freshly made aqueous solution of $NaBH_4$ (3.5 mL, 1.4 mmol, 0.4 M) was added instantly. After further stirring for 12 h the organic layer was separated and evaporated under a stream of dry nitrogen gas. The acetonitrile was removed using a pipette, and the solid was washed with acetonitrile a further five times. ^{1}H NMR ($CDCl_3$, 400 MHz): 3.37 (8H, t, J = 8 Hz), 1.73-1.62 (8H, m), 1.45-1.34 (16H, m), 1.34-1.18 (24H, m), 0.88 (12H, t, J= 6 Hz).

Synthesis of TOAB-stabilised AuNPS – Method C. TOAB-stabilised AuNPs was synthesised using a modified literature method.[48] An aqueous solution of tetrachloroauric acid (6.7 mL, 0.027 M, 0.18 mmol) was mixed with TOAB (0.49 g, 0.9 mmol) in toluene (6 mL) then cooled in an ice bath. After 15 min a cold, freshly made aqueous solution of $NaBH_4$ (6 mL, 1.5 mmol, 0.25 M) was added dropwise over 30s. After further stirring for 12 h the organic layer was separated and evaporated under N_2 to near dryness then washed with water. ^{1}H NMR ($CDCl_3$, 400 MHz): 3.35 (8H, t, J= 8 Hz), 170-1.61 (8H, m), 1.44-1.33 (16H, m), 1.33-1.20 (24H, m), 0.88 (12H, t, J= 7 Hz).

Synthesis of gold(I)dec-1-ynide. Gold(I) dec-1-ynide was synthesised using a modified literature procedure.[26] Chloro(dimethylsulfide)gold(I) (100 mg, 0.34 mmol) was added to dichloromethane (10.0 mL), decyne (77.4 µL, 0.43 mmol), and triethylamine (60.3 µL, 0.43 mmol) in a 20 mL scintillation vial and stirred in the dark for two hours. The solution was then evaporated under a stream of dry nitrogen gas and the resulting powder washed with water, ethanol, and diethyl ether. Yield: 95 mg (84%). ^{1}H NMR ($CDCl_3$, 400 MHz): 2.62 (2H, t, J= 7 Hz), 1.67-1.59 (2H, quint, J= 7 Hz), 1.47-1.38 (2H, m), 1.33-1.21 (8H, m), 0.88 (3H, t, J= 7 Hz).

Synthesis of dec-1-ynide@AuNPs – Method D. Gold(I) dec-1-ynide (30 mg, 0.090 mmol) was dissolved in toluene (1 mL) and then mixed with TOAB (0.19 g, 0.36 mmol)

dissolved in toluene (6.5 mL) then cooled in an ice bath. After 15 min an ice-cold, freshly made aqueous solution of $NaBH_4$ (2.3 mL, 0.90 mmol, 0.4 M) was added instantly. After further stirring for 12 h, the organic layer was separated and concentrated to near dryness under a stream of dry nitrogen gas. The solution was then precipitated in methanol and washed twice. Yield: 15 mg (52% based on gold). ^{1}H NMR ($CDCl_3$, 400 MHz): 2.62 (2H, t, J= 7 Hz), 1.66-1.59 (2H, quint, J= 7 Hz), 1.47-1.37 (2H, m), 1.33-1.22 (8H, m), 0.88 (3H, t, J= 7 Hz).

Synthesis of dec-1-ynide@AuNPs – Method E. Gold(I)dec-1-ynide (30 mg, 0.090 mmol) in toluene (1 mL) was mixed with TOAB (0.19 g, 0.36 mmol,) in toluene (6.5 mL) at 23°C. After 15 min a freshly made ice-cold aqueous solution of $NaBH_4$ (1.2 mL, 0.45 mmol, 0.4M) was added dropwise over 60s. After further stirring for 12 h, the organic layer was separated and concentrated to near dryness under a stream of dry nitrogen gas. The solution was then precipitated in acetonitrile and washed twice. ^{1}H NMR ($CDCl_3$, 400 MHz): 3.31 (8H, t, J= 8 Hz), 1.72-1.48 (m), 1.44-1.34 (16H, m), 1.34-1.21 (24H, m), 0.88 (12H, t, J= 7 Hz).

Acknowledgements

This research is supported by an Australian Government Research Training Program Scholarship: We acknowledge Dr Richard Wuhrer, Dr Laurel George and Dr Daniel Fanna at the Advanced Materials Characterisation Facility of Western Sydney University for access to its instrumentation and staff. We thank microstructural analysis unit (University of Technology Sydney) for assistance with TEM.

5.5 Supplementary Information

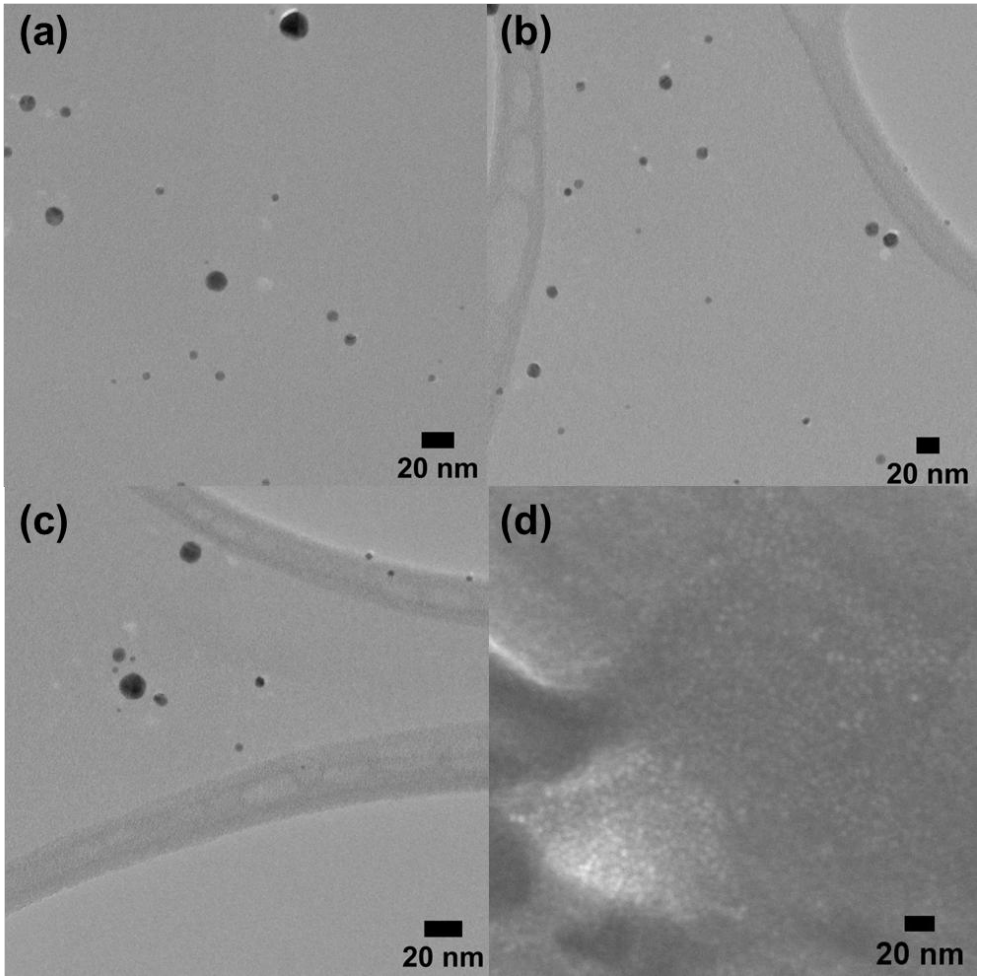

Figure 5.8 TEM of (a) Method A; (b) Method B; (c) Method C and SEM of (d) Method D.

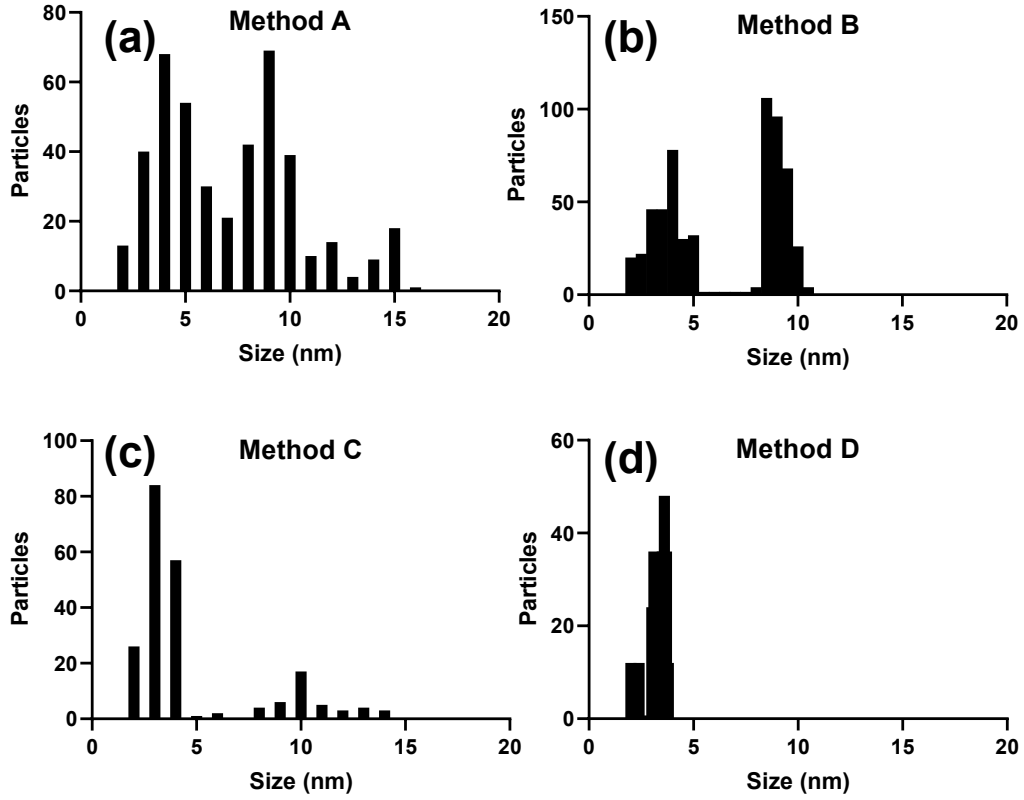

Figure 5.9 TEM Histogram of (a) Method A; (b) Method B; (c) Method C; (d) Method D.

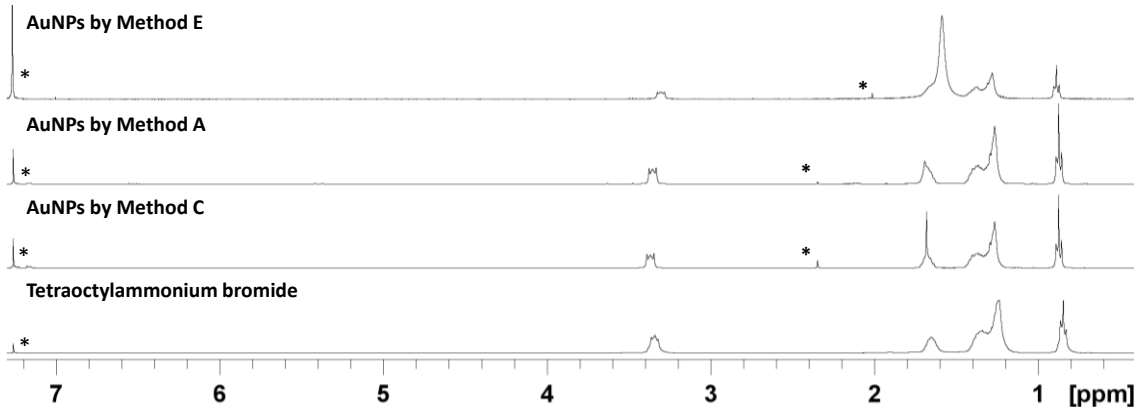

Figure 5.10 ^{1}H NMR spectra of AuNPs synthesised by Method A, C and E, and tetraoctylammonium bromide (* denotes residual solvent).

References

1. Yang, Z., Pujari, S. P., Armstrong, R., Mathwig, K., Rutjes, F. P. J. T., Smulders, M. M. J., Zuilhof, H., Hydrolytic, Thermal, and Electrochemical Stability of Thiol- and Terminal Alkyne-Based Monolayers on Gold: A Comparative Study. *Langmuir.* 2025, *41* (9), 6197-6207.
2. Daniel, M.-C., Astruc, D., Gold Nanoparticles: Assembly, Supramolecular Chemistry, Quantum-Size-Related Properties, and Applications toward Biology, Catalysis, and Nanotechnology. *Chemical Reviews.* 2004, *104* (1), 293-346.
3. Sardar, R., Funston, A. M., Mulvaney, P., Murray, R. W., Gold nanoparticles: past, present, and future. *Langmuir.* 2009, *25* (24), 13840-51.
4. Amendola, V., Pilot, R., Frasconi, M., Marago, O. M., Iati, M. A., Surface plasmon resonance in gold nanoparticles: a review. *Journal of Physics: Condensed Matter.* 2017, *29* (20), 203002.
5. Kimling, J., Maier, M., Okenve, B., Kotaidis, V., Ballot, H., Plech, A., Turkevich method for gold nanoparticle synthesis revisited. *The Journal of Physical Chemistry B.* 2006, *110* (32), 15700-15707.
6. Shan, J., Tenhu, H., Recent advances in polymer protected gold nanoparticles: synthesis, properties and applications. *Chemical Communications* 2007, (44), 4580-98.
7. Kaur, G., Thimes, R. L., Camden, J. P., Jenkins, D. M., Fundamentals and applications of N-heterocyclic carbene functionalized gold surfaces and nanoparticles. *Chemical Communications.* 2022, *58* (95), 13188-13197.
8. Catalán-Toledo, J., Djafari, J., Mas-Torrent, M., Crivillers, N., Redox-Active Au Nanoparticles Self-Assembled at Liquid–Liquid Interface via C–Au Functionalization for Dye Degradation Electrocatalysis. *Applied Nano Materials.* 2024, *7* (5), 5242-5251.
9. Liu, Y.-Q., Chao, Y.-C., Xu, S.-Q., Peng, Y.-R., Syu, J.-J., Yang, X.-H., Pan, Y.-K., Lin, P.-C., Weng, L.-L., Chen, I. C., Tan, K.-T., Surface Functionalization of Gold Nanoparticles Using Alkyne Derivatives: Applications in Chemical Sensing. *Applied Materials & Interfaces.* 2024.
10. Zhang, S., Chandra, K. L., Gorman, C. B., Self-Assembled Monolayers of Terminal Alkynes on Gold. *Journal of the American Chemical Society.* 2007, *129* (16), 4876-4877.
11. Lei, Z., Li, J.-J., Wan, X.-K., Zhang, W.-H., Wang, Q.-M., Isolation and Total Structure Determination of an All-Alkynyl-Protected Gold Nanocluster Au144. *Angewandte Chemie International Edition.* 2018, *57* (28), 8639-8643.
12. Maity, P., Takano, S., Yamazoe, S., Wakabayashi, T., Tsukuda, T., Binding Motif of Terminal Alkynes on Gold Clusters. *Journal of the American Chemical Society.* 2013, *135* (25), 9450-9457.
13. Maity, P., Tsunoyama, H., Yamauchi, M., Xie, S., Tsukuda, T., Organogold Clusters Protected by Phenylacetylene. *Journal of the American Chemical Society.* 2011, *133* (50), 20123-20125.
14. Ma, X., Tang, Z., Qin, L., Peng, J., Li, L., Chen, S., Unravelling the formation mechanism of alkynyl protected gold clusters: a case study of phenylacetylene stabilized Au144 molecules. *Nanoscale.* 2020, *12* (5), 2980-2986.
15. Park, H., Shin, D. J., Yu, J., Categorization of Quantum Dots, Clusters, Nanoclusters, and Nanodots. *Journal of Chemical Education.* 2021, *98* (3), 703-709.
16. Kobayashi, N., Kamei, Y., Shichibu, Y., Konishi, K., Protonation-Induced Chromism of Pyridylethynyl-Appended [core+exo]-Type Au8 Clusters. Resonance-Coupled Electronic Perturbation through π-Conjugated Group. *Journal of the American Chemical Society.* 2013, *135* (43), 16078-16081.

17. Sugiuchi, M., Shichibu, Y., Nakanishi, T., Hasegawa, Y., Konishi, K., Cluster–π electronic interaction in a superatomic Au13 cluster bearing σ-bonded acetylide ligands. *Chemical Communications.* 2015, *51* (70), 13519-13522.
18. Wang, Y., Wan, X.-K., Ren, L., Su, H., Li, G., Malola, S., Lin, S., Tang, Z., Häkkinen, H., Teo, B. K., Wang, Q.-M., Zheng, N., Atomically Precise Alkynyl-Protected Metal Nanoclusters as a Model Catalyst: Observation of Promoting Effect of Surface Ligands on Catalysis by Metal Nanoparticles. *Journal of the American Chemical Society.* 2016, *138* (10), 3278-3281.
19. Hoft, R., Ford, M., García-Suárez, V., Lambert, C., Cortie, M., The effect of stretching thiyl– and ethynyl–Au molecular junctions. *Journal of Physics: Condensed Matter.* 2007, *20*, 025207.
20. Tang, Q., Jiang, D.-e., Insights into the PhC≡C/Au Interface. *The Journal of Physical Chemistry C.* 2014, *119* (20), 10804-10810.
21. Hu, X., Li, P., Xu, D., Liu, H., Hao, Q., Zhang, M., Wang, Z., Wei, T., Dai, Z., Facile Alkyne Assembly-Enabled Functional Au Nanosheets for Photoacoustic Imaging-Guided Photothermal/Gene Therapy of Orthotopic Glioblastoma. *Journal of the American Chemical Society.* 2024, *146* (48), 32965-32978.
22. Weston, R. P., Chen, Y., Dzwonczyk, T. J., Veras, J. A., Sevigny, A. M., Landis, E. C., Electrically Transmissive and Stable Alkyne-Derived Molecular Layers on Nanoporous Gold. *The Journal of Physical Chemistry C.* 2022, *126* (23), 9673-9682.
23. Herrer, L., González-Orive, A., Marqués-González, S., Martín, S., Nichols, R. J., Serrano, J. L., Low, P. J., Cea, P., Electrically transmissive alkyne-anchored monolayers on gold. *Nanoscale.* 2019, *11* (16), 7976-7985.
24. Du, J., Xu, H., Zhu, X., Long, K., Lang, J., Jiang, L., Xiong, E., Liu, J., Yang, R., Robust Peptide-Functionalized Gold Nanoparticles via Ethynyl Bonding for High-Fidelity Bioanalytical Applications. *Angewandte Chemie International Edition.* 2025, e202424351.
25. Duan, H., Yang, T., Sklyar, W., Chen, B., Chen, Y., Hanson, L. A., Sun, S., Lin, Y., He, J., Phenylacetylene-Terminated Poly(Ethylene Glycol) as Ligands for Colloidal Noble Metal Nanoparticles: a New Tool for "Grafting to" Approach. *Nano Letters.* 2024, *24* (19), 5847-5854.
26. Hosier, C. A., Anderson, I. D., Ackerson, C. J., Acetylide-for-thiolate and thiolate-for-acetylide exchange on gold nanoclusters. *Nanoscale.* 2020, *12* (11), 6239-6242.
27. Ito, S., Takano, S., Tsukuda, T., Alkynyl-Protected Au22(C≡CR)18 Clusters Featuring New Interfacial Motifs and R-Dependent Photoluminescence. *The Journal of Physical Chemistry Letters.* 2019, *10* (21), 6892-6896.
28. Guan, Z.-J., Hu, F., Li, J.-J., Wen, Z.-R., Lin, Y.-M., Wang, Q.-M., Isomerization in Alkynyl-Protected Gold Nanoclusters. *Journal of the American Chemical Society.* 2020, *142* (6), 2995-3001.
29. Brust, M., Walker, M., Bethell, D., Schiffrin, D. J., Whyman, R., Synthesis of thiol-derivatised gold nanoparticles in a two-phase Liquid–Liquid system. *Journal of the Chemical Society, Chemical Communications.* 1994, (7), 801-802.
30. Guan, Z.-J., Hu, F., Li, J.-J., Liu, Z.-R., Wang, Q.-M., Homoleptic alkynyl-protected gold nanoclusters with unusual compositions and structures. *Nanoscale.* 2020, *12* (25), 13346-13350.
31. Wan, X.-K., Guan, Z.-J., Wang, Q.-M., Homoleptic Alkynyl-Protected Gold Nanoclusters: Au44(PhC≡C)28 and Au36(PhC≡C)24. *Angewandte Chemie International Edition.* 2017, *56* (38), 11494-11497.

32. Li, J.-J., Liu, Z., Guan, Z.-J., Han, X.-S., Shi, W.-Q., Wang, Q.-M., A 59-Electron Non-Magic-Number Gold Nanocluster Au99(C≡CR)40 Showing Unexpectedly High Stability. *Journal of the American Chemical Society.* 2022, *144* (2), 690-694.
33. Wang, J.-Q., Shi, S., He, R.-L., Yuan, S.-F., Yang, G.-Y., Liang, G.-J., Wang, Q.-M., Total Structure Determination of the Largest Alkynyl-Protected fcc Gold Nanocluster Au110 and the Study on Its Ultrafast Excited-State Dynamics. *Journal of the American Chemical Society.* 2020, *142* (42), 18086-18092.
34. Ma, X., Ma, G., Qin, L., Chen, G., Chen, S., Tang, Z., A synchronous nucleation and passivation strategy for controllable synthesis of Au36(PA)24: unveiling the formation process and the role of Au22(PA)18 intermediate. *Science China Chemistry.* 2020, *63* (12), 1777-1784.
35. Summers, P. K., Wuhrer, R., McDonagh, A. M., Electrically conductive gold films formed by sintering of gold nanoparticles at room temperature initiated by ozone. *Journal of Nanoparticle Research.* 2024, *26* (5), 97.
36. Summers, P. K., Angeloski, A., Wuhrer, R., Cortie, M. B., McDonagh, A. M., The fate of organic species upon sintering of thiol-stabilised gold nanoparticles under different atmospheric conditions. *Physical Chemistry Chemical Physics.* 2023, *25* (10), 7170-7175.
37. King, S. R., Gentle, A. R., Cortie, M. B., McDonagh, A. M., On the Development of Optical Properties during Thermal Coarsening of Gold Nanoparticle Composites. *The Journal of Physical Chemistry C.* 2018, *122* (22), 12098-12105.
38. King, S. R., Shimmon, S., Totonjian, D. D., McDonagh, A. M., Influence of Bound versus Non-Bound Stabilizing Molecules on the Thermal Stability of Gold Nanoparticles. *The Journal of Physical Chemistry C.* 2017, *121* (25), 13944-13951.
39. King, S. R., Shimmon, S., Gentle, A. R., Westerhausen, M. T., Dowd, A., McDonagh, A. M., Remarkable thermal stability of gold nanoparticles functionalised with ruthenium phthalocyanine complexes. *Nanotechnology.* 2016, *27* (21), 215702.
40. Cortie, M. B., Coutts, M. J., Ton-That, C., Dowd, A., Keast, V. J., McDonagh, A. M., On the Coalescence of Nanoparticulate Gold Sinter Ink. *The Journal of Physical Chemistry C.* 2013, *117* (21), 11377-11384.
41. Coutts, M. J., Cortie, M. B., Ford, M. J., McDonagh, A. M., Rapid and Controllable Sintering of Gold Nanoparticle Inks at Room Temperature Using a Chemical Agent. *The Journal of Physical Chemistry C.* 2009, *113* (4), 1325-1328.
42. Singh, R., Nanotechnology based therapeutic application in cancer diagnosis and therapy. *3 Biotech.* 2019, *9* (11), 415.
43. Chang, J., Zhang, A., Huang, Z., Chen, Y., Zhang, Q., Cui, D., Monodisperse Au@ Ag core-shell nanoprobes with ultrasensitive SERS-activity for rapid identification and Raman imaging of living cancer cells. *Talanta.* 2019, *198*, 45-54.
44. Ozcicek, I., Aysit, N., Cakici, C., Aydeger, A., The effects of surface functionality and size of gold nanoparticles on neuronal toxicity, apoptosis, ROS production and cellular/suborgan biodistribution. *Materials Science and Engineering: C.* 2021, *128*, 112308.
45. Bano, A., Dawood, A., Saira, F., Malik, A., Alkholief, M., Ahmad, H., Khan, M. A., Ahmad, Z., Bazighifan, O., Enhancing catalytic activity of gold nanoparticles in a standard redox reaction by investigating the impact of AuNPs size, temperature and reductant concentrations. *Scientific Reports.* 2023, *13* (1).
46. Leff, D. V., Ohara, P. C., Heath, J. R., Gelbart, W. M., Thermodynamic Control of Gold Nanocrystal Size: Experiment and Theory. *The Journal of Physical Chemistry.* 1995, *99* (18), 7036-7041.

47. Hostetler, M. J., Wingate, J. E., Zhong, C.-J., Harris, J. E., Vachet, R. W., Clark, M. R., Londono, J. D., Green, S. J., Stokes, J. J., Wignall, G. D., Glish, G. L., Porter, M. D., Evans, N. D., Murray, R. W., Alkanethiolate Gold Cluster Molecules with Core Diameters from 1.5 to 5.2 nm: Core and Monolayer Properties as a Function of Core Size. *Langmuir.* 1998, *14* (1), 17-30.
48. Wang, Y. Q., Liang, W. S., Geng, C. Y., Coalescence Behavior of Gold Nanoparticles. *Nanoscale Research Letters.* 2009, *4* (7), 684.
49. Yu, C., Zhu, L., Zhang, R., Wang, X., Guo, C., Sun, P., Xue, G., Investigation on the Mechanism of the Synthesis of Gold(I) Thiolate Complexes by NMR. *The Journal of Physical Chemistry C.* 2014, *118* (19), 10434-10440.
50. Casado, R., Contel, M., Laguna, M., Romero, P., Sanz, S., Organometallic Gold(III) Compounds as Catalysts for the Addition of Water and Methanol to Terminal Alkynes. *Journal of the American Chemical Society.* 2003, *125* (39), 11925-11935.
51. Badia, A., Gao, W., Singh, S., Demers, L., Cuccia, L., Reven, L., Structure and Chain Dynamics of Alkanethiol-Capped Gold Colloids. *Langmuir.* 1996, *12* (5), 1262-1269.
52. Terrill, R. H., Postlethwaite, T. A., Chen, C.-h., Poon, C.-D., Terzis, A., Chen, A., Hutchison, J. E., Clark, M. R., Wignall, G., Monolayers in Three Dimensions: NMR, SAXS, Thermal, and Electron Hopping Studies of Alkanethiol Stabilized Gold Clusters. *Journal of the American Chemical Society.* 1995, *117* (50), 12537-12548.
53. Thomas, S. R., Yang, W., Morgan, D. J., Davies, T. E., Li, J. J., Fischer, R. A., Huang, J., Dimitratos, N., Casini, A., Bottom-up Synthesis of Water-Soluble Gold Nanoparticles Stabilized by N-Heterocyclic Carbenes: From Structural Characterization to Applications. *Chemistry – A European Journal.* 2022, *28* (56), e202201575.
54. MacLeod, M. J., Johnson, J. A., PEGylated N-Heterocyclic Carbene Anchors Designed To Stabilize Gold Nanoparticles in Biologically Relevant Media. *Journal of the American Chemical Society.* 2015, *137* (25), 7974-7.
55. King, S. R., Massicot, J., McDonagh, A., A Straightforward Route to Tetrachloroauric Acid from Gold Metal and Molecular Chlorine for Nanoparticle Synthesis. *Metals.* 2015, *5*, 1454-1461.
56. Uson, R., Laguna, A., Laguna, M., Briggs, D. A., Murray, H. H., Fackler Jr, J. P., *(Tetrahydrothiophene)Gold(I) or Gold(III) Complexes*. 1989; p 85-91.

Chapter 6

Conclusions and Future Directions

6.1 Conclusions

The research aims, outlined in Chapter 1.4, have been addressed and new areas for further study have become apparent.

The investigation into the thermal stability of thiol-stabilised AuNPs reported in Chapter 2 determined that increasing the rate of removal of the resultant dialkyl disulfide compounds can decrease the T_{SE} *if* the disulfide is volatile. If the disulfide has low volatility (as was the case with dihexadecyl disulfide), the T_{SE} was not affected. The findings reported in this chapter elucidate some of the intricacies of the chosen alkane thiol ligand on the T_{SE}. That is, the sintering of AuNPs stabilised using short-chain alkanethiols can be controlled by pressure whereas this was not the case for the AuNPs with long-chain ligands.

Prior to the sintering event, AuNPs stabilised with hexadecanethiol ligands entered a liquid phase (at 56°C). This can be explained by considering the equilibrium between the surface thiyl species and the corresponding disulfide compounds. The temperature at which the HDT@AuNPs form a liquid phase corresponds precisely to the melting point of dihexadecyl disulfide (56°C). This molten form decreased the electrical resistance of the AuNPs film when heated from room temperature to 56°C. In contrast, no liquid phase was observed for BT@AuNPs. SAXS data and SEM images showed that BT@AuNPs do not coarsen until after ~140°C. While HDT@AuNPs underwent changes at ~90°C which was attributed to the formation of the liquid phase.

In an ozone-containing atmosphere, BT@AuNPs sintered at significantly lower temperatures than in air. Examination of the ligands post-sintering revealed that the butanethiyl ligands undergo oxidation to form the corresponding butanesulfonate. The formed sulfonate is a poor ligand for gold and induces sintering even at room temperature.

Alkynide-stabilised AuNPs were synthesised using a new method to give stable dec-1-ynide@AuNPs surrounded by gold(I) species. Modification of the method altered the size distribution of the AuNPs, however the larger (>3 nm) AuNPs were stabilised predominantly by TOAB, rather than the alkynide.

6.2 Future Directions

Gold films free from organic residues are desirable for several applications. Thus, organic residues formed on gold films after sintering of ligand-stabilised AuNP should be removed. By incorporating the findings presented in Chapter 2, the knowledge gained about the nature of the compounds that result from sintering thiol-stabilised AuNPs can readily assist the cleaning procedure or remove the process entirely.

Future work could utilise the methods developed here to investigate the nature of compounds that result from sintering of AuNPs bearing other types of stabilising ligands and functional groups, as this has been shown to be a significant factor affecting their thermal stability.

An investigation into thiol-stabilised AuNPs with different chain lengths could explore the extent to which the disulfide species form a liquid phase, such as that presented in Chapter 3. Exploiting this liquid-like state that is formed at low temperatures could remove the requirement for solvents that are used to disperse thiol-stabilised AuNPs as sinter inks. For example, a process whereby the HDT@AuNPs are heated to their liquid phase (56°C) and then poured into a mold to create a solid object once the material is cooled. The formed object could then be used for either its optical properties or sintered with additional heating to form a solid gold object. Additionally, changes in particle polydispersity could be explored as they pass through this phase.

Ozone is a readily available oxidiser that could provide an upscaled process to sinter AuNPs at reduced temperatures. This may provide opportunities to form gold films on temperature sensitive media such as polymer or biological surfaces. Furthermore, the effect of heat on ozone treated samples could be investigated. This may impact the resultant conductivity and film structure.

By implementing the method developed in Chapter 5, further research (such as that shown in Chapter 2) should be conducted to examine the stability of the new alkynide-stabilised AuNPs. With alkynes demonstrated stability as SAMs, this raises the possibility of alkynide-stabilised AuNPs with applications as high temperature sensing technologies and in the improved development of nanomaterials.